Western Graduate&PostdoctoralStudies

Western University
Scholarship@Western

Electronic Thesis and Dissertation Repository

12-2-2014 12:00 AM

Miniature Cone Penetration Test on Loose Sand

Sepideh Damavandinejad Monfared, *The University of Western Ontario*

Supervisor: Abouzar Sadrekarimi, *The University of Western Ontario*

A thesis submitted in partial fulfillment of the requirements for the Master of Engineering Science degree in Civil and Environmental Engineering

© Sepideh Damavandinejad Monfared 2014

Follow this and additional works at: https://ir.lib.uwo.ca/etd

Part of the Geotechnical Engineering Commons

Recommended Citation

Damavandinejad Monfared, Sepideh, "Miniature Cone Penetration Test on Loose Sand" (2014). *Electronic Thesis and Dissertation Repository*. 2533.
https://ir.lib.uwo.ca/etd/2533

This Dissertation/Thesis is brought to you for free and open access by Scholarship@Western. It has been accepted for inclusion in Electronic Thesis and Dissertation Repository by an authorized administrator of Scholarship@Western. For more information, please contact wlswadmin@uwo.ca.

MINIATURE CONE PENETRATION TEST ON LOOSE SAND

(Thesis format: Integrated Article)

by

Sepideh Damavandinejad Monfared

Graduate Program in Civil and Environmental Engineering

A thesis submitted in partial fulfillment
of the requirements for the degree of
Master of Engineering Science

The School of Graduate and Postdoctoral Studies
The University of Western Ontario
London, Ontario, Canada

© Sepideh Damavandinejad Monfared 2014

Abstract

Considering the difficulties associated with preparing loose sand samples in large calibration chambers and wide area of research on the behavior of loose sands, miniature calibration chamber experiments are used to perform cone penetration tests on soils in different states. A miniature cone calibration chamber has been designed and developed in this study. Nineteen tests have been performed on Ottawa sand and the results are compared to the available data in the literature. The accuracy of the results is validated by comparing the results with the suggested rate for the cone resistance in sands in literature. More specifically, results are compared with the results of the large calibration chamber tests performed on the same soil at University of Florida. Results are in a very good agreement with the literature and data available from large calibration chambers. Different soil identification systems are used to further validate and compare the results. Results of the performed tests are presented and discussed in terms of the repeatability of the developed apparatus, the effect of penetration rate, boundary condition effect, scale effect, particle crushing, overburden stress normalization and verification of the measurements. Some available procedures to perform a CPT-based liquefaction analysis including liquefaction susceptibility, triggering and post-liquefaction strength analysis are evaluated using the laboratory miniature CPT experiments performed in the current study. Some of the well-stablished equations to estimate soil properties required for liquefaction studies are also evaluated using the laboratory miniature CPT experiments performed in the current study. The existing methods for estimating state parameter from cone penetration test results are reviewed and an evaluation of the performance of the existing methods using the laboratory miniature CPT experiments performed in the current study is presented.

Keywords

Miniature cone calibration test, loose sand, liquefaction, state parameter.

Co-Authorship Statement

This thesis has been prepared in accordance with the regulations for an Integrated-Article format thesis stipulated by the School of Graduate and Postdoctoral Studies at the University of Western Ontario and has been co-authored as:

Chapter 2: Development of a Miniature Cone Penetrometer

A paper co-authored by Sepideh Damavandinejad Monfared and Abouzar Sadrekarimi will be submitted to the ASTM geotechnical testing journal.

The experimental work and interpretation of test results, and writing the draft of the paper was conducted by Sepideh Damavandinejad Monfared under close supervision of Dr. Abouzar Sadrekarimi.

Chapter 3: CPT-based Static Liquefaction Evaluation

A paper co-authored by Sepideh Damavandinejad Monfared and Abouzar Sadrekarimi will be submitted to the Canadian Geotechnical Journal.

The interpretation of the results and writing the draft of the paper was conducted by Sepideh Damavandinejad Monfared under close supervision of Dr. Abouzar Sadrekarimi.

Acknowledgments

First, I would like to express my sincere gratitude and appreciation to my supervisor Dr. Abouzar Sadrekarimi for his consistent support, advice, and encouragement throughout this research program. It has been a privilege to work under his supervision.

I would like to thank the administrative and laboratory staff at Western University. Special thanks to Erol Tas, Wilbert Logan, Whitney Barrett and Stephanie Laurence.

Many thanks to my friends and colleagues for their helpful discussions and encouragement through this research, particular thanks to Thomas Lardner, Muhammad Safdar, Muhammad Salama and Tarek Omar.

Finally, I can't find the suitable words to express my gratitude for my mother for her love, support, and sacrifices. I am indebted to her for everything I have. Especial thanks to my sister for her continuous support and encouragement.

Table of Contents

Abstract ii

Co-Authorship Statement iii

Acknowledgments iv

Table of Contents v

List of Tables ix

List of Figures x

List of Symbols xvi

List of Appendices xix

Chapter 1 1

1 Introduction 1

1.1 Background 1

1.2 Research Objectives 2

1.3 Scope and Outline of Current Study 2

1.4 The Original Contributions 3

References 4

Chapter 2 6

2 Development of a Miniature Cone Penetrometer 6

2.1 Introduction 6

2.1.1 Previous Miniature Cone Penetration Tests 8

2.2 Design and Construction of the New Miniature CPT Device 11

2.2.1 Miniature-cone 12

2.2.2 Miniature-cone Calibration Chamber 13

2.2.3 Cone Driving Frame and Pressure Pumps 17

2.2.4 Tested Material 17
2.2.5 Specimen Preparation 18
2.2.6 Specimen Uniformity 20
2.2.7 Specimen Saturation and Consolidation 21
2.2.8 Cone Penetration Testing 23
2.3 Results 25
2.4.1 Repeatability 49
2.4.2 Specimen Boundary Conditions and Size Effect 50
2.4.3 Scale Effect 52
2.4.4 Effect of Penetration Rate 54
2.4.5 Particle Crushing 55
2.4.6 Overburden Stress Normalization 56
2.4.7 The Effect of Increase in Mean Effective Stress on q_c and f_s 61
2.4.8 The Effect of Increase in Relative Density on q_c and f_s 62
2.5 Verification of CPT Measurements 64
2.5.1 Comparison with Previous Studies 64
2.5.2 Evaluation for soil classification 66
2.6 Conclusions 71
References 73
Chapter 3 82
3 CPT-based Static Liquefaction Evaluation 82
3.1 Introduction 82
3.2 Background 82
3.2.1 Flow Liquefaction Susceptibility Analysis 83
3.2.2 Liquefaction Triggering Analysis Using s_u(yield) 85

3.2.3 Post-Liquefaction Strength of Soil, s_u(liq) 88
3.3 Evaluation of the available procedures for liquefaction analysis 90
3.3.1 Liquefaction susceptibility 90
3.3.2 Liquefaction triggering analysis 96
3.3.3 Methods for estimating liquefied strength 100
3.4 Estimation of Loose Sand Parameters from CPT 102
3.4.1 Estimation of Soil Unit Weight 102
3.4.2 Estimation of Soil Relative Density 105
3.4.3 Estimation of in Situ State Parameter 109
3.4.3.1 Empirical Methods 110
3.4.3.2 Numerical Methods 111
3.4.3.3 Comparison with Laboratory Miniature CPT Experiments Results 113
3.5 Conclusions 116
References 117
Chapter 4 122
4 Conclusions 122
4.1 Summary and Conclusions 122
4.2 Suggestions for Future Research 124
Appendix A 125
(Sensors Calibration Factors) 125
Appendix B 129
(Photographs of the Developed Device and Experiments) 129
Appendix C 132
(Repeatability Tests Results) 132
Appendix D 138

(Triaxial Compression Test Results) 138

Curriculum Vitae 140

List of Tables

Table 2-1: Geometrical characteristics and boundary conditions of past miniature calibration chamber CPT tests 10

Table 2-2: Physical characteristics of Barco 71 sand 17

Table 2-3: Summary of miniature CPT tests performed in this study 24

Table 2-4: Boundary conditions in calibration chamber tests (Parkin et al. 1980)..... 50

Table 2-5: CPT overburden stress normalization methods..... 56

Table 2-6: Normalized tip resistance 59

Table 2-7: Comparison with the available data in the literature. 64

Table 2-8: Critical State parameters of Barco 71 (Omar 2013). 65

Table 3-1: Summary of miniature CPT tests performed in this study 91

Table 3-2: s_u(yield) and q_{c1} values used to evaluate the available correlations 98

Table 3-3: s_u(liq) and q_{c1} values used to evaluate the available correlations..... 100

Table 3-4: State parameter interpretation methods from CPT..... 109

List of Figures

Figure 2-1: Calibration chamber experiment setup 11

Figure 2-2: Schematics of the miniature cone 13

Figure 2-3: Schematics of the large triaxal cell used as a calibration chamber (a: top Plate, b: Acrylic Cell, c: Bottom Plate, d: PWP measurement Connection, e: Specimen Drain Lines Connected to Pressure Lines, f: Specimen Drain Lines Connected to Atmosphere, g: Bottom Cap, h: Top Cap, i: Specimen, j: Bushing) 14

Figure 2-4: Bottom plate 15

Figure 2-5: (a) Top plate assembly and (b) Top specimen cap 16

Figure 2-6: Particle size distribution of Ottawa sand (Barco 71) used in this study 18

Figure 2-7: Containers used to get plug samples and check the density uniformity 21

Figure 2-8 : Back-pressure, pore water and cell fluid pressure measurements 25

Figure 2-9: Internal and external load cell readings. 26

Figure 2-10: Forces measured by the external load cell (Q_c: compressive force on the cone tip; Q_s: friction along the cone sleeve; f_{v1}: frictional resistance of the wiper ring within the top cap; f_w: weight of the cone assembly; f_{v2}: frictional resistance of the wiper ring used to seal the top platen; f_E: external load cell reading) 28

Figure 2-11: Cone penetration resistances mobilized in Test No. 1: (a) q_c, (b) f_s, and (c) R_f 30

Figure 2-12: Cone penetration resistances mobilized in Test No. 2: (a) q_c, (b) f_s, and (c) R_f 31

Figure 2-13: Cone penetration resistances mobilized in Test No. 3: (a) q_c, (b) f_s, and (c) R_f. 32

Figure 2-14: Cone penetration resistances mobilized in Test No. 4: (a) q_c, (b) f_s, and (c) R_f 33

Figure 2-15: Cone penetration resistances mobilized in Test No. 5: (a) q_c, (b) f_s, and (c) R_f 34

Figure 2-16: Cone penetration resistances mobilized in Test No. 6: (a) q_c, (b) f_s, and (c) R_f 35

Figure 2-17: Cone penetration resistances mobilized in Test No. 7: (a) q_c, (b) f_s, and (c) R_f 36

Figure 2-18: Cone penetration resistances mobilized in Test No. 8: (a) q_c, (b) f_s, and (c) R_f 37

Figure 2-19: Cone penetration resistances mobilized in Test No. 9: (a) q_c, (b) f_s, and (c) R_f 38

Figure 2-20: Cone penetration resistances mobilized in Test No. 10: (a) q_c, (b) f_s, and (c) R_f 39

Figure 2-21: Cone penetration resistances mobilized in Test No. 11: (a) q_c, (b) f_s, and (c) R_f 40

Figure 2-22: Cone penetration resistances mobilized in Test No. 12: (a) q_c, (b) f_s, and (c) R_f 41

Figure 2-23: Cone penetration resistances mobilized in Test No. 13: (a) q_c, (b) f_s, and (c) R_f 42

Figure 2-24: Cone penetration resistances mobilized in Test No. 14: (a) q_c, (b) f_s, and (c) R_f 43

Figure 2-25: Cone penetration resistances mobilized in Test No. 15: (a) q_c, (b) f_s, and (c) R_f 44

Figure 2-26: Cone penetration resistances mobilized in Test No. 16: (a) q_c, (b) f_s, and (c) R_f 45

Figure 2-27: Cone penetration resistances mobilized in Test No. 17: (a) q_c, (b) f_s, and (c) R_f 46

Figure 2-28: Cone penetration resistances mobilized in Test No. 18: (a) q_c, (b) f_s, and (c) R_f 47

Figure 2-29: Cone penetration resistances mobilized in Test No. 19: (a) q_c, (b) f_s, and (c) R_f 48

Figure 2-30: Repeatability of penetration resistances for Test No. 7: (a) q_c, (b) f_s 133

Figure 2-31 : Correction factor for calibration chamber size and boundary conditions (Been et al. 1987) 52

Figure 2-32: Effect of cone penetration rate on: (a) q_c, and (b) f_s in samples with D_{rc} = 11% at p'_c = 200 kPa (Test No. 3.) 55

Figure 2-33: Comparison of the Coefficient of Normalization using different methods with data from tests No 11-19 (Numbers next to the data points show the Test. No.)..... 60

Figure 2-34: Cone tip resistance versus effective mean stress for tests No 11-19. (Numbers next to the data points show the Test. No.)..... 61

Figure 2-35: Sleeve friction versus effective mean stress for tests No 11-19. (Numbers next to the data points show the Test. No.)..... 62

Figure 2-36: Cone tip resistance versus consolidated relative density for tests No. 4 to 11. (Numbers next to the data points show the Test. No.)..... 63

Figure 2-37: Sleeve friction versus consolidated relative density for tests No. 4 to 11. (Numbers next to the data points show the Test. No.)..... 63

Figure 2-38: Comparison of normalized cone tip resistances of this study with those of Harman (1976) based on ψ_{cs}. (* Note that the state parameters were calculated based on the critical state parameters reported by Omar (2013) for Barco 71) 66

Figure 2-39: Comparison of CPT data of this study with soil type boundaries of Eslami and Fellenius (1997) 67

Figure 2-40: Comparison of CPT data of this study with soil identification zones of Mayne (2006) 68

Figure 2-41: Comparison of CPT data of this study with soil identification zones of Robertson (1990) 69

Figure 2-42: Comparison of CPT data of this study with soil type zones of Schneider et al. (2008) 70

Figure 3-1: Definition of state parameter, ψ_{cs} 84

Figure 3-2: Comparison of yield strength ratios and corrected CPT tip resistance for liquefaction flow failures (Olson 2001) 86

Figure 3-3: Comparison of $s_u(liq)/\sigma'_{vo}$ and corrected CPT tip resistance from the back-analyses of liquefaction flow failures (Olson 2001) 89

Figure 3-4: Stress-Strain response of undrained triaxial compression test on a sample with D_{rc} = 29% at p'_c = 100 kPa (Test No. 10.) 92

Figure 3-5: Effective stress path of undrained triaxial compression test on a sample with D_{rc} = 29% at p'_c = 100 kPa (Test No. 10.) 92

Figure 3-6: Approximate boundary between dilative and contractive soil response from Robertson (2010) and data from current study 95

Figure 3-7: Boundary between dilative and contractive soil response from Fear and Robertson (1995) and data from current study 96

Figure 3-8: Comparison of yield strength ratios predicted by Olson (2001) and the data from the current study (Numbers next to the data points show the CPT Test. No. , * Note that the s_u values for Test No. 1,2,3 and 4 were reported by Omar (2013)) 98

Figure 3-9: Comparison of the yield strength ratios predicted by Sadrekarimi (2014) and the data from the current study (Numbers next to the data points show the CPT Test. No, *Note that the s_u values for Test No.1,2,3 and 4 were reported by Omar (2013)) 99

Figure 3-10: Comparison of the liquefied strength ratios predicted by Olson (2001) and the data from the current study (Numbers next to the data points show the CPT Test. No, *Note that the s_u values for Test No.1,2,3 and 4 were reported by Omar (2013)) 101

Figure 3-11: Comparison of the liquefied strength ratios predicted by Sadrekarimi (2014) and the data from the current study (Numbers next to the data points show the CPT Test. No, *Note that the s_u values for Test No.1,2,3 and 4 were reported by Omar (2013)) .. 101

Figure 3-12: Comparison of the dry unit weights predicted by Mayne (2007) and the data from the current study (Numbers next to the data points show the Test. No.) 103

Figure 3-13: Comparison of the saturated unit weights predicted by Mayne et al. (2010) and the data from the current study..... 104

Figure 3-14: Relationship between soil relative density, cone tip resistance and mean effective stress (Baldi et al. 1986)..... 105

Figure 3-15: Comparison of the relative density predicted by Baldi et al. (1986) and the data from the current study (Numbers next to the data points show the tested relative density in percentage). 106

Figure 3-16: Comparison of the relative density predicted by Schemertmann (1976) and the data from the current study (Numbers next to the data points show the tested relative density in percentage). 107

Figure 3-17: Comparison of the relative density predicted by Baldi et al. (1986), Schemertmann (1976) and the data from the current study (Number next to the data points is the Test. No.) 108

Figure 3-18: Comparison of σ'_c from cavity expansion analysis (Russell and Khalili 2002) and equation (3-17) for CCT on Ticino sand. 113

Figure 3-19: Q_c versus ψ_{cs} for Barco 71 from current study (* Note that the state parameters were calculated based on the critical state parameters reported by Omar (2013) for Barco 71) 114

Figure B-1: Prepared sample (a) before and (b) after assembling the cell 130

Figure B-2: Miniature cone calibration chamber assembly 131

Figure C-1: Stress-Strain response of undrained triaxial compression test on a sample with D_{rc} = 20% at p'_c = 450 kPa (CPT Test No. 17.) 139

Figure C-2: Stress-Strain response of undrained triaxial compression test on a sample with D_{rc} = 20% at p'_c = 300 kPa (CPT Test No. 16.) 139

List of Symbols

$\mathbf{A_c}$	Cone base area
$\mathbf{a_n}$	Net area ratio
B	Skempton's pore pressure coefficient
BC	Chamber boundary condition
c	Tip normalization exponent
$\mathbf{C_f}$	Coefficient of friction normalization for overburden stress
Cq	Coefficient of tip normalization for overburden stress
$\mathbf{d_c}$	Cone diameter (mm)
$\mathbf{D_c}$	Chamber diameter (mm)
$\mathbf{D_r}$	Relative density (%)
$\mathbf{D_{ri}}$	Initial relative density (%)
$\mathbf{D_{rc}}$	Consolidated relative density (%)
$\mathbf{D_{50}}$	Particle size corresponding to 50% finer soil-size particles, (mm)
$\mathbf{e_i}$	Initial void ratio
$\mathbf{e_c}$	Consolidated void ratio
$\mathbf{e_{max}}$	Maximum void ratio
$\mathbf{e_{min}}$	Minimum void ratio
FC	Fine contents
$\mathbf{F_R}$	Normalized friction ratio
$\mathbf{f_s}$	Sleeve friction resistance (kPa)
$\mathbf{f_w}$	Weight of the cone assembly (N)
$\mathbf{f_{v1}}$	Friction offered by the V-ring placed in the top cap (N)
$\mathbf{f_{v2}}$	Friction offered by the V-ring used to seal the top platen (N)
$\mathbf{f_E}$	External load cell measurement (N)
$\mathbf{G_s}$	Specific gravity
$\mathbf{K_0}$	Coefficient of lateral earth pressure at rest
n	Tip normalization exponent
p	Total mean stress (kPa)
$\mathbf{p'}$	Effective mean stress (kPa)
$\mathbf{p'_c}$	Target consolidation effective mean stress (kPa)

P_a	Atmospheric pressure
q_c	Cone tip resistance (MPa)
q_t	Corrected total cone resistance
q_E	Corrected cone resistance
$q_{c,1}$	Normalized cone resistance
$q_{c,cc}$	Cone tip resistance observed in the calibration chamber tests
$q_{c,field}$	Cone tip resistance expected to be measured in the field for the same sand with the same relative density and the same in-situ stresses as in the chamber.
Q	Normalized cone resistance
Q_s	Force on friction sleeve (N)
Q_c	Force at the cone tip (N)
Q_t	Normalized cone resistance
R_d	Chamber to cone diameter ratio
R_f	Friction ratio, (%)
s	Friction normalization exponent
u_2	Porewater pressure generated immediately behind the cone tip
λ	Slope of critical state line
Γ	Critical state void ratio at p′=1 kPa
ψ_{cs}	State parameter
σ_{v0}	Total overburden stresses (kPa)
σ'_{v0}	Effective overburden stresses (kPa)
σ'_c	Cavity expansion pressure
σ_{atm}	Atmospheric pressure
s_u**(liq)**	Post-liquefaction strength
s_u**(yield)**	Yield shear strength
G/G_{max}	Shear modulus ratio
RMSD	Root mean square deviation
R^2	least square regression coefficient
K_c	Anisotrpic consolidation coefficient
I_B	Brittleness index

γ_d	Dry unit weight
γ_t	Total unit weight
B_q	Normalized pore water pressure

List of Appendices

Appendix A: Sensor Calibration Factors 127

Appendix B: Photographs of the Developed Device and Experiments 127

Appendix C: Repeatability Test Results 132

Appendix D: Triaxial Compression Test Results 138

Chapter 1

1 Introduction

1.1 Background

Difficulties in obtaining undisturbed samples in cohessionless soils have encouraged geotechnical engineers to depend largely on field tests to obtain soil properties. An alternative mean to the conventional exploration methods is using direct-push technologies. The cone penetration test (CPT) has been used for a long time as an in-situ test for site investigation and geotechnical design. Mechanical in-situ tests, including CPT, do not measure any particular property of the soil directly. Basically, cone penetration tests provide engineers with the load response to an imposed deformation through the applied compressive forces on the cone and the friction sleeve along the penetration depth, as well as the pore pressure generated at the tip of the cone. Therefore, extensive research has been conducted to provide correlations between CPT data and soil properties or soil stratigraphy using either laboratory calibration chamber experiments such as Been et al. (1987), Been and Jefferies (1992), Konrad (1997), comparison with in-situ field tests such as (Olson and Stark 2003), or numerical analyses including cavity expansion, finite element, or discrete element analyses (Shuttle and Jefferies 1998; Russell and Khalili 2002, Ahmadi et al. 2005, Butlanska et al. 2014).

CPT calibration chamber experiments provide reliable values for the interpretation of CPT measurements, as the entire procedure (including sample preparation and consolidation) is conducted in the laboratory and can be readily monitored and controlled. Therefore data obtained from the calibration chamber experiments can be reliably used to derive correlations between soil mechanical properties and tip or friction resistance.

Calibration chamber studies can be carried out at a wide range of densities and confining stress levels, however each experiment typically provides a single set of cone tip resistance and sleeve friction corresponding to the prepared sample density and stress

state. Therefore, a large number of calibration chamber tests are often required to derive reliable correlations between soil's mechanical properties and state (or relative density) with cone tip resistance, and sleeve friction. This becomes further difficult for preparing loose sand samples in large chamber tests. Therefore, several studies have conducted tests with miniature cones and calibration chamber devices and investigated different properties of soils (e.g., Abedin 1995; Kokusho et al. 2003; Löfroth 2008).

1.2 Research Objectives

This study presents the development and operation of a new miniature cone penetrometer at Western University in order to test loose sands susceptible to liquefaction and enhance the scientific understanding of liquefaction phenomenon. To achieve this goal, the following specific objectives are devised.

1. To develop and calibrate a new miniature cone penetrometer at Western University using a triaxial load frame.

2. To perform a number of tests on loose sands using the developed apparatus and evaluate the application of the apparatus in terms of repeatability, penetration rate, boundary condition effect, scale effect, particle crushing, overburden stress normalization and verification of the measurements.

3. To evaluate a CPT-based liquefaction analysis including liquefaction susceptibility, triggering and post-liquefaction strength analysis using the laboratory miniature CPT experiments performed in the current study.

1.3 Scope and Outline of Current Study

This thesis has been prepared in "Integrated-Article" format. It is organized into 4 chapters. A brief description of the following three chapters is as follow:

Chapter 2 is the development and calibration of a new miniature cone penetrometer at Western University using a triaxial load frame. A series of tests are performed and the results are presented and discussed in terms of the repeatability of the developed apparatus, the effect of penetration rate, boundary condition effect, scale effect, particle crushing, overburden stress normalization and verification of the measurements.

Chapter 3 evaluates some available procedures to perform a CPT-based liquefaction analysis including liquefaction susceptibility, triggering and post-liquefaction strength analysis using the laboratory miniature CPT experiments performed in the current study. Some of the well-stablished equations to estimate soil properties, including soil unit weight, relative density and state parameter, required for liquefaction studies are also evaluated using the laboratory miniature CPT experiments performed in the current study.

Chapter 4 is a summary of the research work carried out and the conclusions drawn.

1.4 The Original Contributions

The original contributions of this thesis are:

1. A new miniature cone penetrometer was developed and calibrated using a triaxial load frame. A series of tests were performed and the results were presented and discussed in terms of the effect of penetration rate, boundary condition effect, scale effect, particle crushing, overburden stress normalization and verification of the measurements (Chapter 2).

2. Some of the available procedures to perform a CPT-based liquefaction analysis including liquefaction susceptibility, triggering and post-liquefaction strength analysis and some of the well-stablished equations to estimate soil properties, including soil unit weight, relative density and state parameter, required for liquefaction studies were reviewed and evaluated using the laboratory miniature CPT experiments performed in the current study (Chapter 3).

References

Abedin, M. Z., (1995), "The characterization of unsaturated soil behaviour from penetrometer performance and the critical state concept," PhD Thesis, The University of Newcastle upon Tyne, UK.

Ahmadi, M. M., Byrne, P. M., Campanella R. G., (2005) "Cone tip resistance in sand: modeling, verification, and applications" *Canadian Geotechnical Journal*, 42(4): 977-993, 10.1139/t05-030

Been, K. Jefferies, M.B. Crooks, J.H.A. and Rothenburg, L., (1987), "The cone penetration test in sands, part 2. General inference of state," *Géotechnique*, 37(3): 285–299.

Been, K. and Jefferies, M.G., (1992), "Towards systematic CPT interpretation," *In Proceedings of the Wroth Symposium*, Oxford, U.K. pp. 44–55.

Butlanska, J., Arroyo M., Gens, A., O'Sullivan, C., (2014) "Multi-scale analysis of cone penetration test (CPT) in a virtual calibration chamber" *Canadian Geotechnical Journal*, 51(1): 51-66, 10.1139/cgj-2012-0476.

Kokusho, T. Murahata, K. Hushikida, T. and Ito, N., (2003), "Introduction of miniature cone in triaxial apparatus and correlation with liquefaction strength," *Proc., Annual Convention of Japan Society of Civil Engineers (JSCE),* Tokyo, Japan, III-96, Japan Society for Civil Engineers, 191–192 (in Japanese).

Konrad, J. M., (1997), "In situ sand state from CPT: evaluation of a unifed approach at two CANLEX sites," *Canadian Geotechnical Journal*, 1: 120-130.

Löfroth, H., (2008), "Undrained shear strength in clay slopes – Influence of stress conditions, A model and field test study," Phd Thesis. Chalmers University of Technology. Gothenburg.

Olson, S. M., and Stark, T. D. (2003). "Yield strength ratio and liquefaction analysis of slopes and embankments." *J. Geotech. Geoenviron. Eng.*, 129_8_, 727–737.

Russell, A. R. and Khalili, N., (2002), "Drained cavity expansion in sands exhibiting particle crushing," *International Journal for Numerical and Analytical Methods in Geomechanics*, 26: 323–340 (DOI: 10.1002/nag.203)

Shuttle, D. and Jefferies, M., (1998), "Dimensionless and unbiased CPT interpretation in sand," *International Journal for Numerical and Analytical Methods in Geomechanics*, 22: 351-391.

Chapter 2

2 Development of a Miniature Cone Penetrometer

2.1 Introduction

Difficulties in obtaining undisturbed samples in cohessionless soils have encouraged geotechnical engineers to depend largely on field tests to obtain soil properties. An alternative mean to the conventional exploration methods is using direct-push technologies. The cone penetration test (CPT) has been used for a long time as an in-situ test for site investigation and geotechnical design. The first cone penetrometers were developed in 1932 in the Netherlands (Lunne et al. 1997). Nowadays, the cone penetration test is one of the most widely used in-situ field testing and exploration methods due to its continuous data measurement with excellent repeatability and accuracy at relatively low cost (Jefferies and Been 2006). CPT tests are performed to obtain data about: (1) stratigraphy of the soil deposit, (2) soil type identification, (3) mechanical soil characteristics (relative density, friction angle, OCR), (4) drivability and bearing capacity of piles, and (5) liquefaction potential of saturated cohesionless soils.

CPT is conducted by pushing a cone on the end of series of rods, into the ground at a controlled rate of 2 cm/s. The standard CPT cone has a 60˚ apex angle and a diameter of 35.7 mm which corresponds to a projected cone base area of 10 cm^2. The standard cone has a friction sleeve with a surface area of 150 cm^2 for the 10 cm^2 cone (ASTM D5778- 2012).

Mechanical in-situ tests, including CPT, do not measure any particular property of the soil directly. Basically, cone penetration tests provide engineers with the load response to an imposed deformation through the applied compressive forces on the cone and the friction sleeve along the penetration depth, as well as the pore pressure generated at the

---

A version of this chapter will be submitted to the ASTM geotechnical testing journal.

tip of the cone. Measured forces are converted to cone tip resistance, sleeve friction resistance and friction ratio using the equations suggested by ASTM D5778-2012, which will be discussed later.

Therefore, extensive research has been conducted to provide correlations between CPT data and soil properties or soil stratigraphy using either laboratory calibration chamber experiments (e.g., Been et al. 1987; Been and Jefferies 1992; Konrad 1997), comparison with in-situ field tests (Olson and Stark 2003; Idriss and Boulanger 2007), or numerical analyses such as cavity expansion, finite element, or discrete element analyses (Shuttle and Jefferies 1998; Russell and Khalili 2002, Ahmadi et al. 2005, Butlanska et al. 2014).

A calibration chamber is essentially a large circular soil specimen, in which soil is deposited at a known density and compressed from the external boundaries. A CPT cone is then inserted into the soil sample to provide the tip and sleeve (along the sides of the cone) resistances under given boundary conditions. CPT calibration chamber experiments provide reliable values for the interpretation of CPT measurements, as the entire procedure (including sample preparation and consolidation) is conducted in the laboratory and can be readily monitored and controlled.

Therefore data obtained from the calibration chamber experiments can be reliably used to derive correlations between soil mechanical properties and tip or friction resistance.

Calibration chamber studies can be carried out at a wide range of densities and confining stress levels, however each experiment typically provides a single set of cone tip resistance and sleeve friction corresponding to the prepared sample density and stress state. Therefore, a large number of calibration chamber tests are often required to derive reliable correlations between soil's mechanical properties and state (or relative density) with cone tip resistance, and sleeve friction. This becomes further difficult for preparing loose sand samples in large chamber tests. After a brief description of the previous miniature CPT calibration chamber laboratory tests, this study presents the development and operation of a new miniature cone penetrometer at Western University which is used for testing loose sands for liquefaction studies.

2.1.1 Previous Miniature Cone Penetration Tests

Carrying out controlled CPT calibration chamber tests with a standard cone (with a diameter of 35.7 mm) requires a very large diameter (typically more than 1.2 m) calibration chamber (Ghionna and Jamiolkowski, 1991; Harman, 1976; Baldi et al, 1986; Huntsman, 1985; Lhuer, 1976). Such an experiment can be expensive and time consuming, as sample preparation would involve placing a large volume of sand (over 2 tons) in the testing chamber at a uniformly controlled density. This could become even much more difficult when dealing with loose samples. Therefore, several studies have conducted tests with miniature cones and calibration chamber devices (e.g., Abedin 1995; Kokusho et al. 2003; Löfroth 2008).

For example, Abedin (1995) designed and developed a miniature CPT by adapting an existing triaxial compression cell which could accommodate specimens of 100 mm in diameter and 185 mm in height. A miniature cone with a 10 mm diameter was driven into the soil at a rate of 0.012 mm/s under controlled boundary stresses. The CPT data were later used to predict the density of unsaturated loam soils (Abedin and Hettiaratchi 2002).

Kokusho et al. (2003) modified a cyclic triaxial apparatus to measure the resistance of specimens to the penetration of a 6 mm diameter cone prior to cyclic loading. The miniature cone was attached to the base of the cell and protruded up into a 100 mm in diameter specimen at a rate of 2 mm/s.

At the University of Rhode Island, Franzen (2006) designed and built a calibration chamber for miniature cone penetration testing by modifying a large-scale triaxial cell which could accommodate specimens of 450 mm in diameter and 560 mm tall. A 1 cm^2 cone manufactured by FUGRO Engineers B.V., Netherlands was used in the experiments. The miniature cone was mounted on the base of the chamber and pushed upwards into the sample using a hydraulic piston at an average rate of 20 mm/s. This testing system has been used for studying the CPT resistance of Rhode Island silt soils and developing empirical correlations with relative density (Jasinski 2008; Seher 2008).

A modified triaxial cell (with a specimen diameter of 91 mm) was also used by Kumar and Raju (2008) for conducting miniature CPT with a cone diameter of 19.5 mm. As described by Kumar and Raju (2008), vertical stress was applied by a compressed rubber chamber from the bottom of the specimen while the cone was driven at a fixed rate of 0.021 mm/second. Although this devices was used by Kumar and Raju (2008) to investigate the CPT resistance of loose sands and silty sands (with 15% and 25% fines contents), the large boundary effects associated with the relatively small chamber size makes it questionable to compare their CPT measurements with standard field tests.

More recently, Pournaghiazar et al. (2011) developed a calibration chamber to conduct laboratory-controlled cone penetration tests in unsaturated soils. The chamber developed by Pournaghiazar et al. (2011) could accommodate cylindrical specimens with a height of 840 mm and diameter of 460 mm. They conducted cone penetration tests using a 16 mm diameter electrical cone which was driven into soil at a constant rate of 20 mm/s. They found that the correlations developed for saturated (or dry) soils are not applicable to unsaturated soils and new correlations that take suction into account should be developed for unsaturated soils.

Table 2-1 summarizes the geometrical characteristics and the boundary conditions of the aforementioned CPT calibration chamber studies. Different boundary conditions (BC) will be discussed in section 2.5.1.

Table 2-1: Geometrical characteristics and boundary conditions of past miniature calibration chamber CPT tests

Institution	Sample Dimensions (mm)		Cone diameter (mm)	Penetration rate (mm/s)	Chamber to cone diameter ratio	BC[1]	Measured data	Material tested	Reference
	Diameter	Height							
Indian Institute of Science	91	133.5	19.5	0.021	4.67	BC3	q_c	Clean sand/ Silty sand	Kumar and Raju (2008)
Chuo University	100	200	6	2	16.67	Not reported	q_c	NA	Kokusho et al. (2003)
University of Rhode Island	450	560	11.3	20	39.82	BC1	q_c/f_s	NA	Franzen (2006)
The University of Newcastle	100	185	10	0.012	10	BC1	q_c	Sandy clay loam	Abedin (1995)
The University of New South Wales	460	840	16	20	52.5	BC1	q_c/f_s	Sydney sand	Pournaghiazar et al. (2011)

[1] BC1: Both side and bottom restraints are constant stress, BC2: Both side and bottom restraints are constant volume
BC3: Side restrain is constant volume and bottom restraint is constant stress, BC4: Side restrain is constant stress and bottom restraint is constant volume

2.2 Design and Construction of the New Miniature CPT Device

The calibration chamber designed and used in this study was adapted from a large triaxial compression testing cell having the ability to accommodate 150 mm diameter by 195 mm height specimens. The top acrylic cap, sitting on the surface of the specimen, was drilled to accommodate the shaft of a miniature cone with 6 mm diameter. Triaxial pressure pumps were used to saturate and consolidate the sample and then a uniaxial loading frame pushed the cone into the specimen while the cone tip resistance and side friction were measured. A schematic of the designed calibration chamber and the triaxial apparatus are illustrated in Figure 2-1.

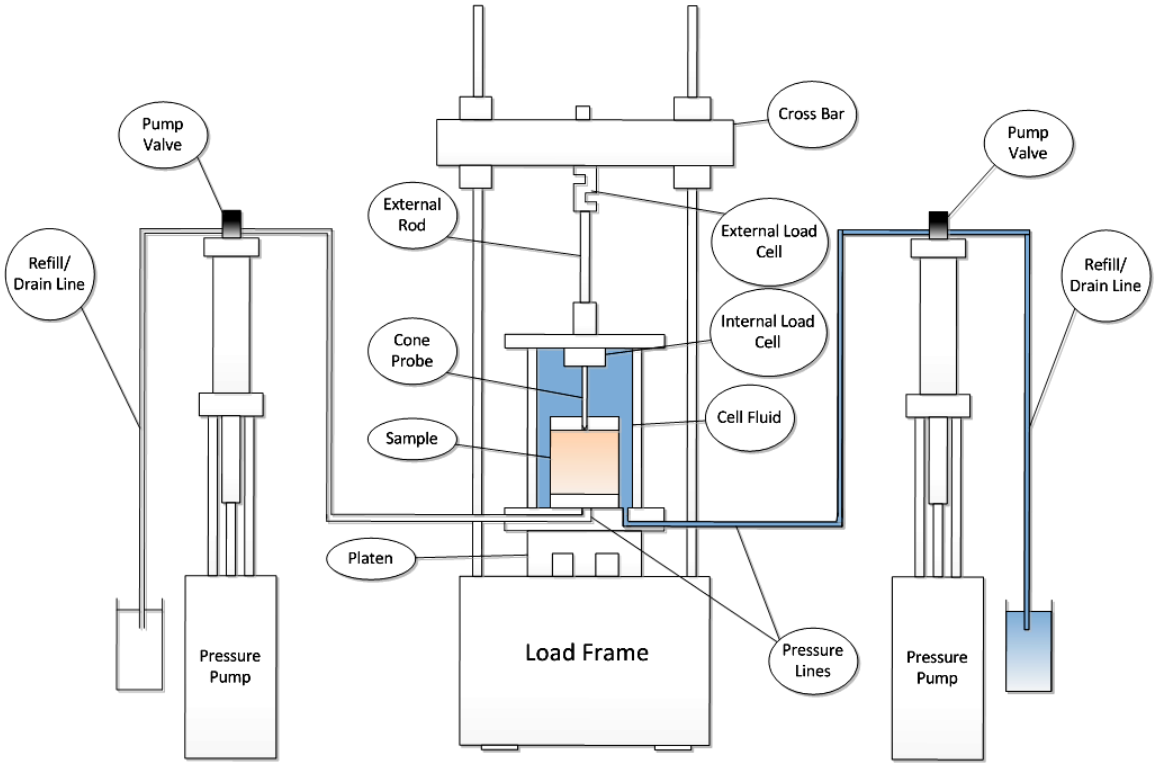

Figure 2-1: Calibration chamber experiment setup

2.2.1 Miniature-cone

A 6 mm-diameter cone with an apex angle of 60 degrees and a net area ratio of $a_n = 0.75$ was used in the calibration chamber tests. The miniature cone designed in this study is a subtraction-type penetrometer in which the cone and sleeve both produce compressive forces on the load cells attached to each other in series. As illustrated in Figure 2-2, the cone tip resistance (Q_c) is directly measured by an internal load cell which is connected to the cone by a steel rod (b) passing through a hollow steel shaft (a). An external load cell (shown in Figure. 2-1), attached to the external shaft (h), measures the total cone tip resistance as well as the friction on the outside surface of the hollow shaft (a), Q_s. Therefore, sleeve friction is readily obtained from the subtraction of the load cells' measurements. The external load cell has a maximum capacity of 8896 N which was calibrated using dead loads prior to testing. The internal load cell, with the maximum capacity of 889.6 N which was used to measure the cone tip resistance, was also calibrated using dead weights. Sample pore water pressure including any excess pore pressure developed during cone penetration (u_2) is measured at the cone's shoulder just above its tip similar to a type 2 cone (Lunne et al. 1997). The pore pressure is transferred through the hollow shaft to an outlet tube (d) and measured by a pressure sensor. A plastic collar with small notches (c) was used above the cone tip to allow the passage of water while blocking sand particles. A rubber ring (e) was inserted between the plastic collar and the cone tip in order to ensure that the stresses at the cone tip were effectively transferred to the internal load cell (without being partially carried by the hollow shaft) while also inhibiting the sand particles from jamming and wedging in between the cone tip and the plastic collar. As the housing for the internal load cell was not sealed, another rubber ring was placed below the internal load call (at location f in Figure. 2-2) and pressed against the housing to seal and separate sample pore pressure from the cell fluid pressure.

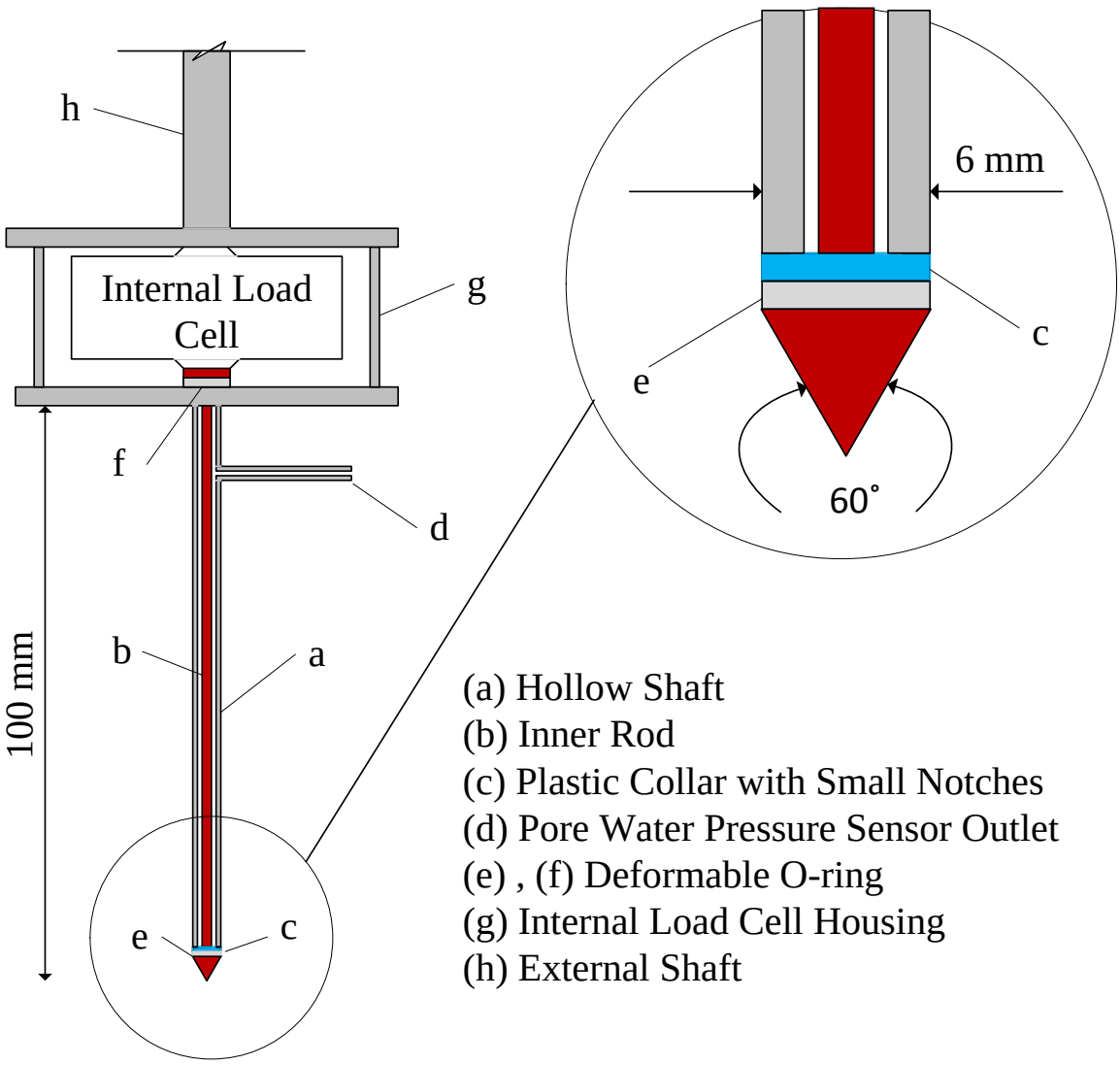

Figure 2-2: Schematics of the miniature cone

2.2.2 Miniature-cone Calibration Chamber

A large triaxial cell was adopted as a calibration chamber to incorporate the miniature cone. The largest possible cell that could be accommodated by the load frame was designed in this study and constructed by the university machine shop. The cell assembly consists of top and bottom steel plates and an acrylic cell as shown in Figure 2-3.

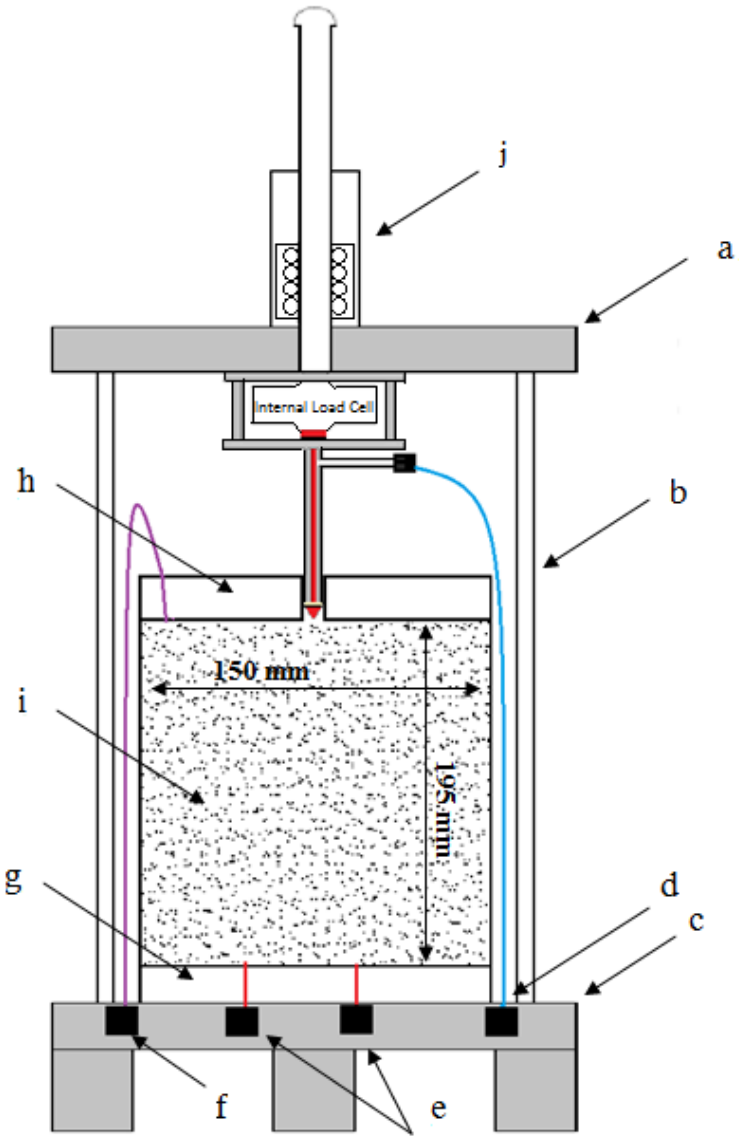

Figure 2-3: Schematics of the large triaxal cell used as a calibration chamber (a: top Plate, b: Acrylic Cell, c: Bottom Plate, d: PWP measurement Connection, e: Specimen Drain Lines Connected to Pressure Lines, f: Specimen Drain Lines Connected to Atmosphere, g: Bottom Cap, h: Top Cap, i: Specimen, j: Bushing)

As shown in Figure 2-4, the bottom plate consists of five connections to control the cell pressure, sample pore pressure, drainage and the measurement of cone tip pore water pressure. A 150-mm diameter disc-shaped acrylic cap was attached to the bottom plate on

which the specimen is built. The bottom cap includes a 5 cm in diameter porous stone embedded at its center which connects the specimen to the drainage lines and a pressure pump through which water is percolated into the specimen.

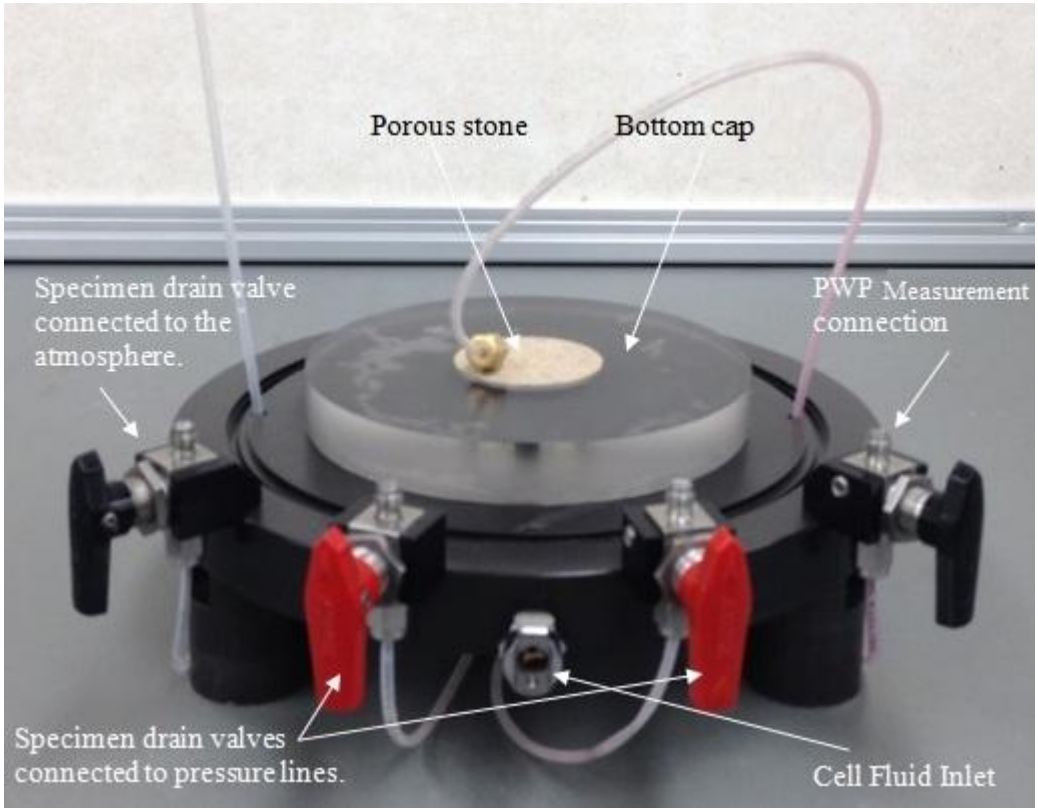

Figure 2-4: bottom plate

A latex rubber membrane, held in place by two O-rings and a hose clamp around the bottom cap, surrounded the specimen and therefore creating a flexible boundary. The latex membrane was 0.635 mm thick with sufficient length to enclose full height of the specimen as well as the top and bottom caps. A special specimen cap was designed for the top of the sample which had a central hole for the passage of the miniature cone probe. One of the main challenges was sealing the contact between the cone probe and the top cap to maintain the differential pressure between cell fluid and sample pore water. This was achieved by using a V-ring around the hole with its notch towards the cell fluid. The greater pressure of the cell fluid expanded the V-ring, pressing it against the cone

and the inner circumference of the hole and therefore providing an effective seal. Two porous stones were placed at the sides of the hole to connect the specimen to the drainage line. These two porous stones were connected to each other through a small hole, and connected to the drainage line. Figure 2-5 shows the top plate (of the cell) and specimen cap with the cone assembly.

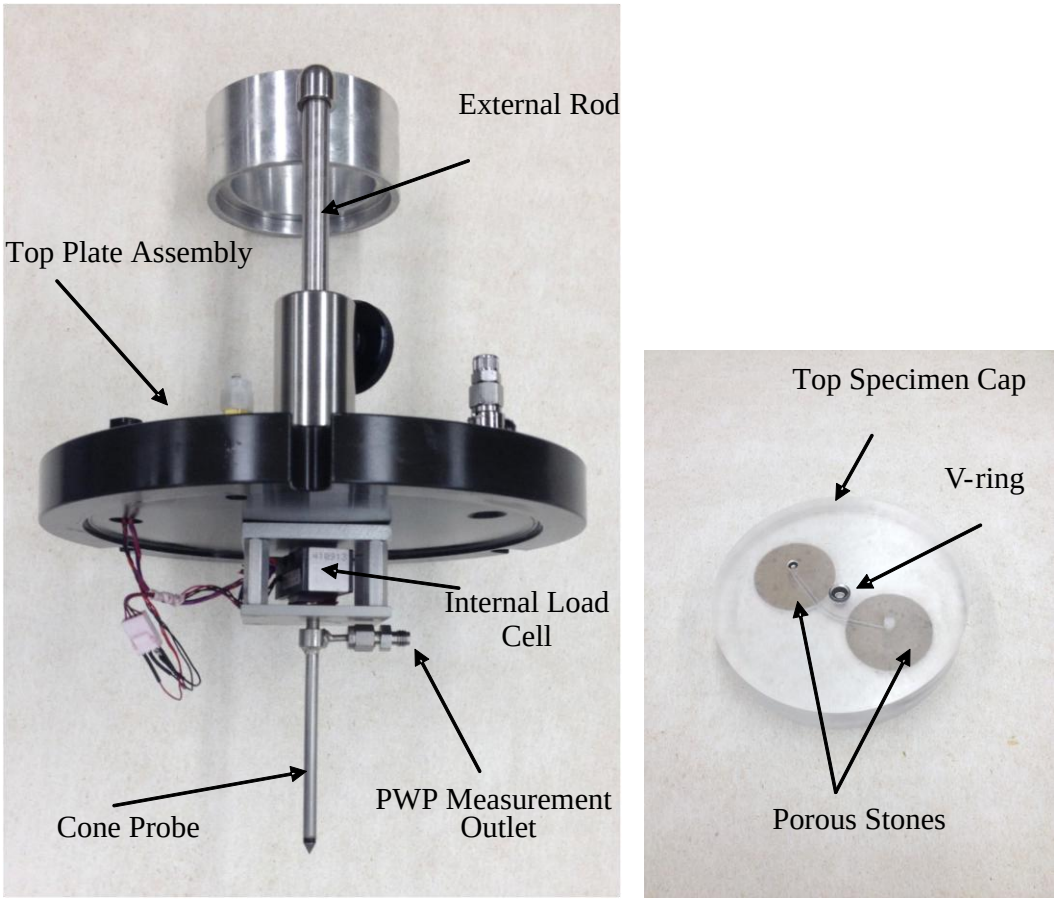

(a) (b)

Figure 2-5: (a) Top plate assembly and (b) Top specimen cap

Similar to the bottom specimen cap, two O-rings and a hose clamp were also used to keep the membrane around the top cap and provide sealing of the sample. A 360 mm high acrylic cylinder with an inner diameter of 190 mm was then placed around sample.

2.2.3 Cone Driving Frame and Pressure Pumps

As illustrated in Figure 2-1, a GEOTAC Sigma-1 loading frame manufactured by Trautwein Soil Testing Equipment Company, Texas (USA), was used to push the penetrometer into the specimen. The load frame has an encoder which records its travel distance automatically. The encoder was calibrated with a high resolution LVDT (see Appendix A). The maximum travel rate of the load frame is 0.423 mm/s which has been used in this study for cone penetration. Details of the calibrations are presented in Appendix A. Two flow pumps were used to apply the cell and back pressures. Pore water, back and cell pressures were measured using three pressure sensors with the maximum capacity of 1379 kPa. Manufacture calibrations were verified and confirmed for these sensors by connecting them to a single pressure pump and cross-checking their measurements at several pressures. A total number of 42 trial tests have been performed in order to solve the leakage of cell fluid into the sample and calibrate the device.

2.2.4 Tested Material

Reconstituted specimens of fine Ottawa sand were prepared and tested in this experimental program. The Ottawa sand used in this study (with a commercial name of "Barco 71") is composed of white-colored quartz particles with rounded to sub-angular particle shapes. Figure 2-6 presents the particle size distribution of this sand and table 2-2 presents the physical characteristics of the Barco 71. Maximum (e_{max}) and minimum (e_{min}) void ratios were determined in accordance to the ASTM D4254-2006 and ASTM D4253-2006 standard codes respectively.

Table 2-2: Physical characteristics of Barco 71 sand

Property	**value**
Specific Gravity, G_s	2.65
Fines Content, FC	< 1%
D_{50} (mm)	0.193
Maximum Void Ratio, e_{max}	0.82
Minimum Void Ratio, e_{min}	0.49

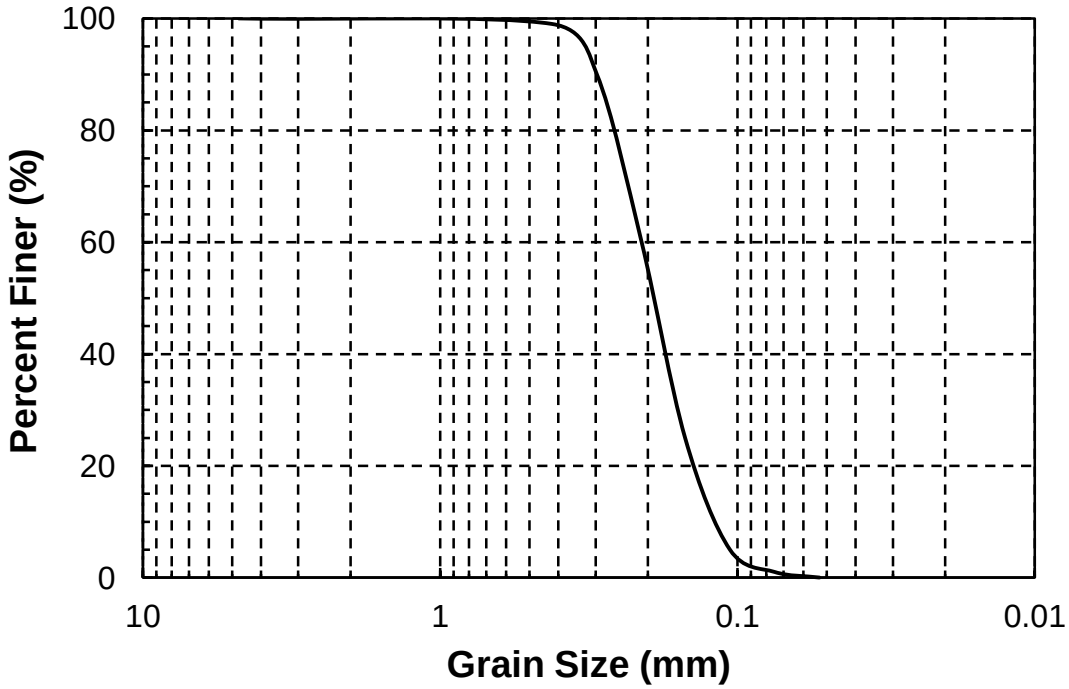

Figure 2-6: Particle size distribution of Ottawa sand (Barco 71) used in this study

2.2.5 Specimen Preparation

The laboratory tests on sands are performed on reconstituted specimens mostly prepared using pluviation and moist compaction methods. Moist tamping is preferred to be used in the laboratory as it is relatively easy and particle segregation can be minimized (Chen 2000) while achieving a more isotropic structure than air pluviated specimens (Yang 2005).

The miniature CPT device developed in this study is designed to test loose sands and the following experiments, performed to calibrate and verify the designed device, are conducted on loose specimens for liquefaction studies which cannot be prepared using the pluviation methods. Therefore, moist tamping method was used to prepare loose enough soil specimens to liquefy. Moreover, moist tamping has been used so that the suction developed during the sample preparation helps the sample to maintain itself and remain stable before filling the cell and applying confining pressure. Note that, pluviation

methods cannot be used as suction cannot be applied to the sample prior to filling the cell which is because of the hole inside the top specimen cap through which cone probe penetrates into the sample. The hole is sealed once the top platen is placed on top of the acrylic cell so that the cone is touching the soil surface.

All specimens were prepared with an initial moisture content of 5% which is adequate for moist tamping (Park 1999). Specimen preparation was done using the undercompaction method suggested by Ladd (1987) to account for the increased density of the lower layers by compaction of the upper layer soils to produce homogenous specimens. In this technique, the lower layers are initially compacted to a looser than the final desired density by predetermined amounts therefore the final density of each layer is equal to the target density. The difference in density between successive layers is defined as the undercompaction ratio (Ladd 1978).

Required amount of soil for each layer was calculated using an undercompaction ratio of 10% and thoroughly mixed with 5% moisture. Soil was placed into the steel mold and tamped in 13 layers of 1.5 cm thick. The height of each layer was checked after tamping using a ruler. Specimens prepared for this study were cylindrical in shape with a diameter of 150 mm and 195 mm height according to the miniature cone testing assembly requirements. The diameter and height of the samples were carefully measured at the end of the sample preparation to ensure the accuracy of the initial void ratio (e_i) and relative density (D_{ri}) determination of the sample.

As shown in Figure 2-1, the miniature cone assembly is connected to an external load cell through a steel rod. The rod travels outside of the specimen chamber through a double-bearing bushing system. The height of the acrylic cylinder was selected to accommodate the heights of the specimen, cone and the internal load cell housing. Therefore, after preparing the specimen and assembling the cell, the tip of the cone would rest on the top surface of the specimen before cone penetration.

Subsequent to specimen preparation, the acrylic cylinder was filled with silicone oil, through which the specimen was subjected to isotropic confining pressure.

2.2.6 Specimen Uniformity

Having a uniform sample in terms of density is an essential factor which contributes to the accuracy of results when testing reconstituted specimens. This has been investigated by many researchers (e.g Mulilis et al. 1977; Jang 1997; Park 1999; Chen 2000; Yang 2002). The density distribution over the height of specimen has been argued to be nonuniform in moist tamped samples (Mitchell et al. 1976). Undercompaction was developed to overcome this nonuniformity in the compaction method (Ladd, 1978). The uniformity of the specimens prepared in this study was evaluated as below.

During the preliminary trials, specimens were made in 5 layers using an undercompaction ratio of 15% which produced non-uniform specimens as the measured cone tip resistance with depth was not uniform and indicated a stepwise change among layers. Using a series of trial and error tests, the number of layers was increased to 13 and the undercompaction ratio was reduced to 10% to prepare more uniform specimens with relatively uniform cone resistance profiles as an indication of reasonable specimen uniformity.

Specimen uniformity was also evaluated by taking plug samples. Local density of the specimens where measured at the top, middle and bottom of the specimen by placing three aluminum containers at different levels within the specimen while pouring the soil inside the specimen chamber and tamping layers in a circular pattern. After tamping the last layer, the containers were extracted by carefully excavating the specimen as shown in Figure 2-7. The top surfaces of the containers were leveled by scraping off the excessive soil from the top of the containers. The containers were then kept inside the oven for 24 hours and the mass of the dry soil in each container was measured. After removing the soil, the volume of a distilled and deaired water required to fill each container was measured and used to precisely calculate the volume of each container. Having the volume of each container and the mass of the dry soil, the void ratios of the specimen were calculated at corresponding elevations. A void ratio variation of about ±0.006 (corresponding to a relative density change of ±1.5%) was obtained from the top to the bottom of the specimen for an average relative density of 0%. The same test was repeated for the densest state of the soil tested with a relative density of 25%. In this test, a void

ratio variation of about ±0.003 (corresponding to a relative density change of ±0.9%) These variations of specimen void ratio is close to what Sivathayalan (1994) reported (a void ratio variation of 0.003 in a sample of loose Ottawa sand which was 125 mm in height) using freezing technique.

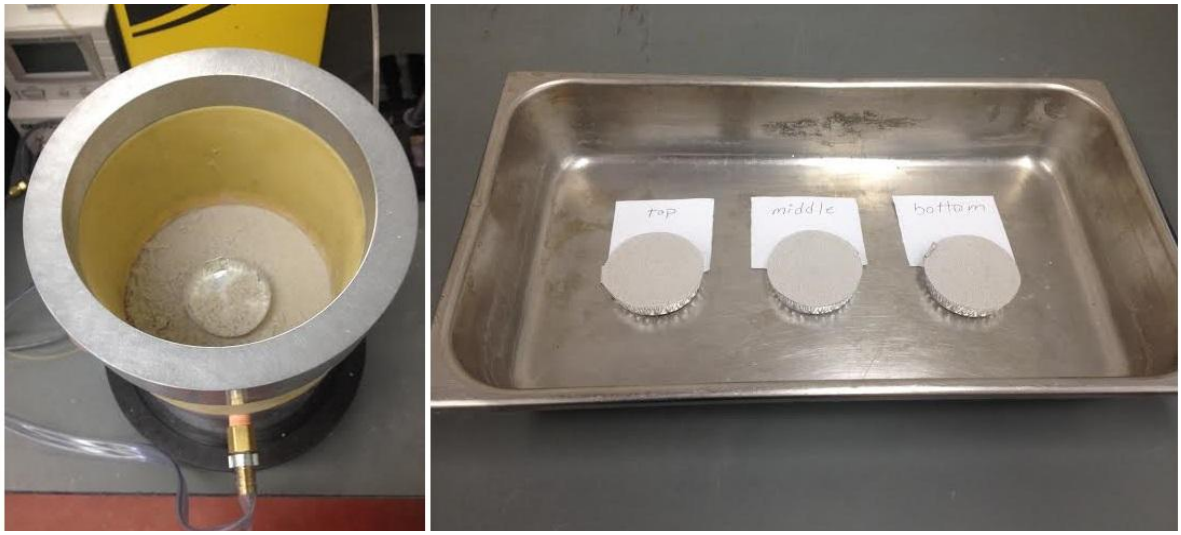

Figure 2-7: Containers used to get plug samples and check the density uniformity

2.2.7 Specimen Saturation and Consolidation

Specimens were saturated before consolidation up to a Skempton's (1954) pore pressure coefficient B, of higher than 0.96 in order to release the negative pore water pressure generated during sample preparation. Moreover, the change in void ratio of the sample can be measured precisely in a fully saturated sample by monitoring the pore pump volume change which has been done in this study. Sample saturation was achieved by flushing the soil specimen with CO_2 prior to inundation with water and the application of back-pressure. Cell volume change was carefully monitored to take into account any possible change in the volume of the specimen during saturation. In most of the tests the volume change during saturation was negligible as the effective stress was kept as low as 10 to15 kPa.

The effect of saturation on penetration resistances has been studied by many researchers. For example, Bellotti et al (1988) performed a few number of tests on dry and saturated samples and concluded that there is only a little influence of saturation on the measured penetration resistance. This confirmed the findings of Schmertmann (1976) reporting that there is a very small difference between the cone resistance measured for dry and nearly saturated Ottawa sand samples. Huang (1992) reported that penetration resistance was not affected significantly by saturation of the specimens provided that induced pore pressures were negligible. Bonita (2000) performed a comprehensive study on both dry and saturated samples in calibration chambers and reported that the static penetration resistance measured at the center of the sample in dry samples was approximately equal to that in saturated samples for static tests performed at similar stress and density conditions. Relying on the literature, the effect of saturation on penetration resistances is assumed to be negligible.

After specimen saturation, samples were isotropically consolidated to the target consolidation stress (p'_c) using the triaxial pressure pumps. Pore volume change during consolidation was measured to define the precise void ratio of the sample after consolidation (e_c) as well as consolidatied relative density (D_{rc}). The consolidation pressure was maintained for at least 30 minutes before pushing the cone in order to ensure excess pore pressure dissipation and reduce the amount of secondary compression during cone penetration. Figure 2-8 presents the normal compression line of Test No. 3.

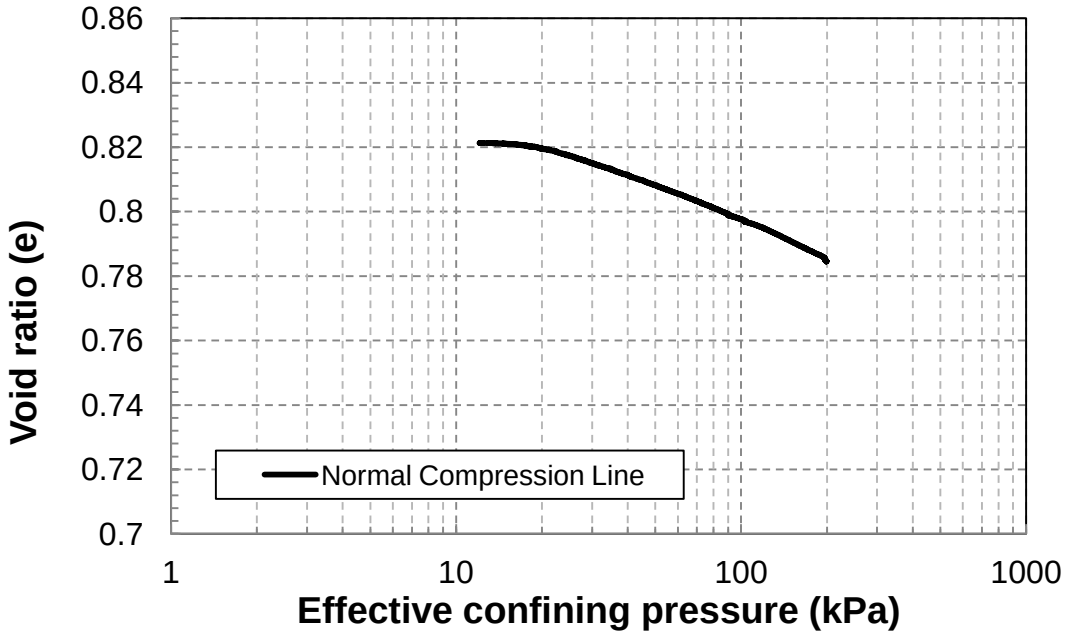

Figure 2-8 : Normal Compression Line of Test. No. 3.

2.2.8 Cone Penetration Testing

A computer controlled automatic loading and control system provided by Trautwein Soil Testing Equipment Company (Texas, Austin) was used to drive the cone into the specimen at a maximum rate of 0.423 mm/s up to a depth of 60 mm. The change in relative density during penetration was measured based on the pore water volume change measurements. It was found that the global void ratio of the sample slightly reduced by about 0.24% at the end of the penetration. Most likely, the soil around the cone was densified during penetration, but we could not measure the local void ratio variation with the current setup.

During loading, the pressure transducers and load cell readings were automatically recorded. Table 2-3 summarizes the density and stress characteristics of the miniature cone penetration tests conducted in this study. Note that the specimens were all prepared in a very loose state to provide a database on the behaviour of loose Ottawa sand for liquefaction studies.

Table 2-3: Summary of miniature CPT tests performed in this study

Test No	D_{ri} (%)	D_{rc} (%)	p'_c (kPa)	q_c (MPa)	f_s (kPa)	R_f (%)
1	0	17	500	10.29	42.64	0.41
2	0	13.5	300	6.55	51.31	0.78
3	0	11	200	5.45	45.41	0.83
4	0	8	100	4.08	38.69	0.95
5	5	10.5	100	4.01	32.85	0.82
6	7	12	100	4.22	41.29	0.98
7	9	16	100	4.42	62.83	1.42
8	17	23	100	4.97	55.66	1.12
9	20	25	100	5.07	50.59	1.00
10	25	29	100	5.62	65.70	1.17
11	15	20	100	4.80	48.25	1.01
12	17	20	45	2.41	16.05	0.67
13	16	20	75	4.23	31.49	0.74
14	13	19.6	150	6.10	46.85	0.77
15	9	20	200	7.06	48.29	0.68
16	7	19.4	300	10.40	49.71	0.48
17	5	20	450	13.54	64.88	0.48
18	3	19.4	600	13.74	67.74	0.49
19	0	19	700	13.99	74.26	0.53

2.3 Results

Figures 2-9 and 2-10 present typical results from test number 15 of Table 2-3. The isotropic compression line of the sand from previous trial CPT tests was used to estimate the D_{ri} (= 9%) required to produce D_{rc} = 20% at p'_c = 200 kPa.

As illustrated in Figure 2-9, as a result of drained penetration and the large hydraulic conductivity of Barco 71 sand, back-pressure and the pore water pressure measured adjacent to the cone tip (u_2) remained constant and equal during cone penetration, indicating no excess pore water pressure generation.

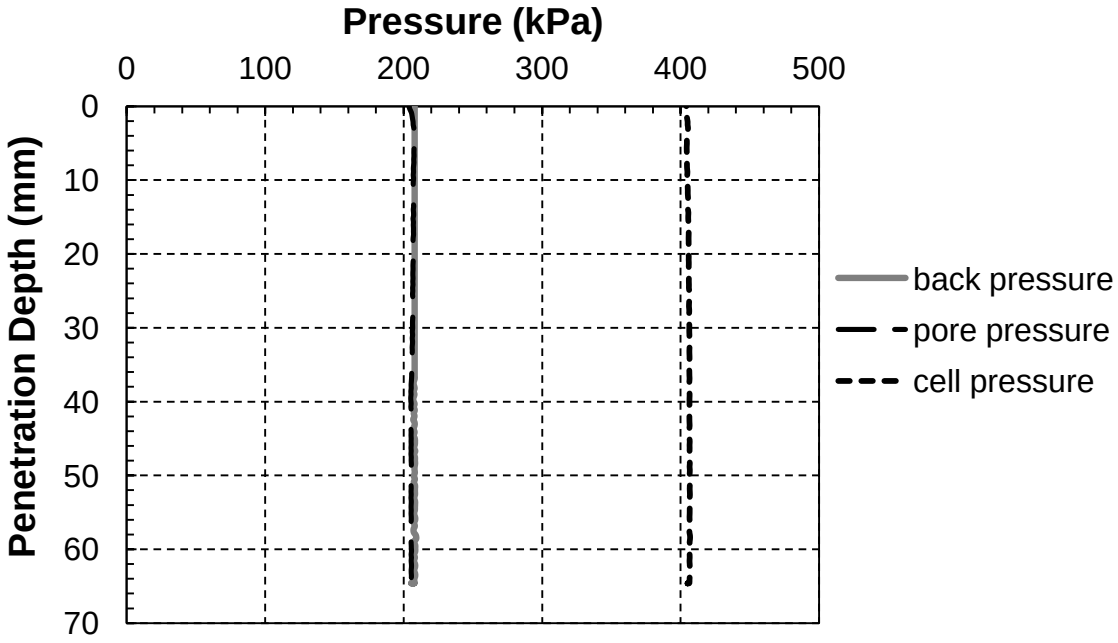

Figure 2-9 : Back-pressure, pore water and cell fluid pressure measurements
(Note: the back and pore responses overlap each other)

Figure 2-10 shows the internal and external load cell readings as well as the subtraction of the two sensor readings. In general, internal and external load cell readings with depth can be divided into four segments. At very small penetration depth (<1mm), the recorded load cell readings exhibit an abrupt increase. For the internal load cell, the initial increase is due to the mobilization of soil resistance against the penetration of the cone. However,

the external load cell registers a larger increase because of the additional friction produced by the V-ring surrounding the cone probe. During the first 6 mm of cone penetration, the load cell measurements are also affected by the top cap of the specimen and exhibit a local peak. For the relatively uniform specimens of this study, cone resistance measurements subsequently increase with penetration depth as soil resistance to the insertion of the cone is fully mobilized. After about 20 mm, both load cells measure more-or-less uniform and constant loads with depth. Note that because of the large distance of the cone to the bottom cap, the cone does not sense the lower boundary of the specimen as observed in some other laboratory CPT studies (Pournaghiazar et al. 2011) and numerical Analysis (Ahmadi 2005).

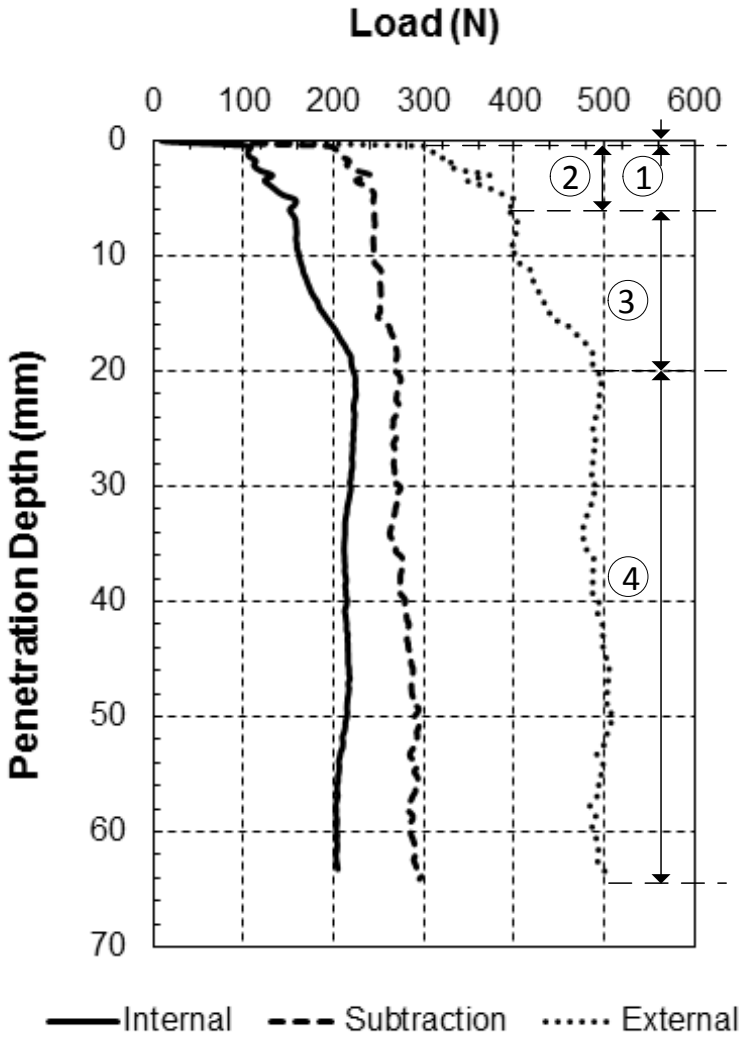

Figure 2-10: Internal and external load cell readings.

Sensor readings are converted to cone tip resistance, q_c (kPa), by dividing the load at the cone tip, Q_c (kN) from the internal load cell measurements by the base area of the cone, A_c (= 0.2827×10^{-4} m^2 for the miniature cone of this study). In the calculation of cone resistance, it is customary to account for the effect of excess pore water pressure applied on unequal cone areas. However, in the experiments of this study since there was no excess pore water pressure and both load cells were zeroed just before cone penetration, the effect of pore water pressure and u_2 on calculating cone tip resistance was effectively eliminated.

Average q_c is determined based on the average readings taken from depths of 20 to 60 mm where q_c reaches a more or less steady value. Sleeve frictional resistance is calculated using the following procedure. As illustrated in Figure 2-11, load cells were combined in a manner that an internal load cell measured the cone tip compressive force (Q_c), while an external load cell measured (f_E) the combined forces of Q_c, sleeve friction (Q_s), weight of the cone (f_w), and the friction provided by the wiper rings used to seal the top cap (f_{v1}) and the top platen (f_{v2}).

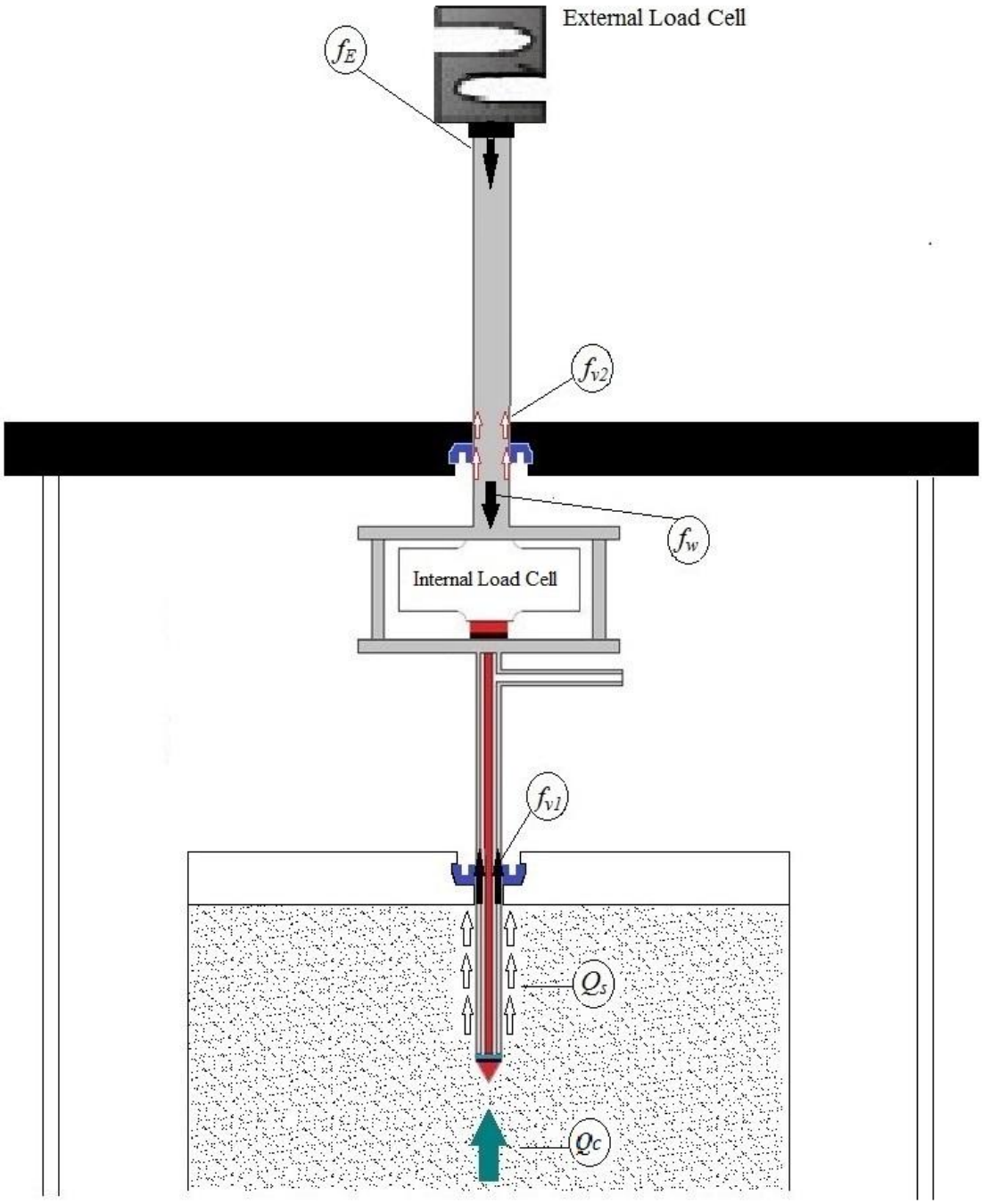

Figure 2-11: Forces measured by the external load cell (Q_c: compressive force on the cone tip; Q_s: friction along the cone sleeve; f_{v1}: frictional resistance of the wiper ring within the top cap; f_w: weight of the cone assembly; f_{v2}: frictional resistance of the wiper ring used to seal the top platen; f_E: external load cell reading)

The amount of friction applied by the V-ring increased with increasing the differential pressure between the cell fluid and sample pore water. Therefore, a calibration test was conducted on a hollow steel cylinder for each test condition to precisely measure the friction developed by the wiper rings. In these experiments, the external load cell measured the combined force of cone weight and the friction developed by two wiper rings ($f_{v1} + f_{v2} - f_w$). Therefore, sleeve friction (Q_s) was obtained by subtracting the load cells readings and taking into account the wiper rings friction (i.e. $Q_s = f_E - Q_c - [f_{v1} + f_{v2} - f_w]$). Sleeve frictional resistance, f_s (kPa) is subsequently calculated as Q_s (kN) divided by the external surface area of the hollow shaft (a) (see Fig. 2-10) inserted into the specimen. A friction ratio, R_f (%) is then obtained as $f_s/q_c \times 100$. These parameters (q_c, f_s, and R_f) are presented for some of the miniature CPT tests conducted in this study in Figures 2-12 to 2-30. Note that f_s and R_f are plotted for penetration depths of greater than 10 mm where the friction sleeve is effectively inserted into the soil away from the specimen's top cap. The average penetration resistances mobilized from a depth of 20 to 60 mm are also summarized in Table 2-3.

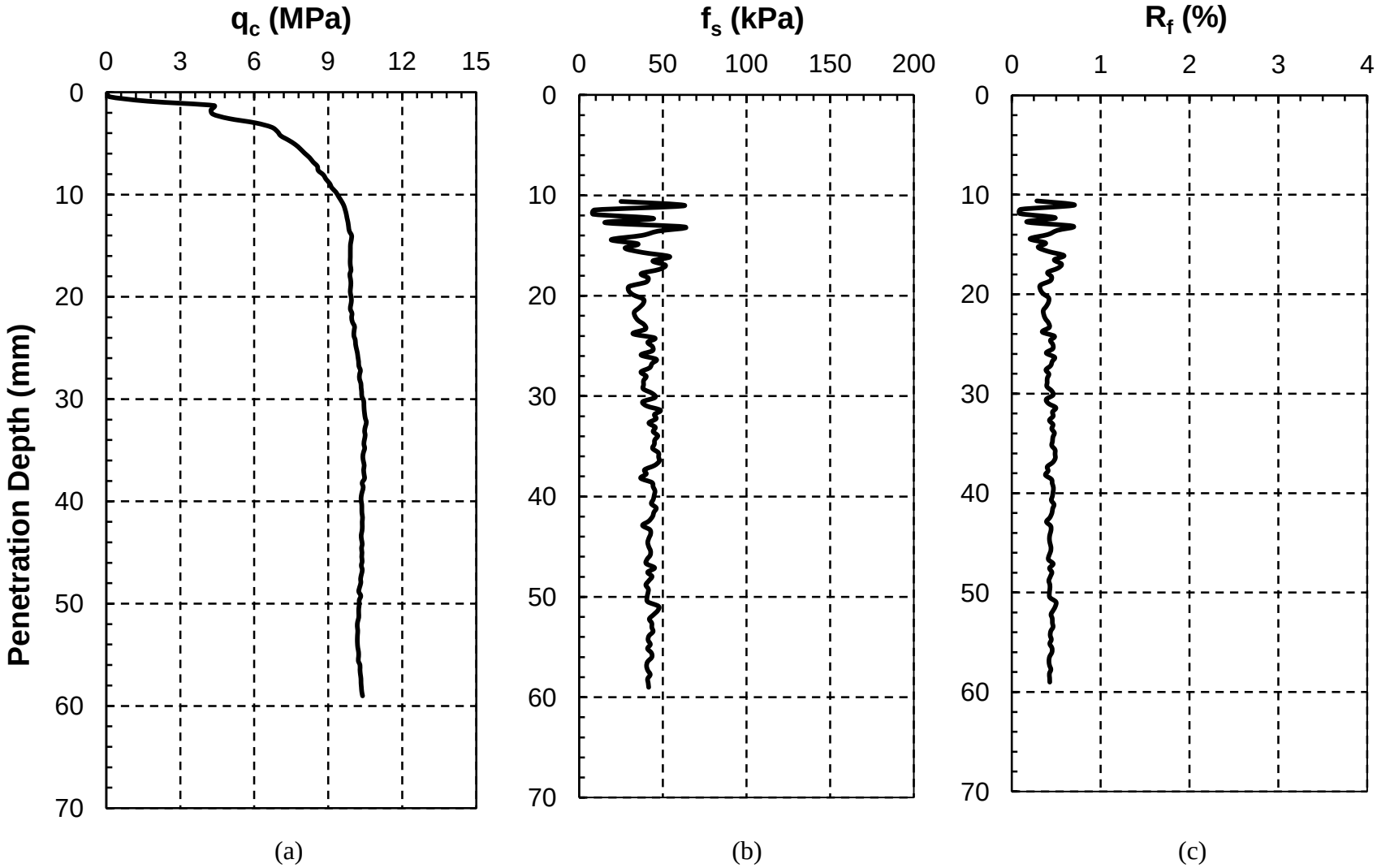

Figure 2-12: Cone penetration resistances mobilized in Test No. 1: (a) q_c, (b) f_s, and (c) R_f

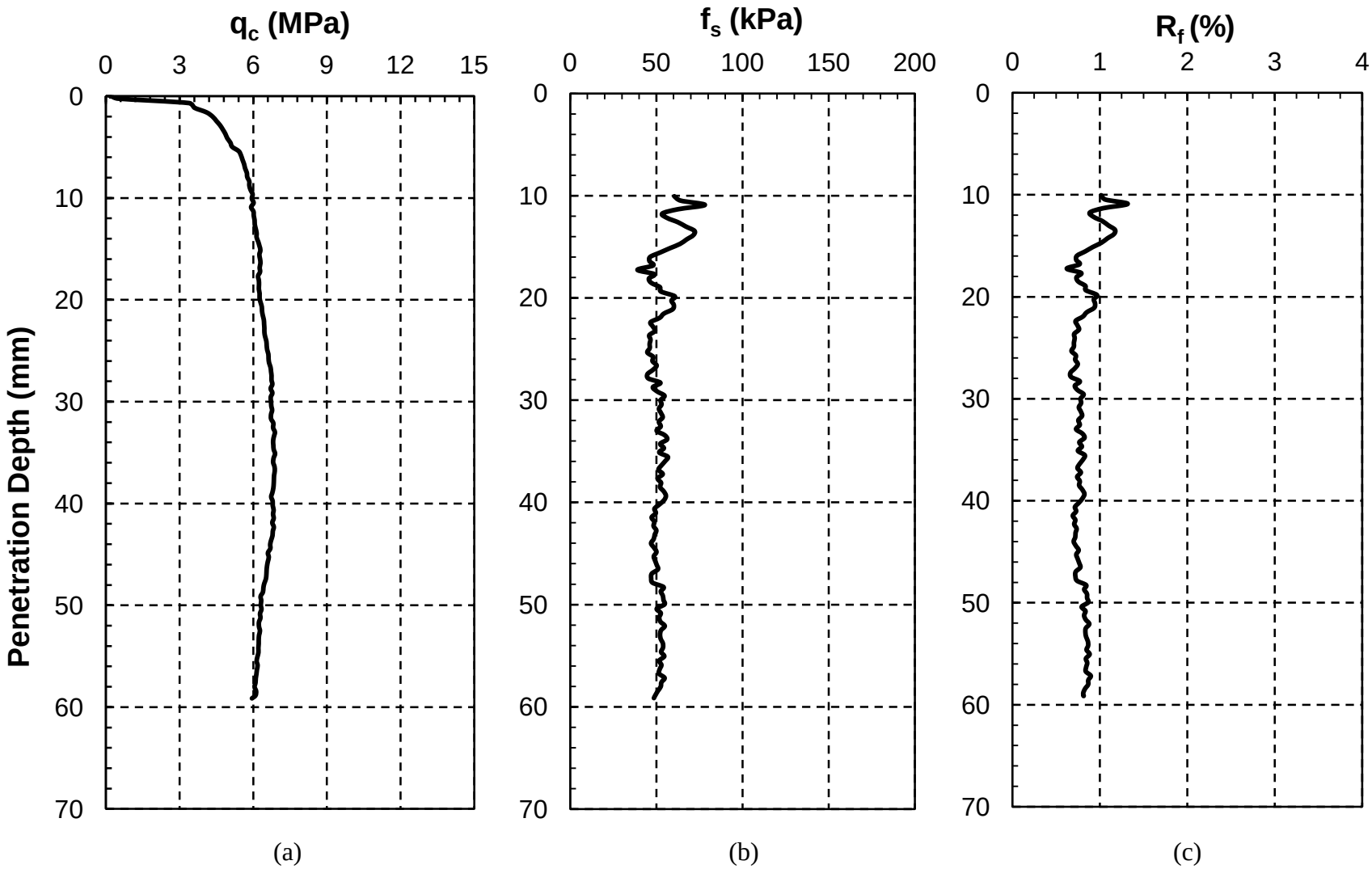

Figure 2-13: Cone penetration resistances mobilized in Test No. 2: (a) q_c, (b) f_s, and (c) R_f

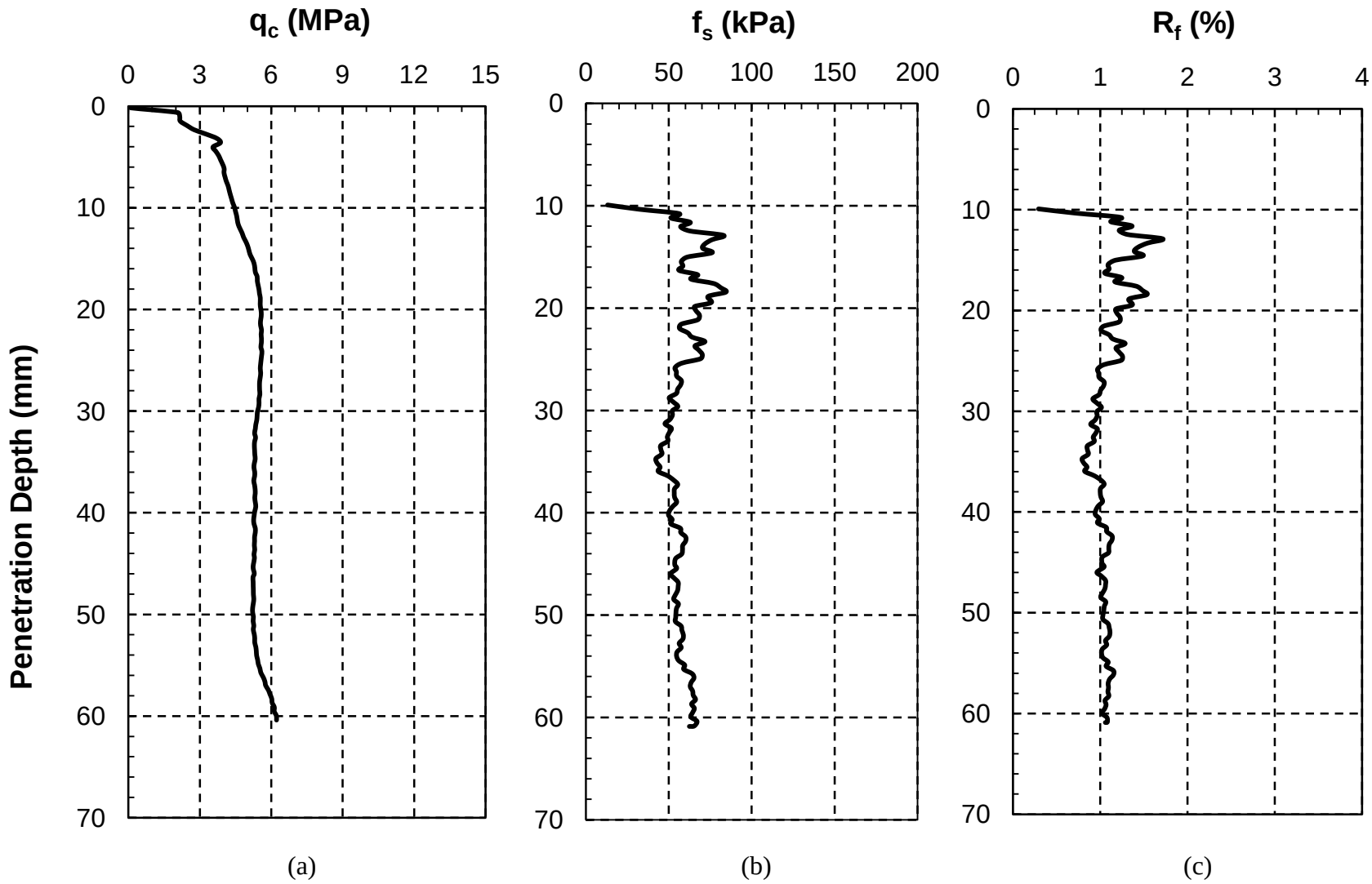

Figure 2-14: Cone penetration resistances mobilized in Test No. 3: (a) q_c, (b) f_s, and (c) R_f.

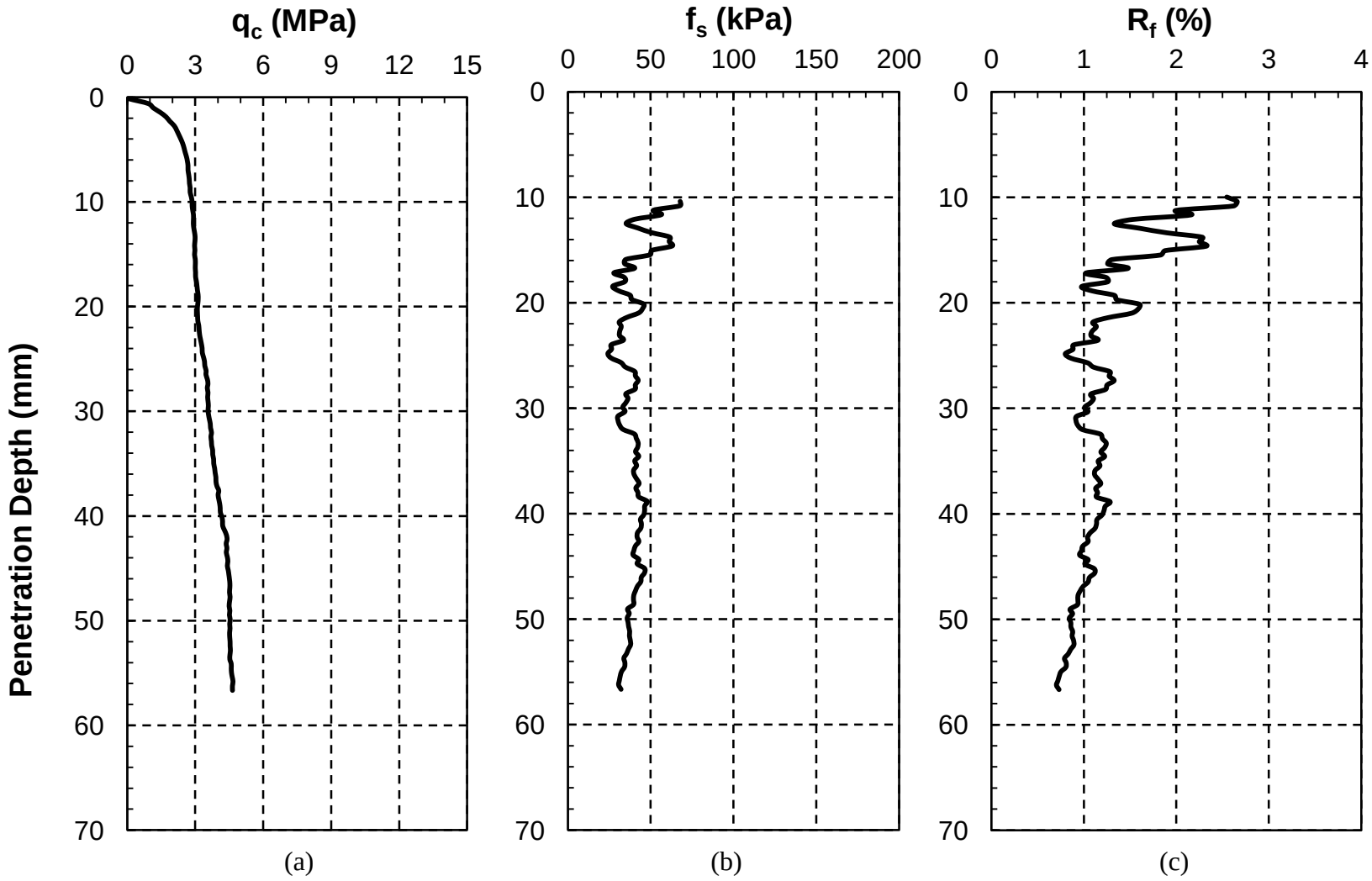

Figure 2-15: Cone penetration resistances mobilized in Test No. 4: (a) q_c, (b) f_s, and (c) R_f

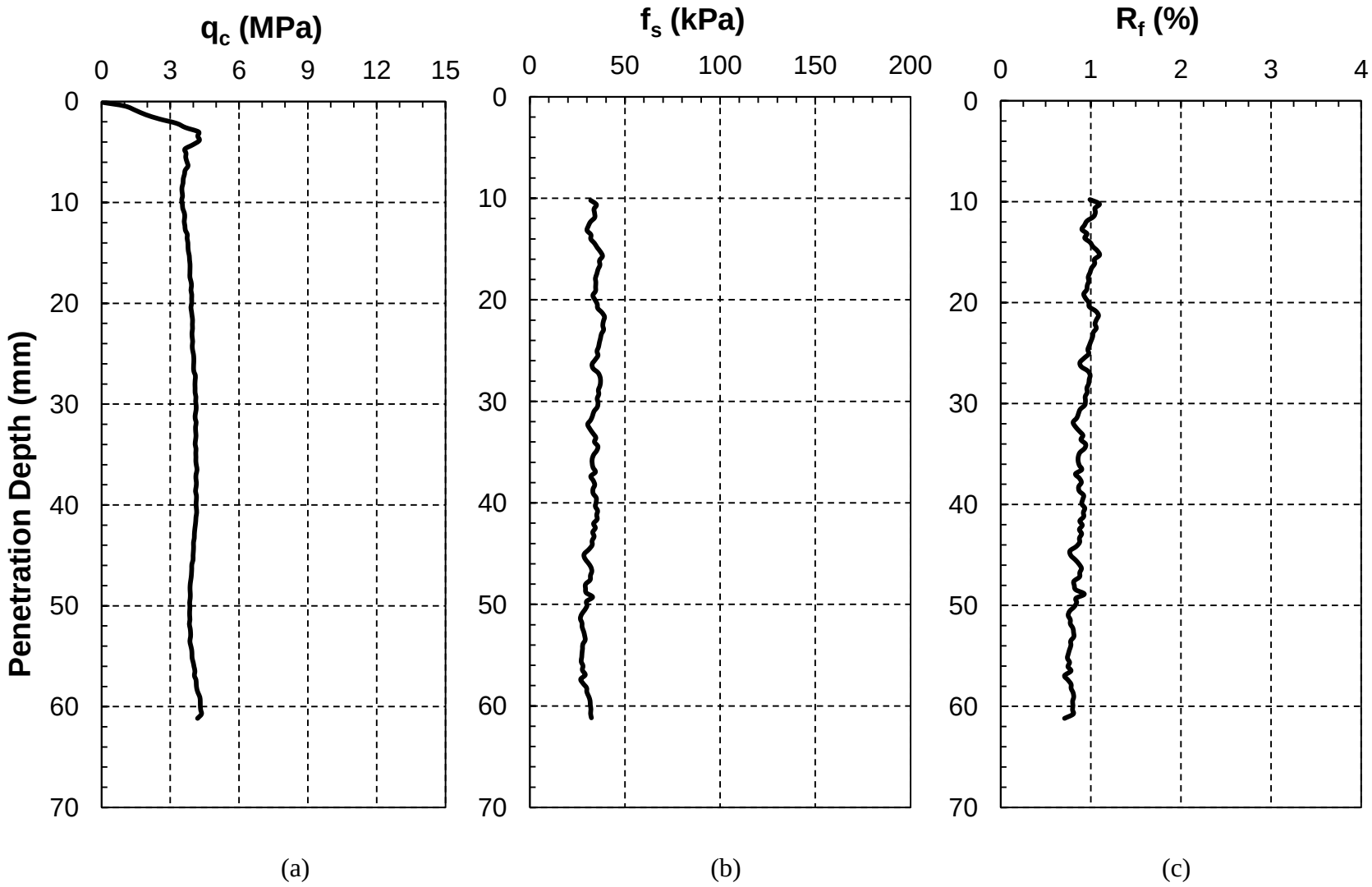

Figure 2-16: Cone penetration resistances mobilized in Test No. 5: (a) q_c, (b) f_s, and (c) R_f

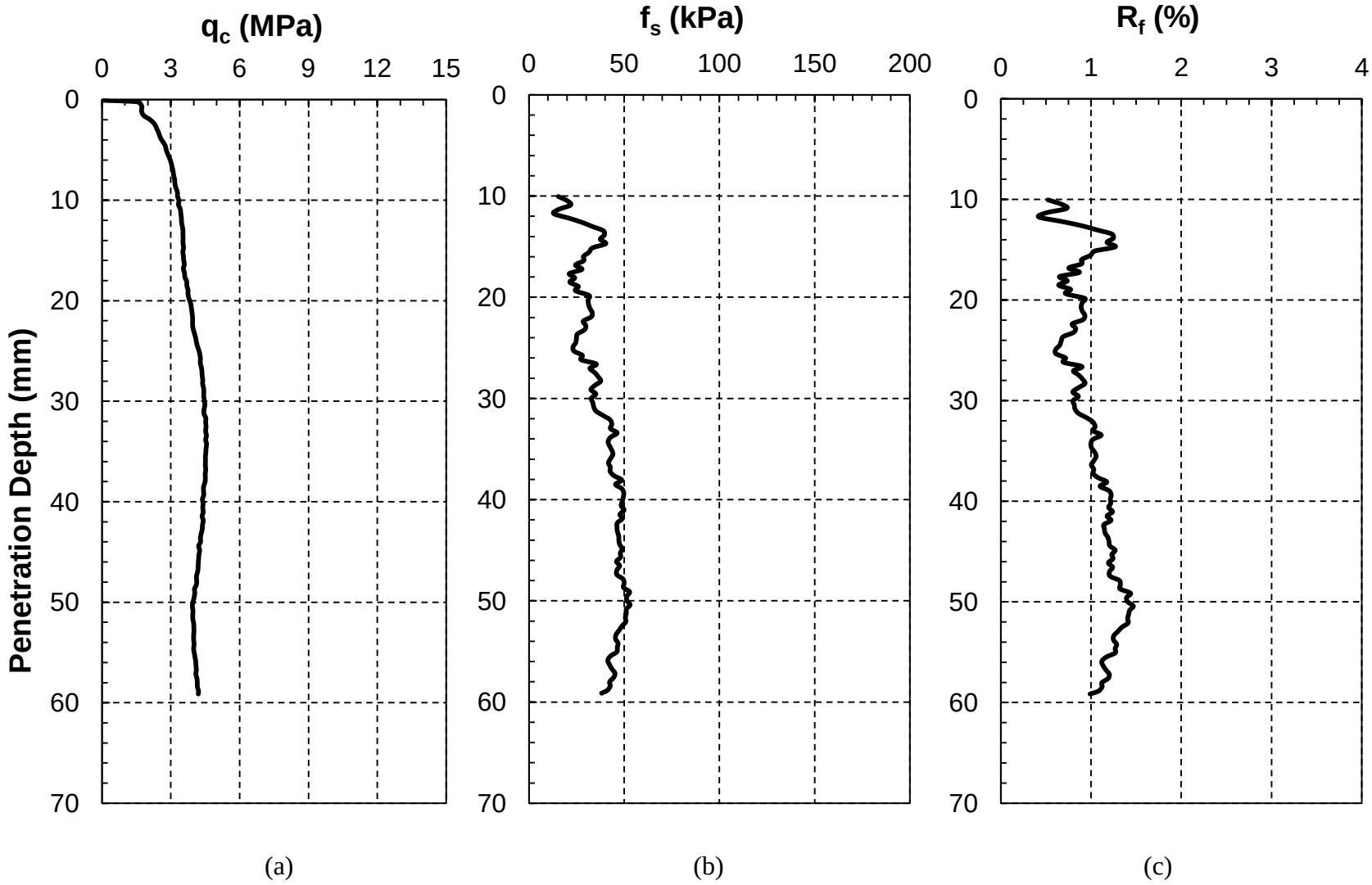

Figure 2-17: Cone penetration resistances mobilized in Test No. 6: (a) q_c, (b) f_s, and (c) R_f

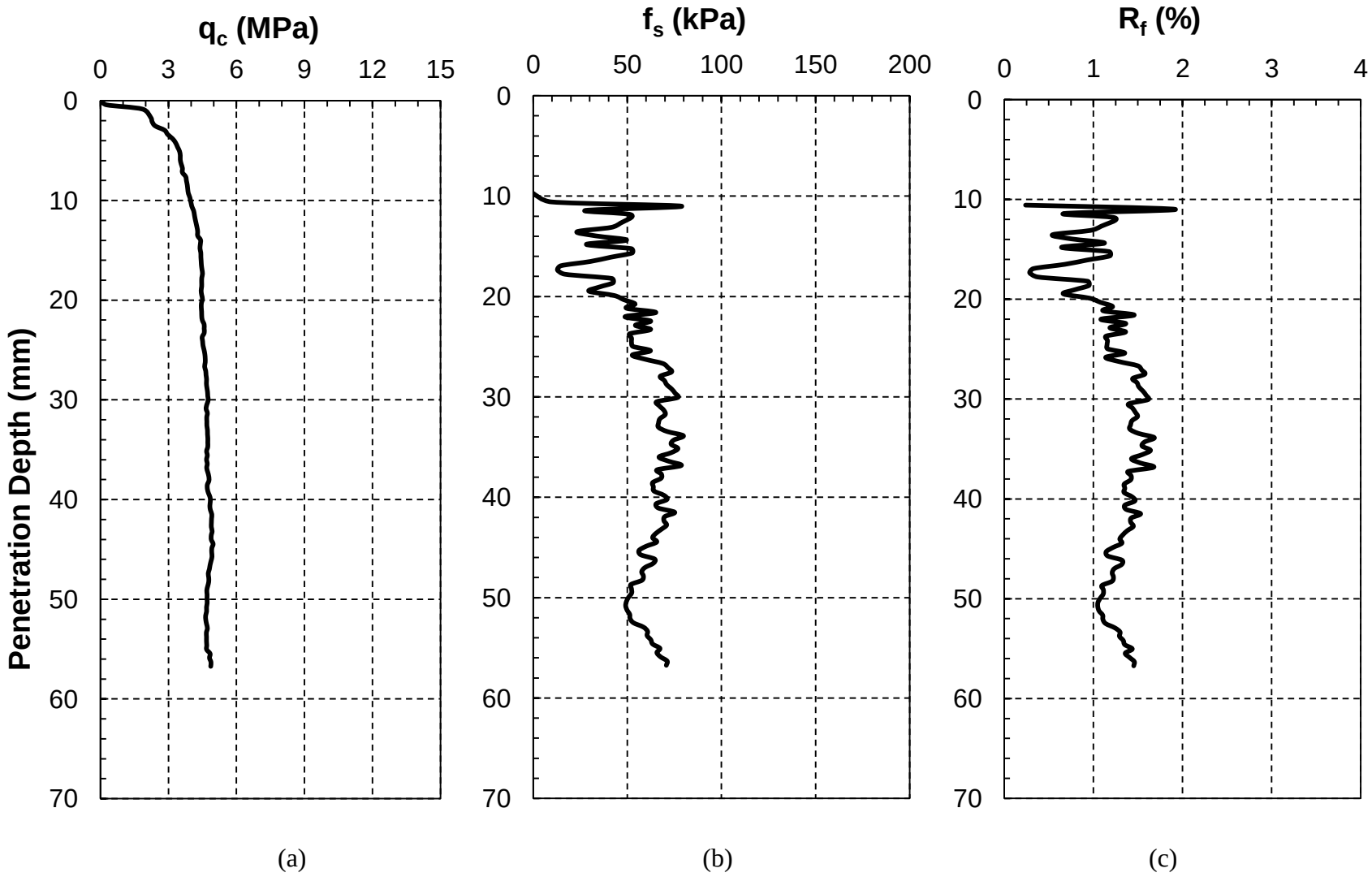

Figure 2-18: Cone penetration resistances mobilized in Test No. 7: (a) q_c, (b) f_s, and (c) R_f

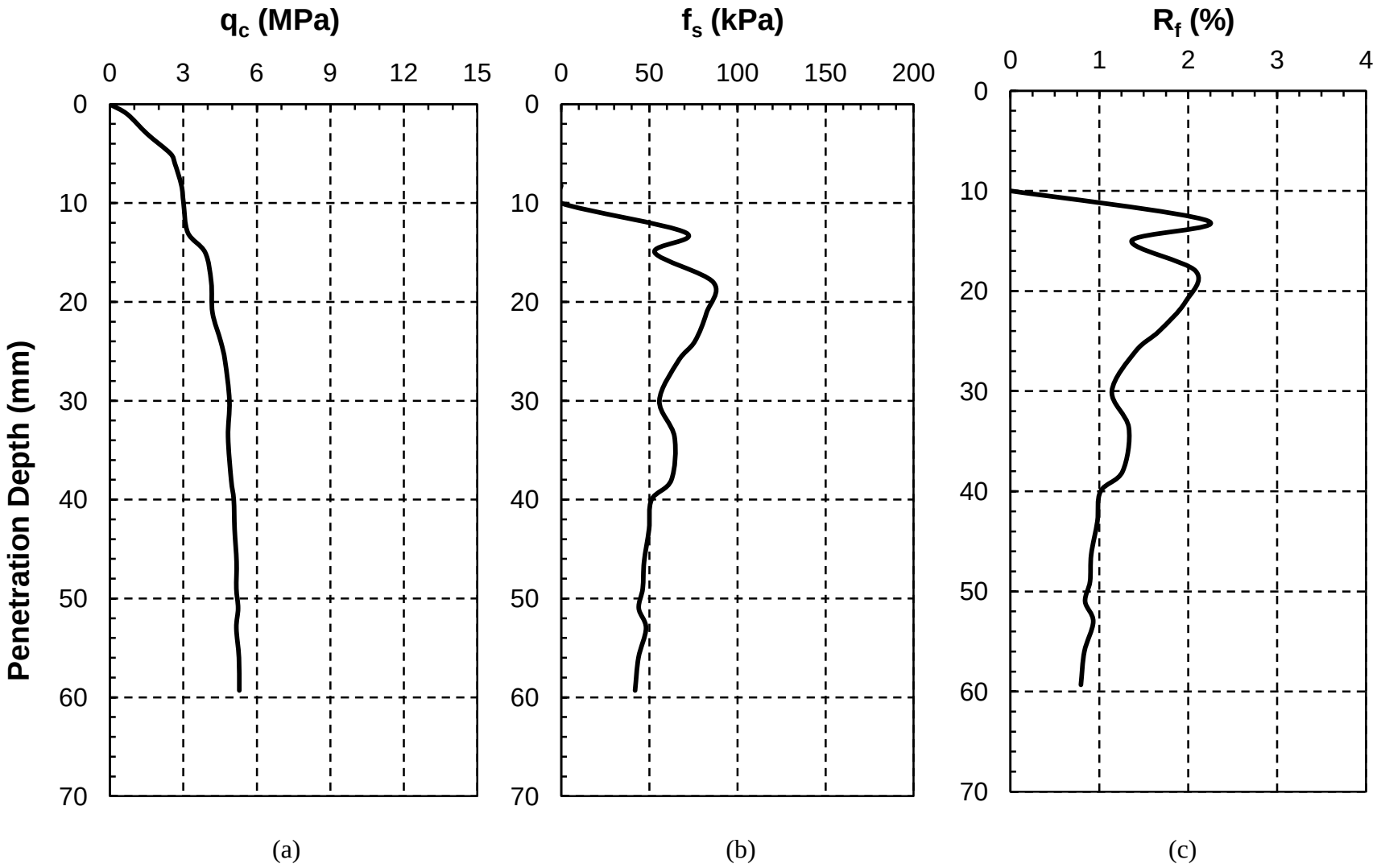

Figure 2-19: Cone penetration resistances mobilized in Test No. 8: (a) q_c, (b) f_s, and (c) R_f

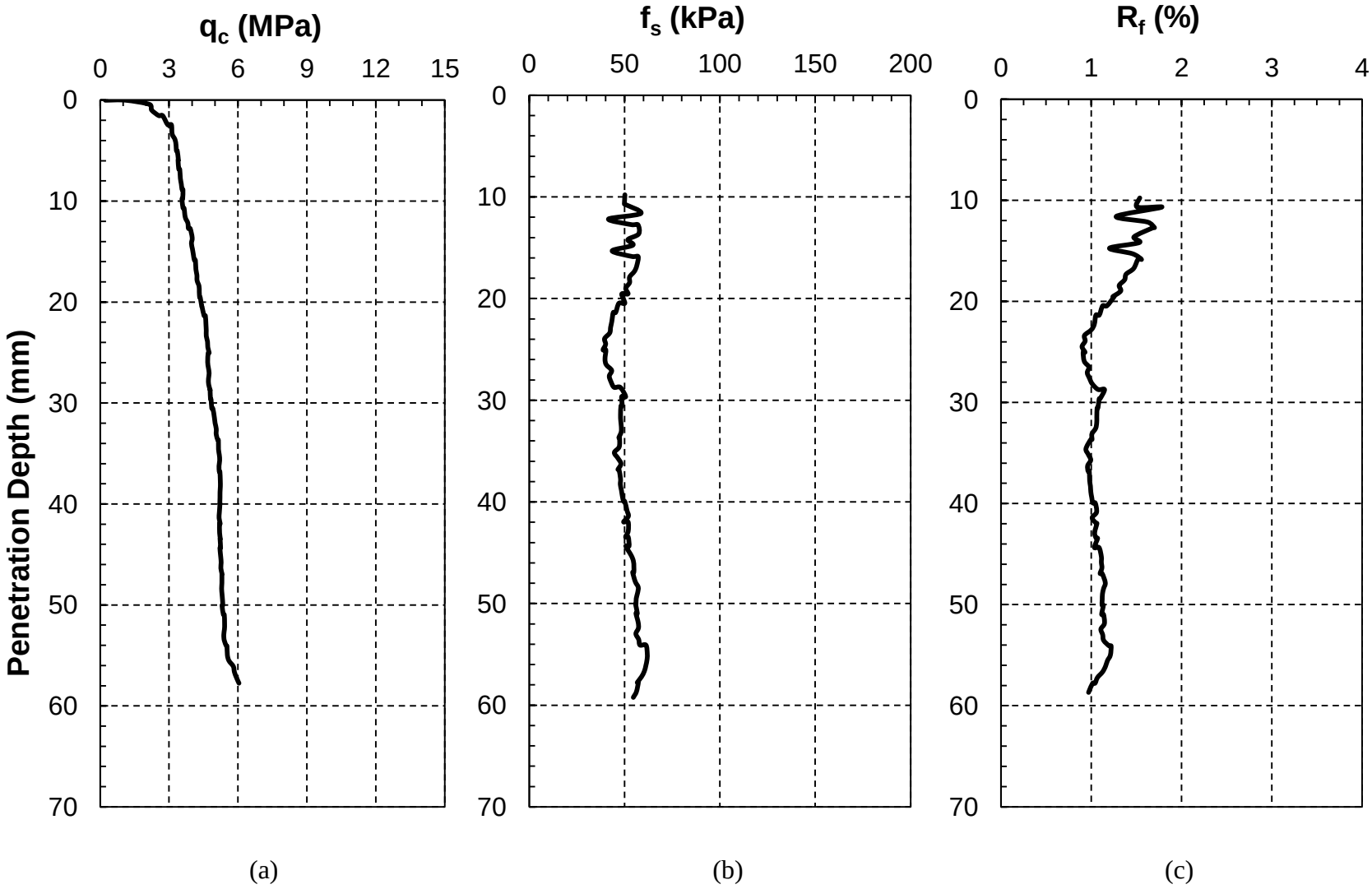

Figure 2-20: Cone penetration resistances mobilized in Test No. 9: (a) q_c, (b) f_s, and (c) R_f

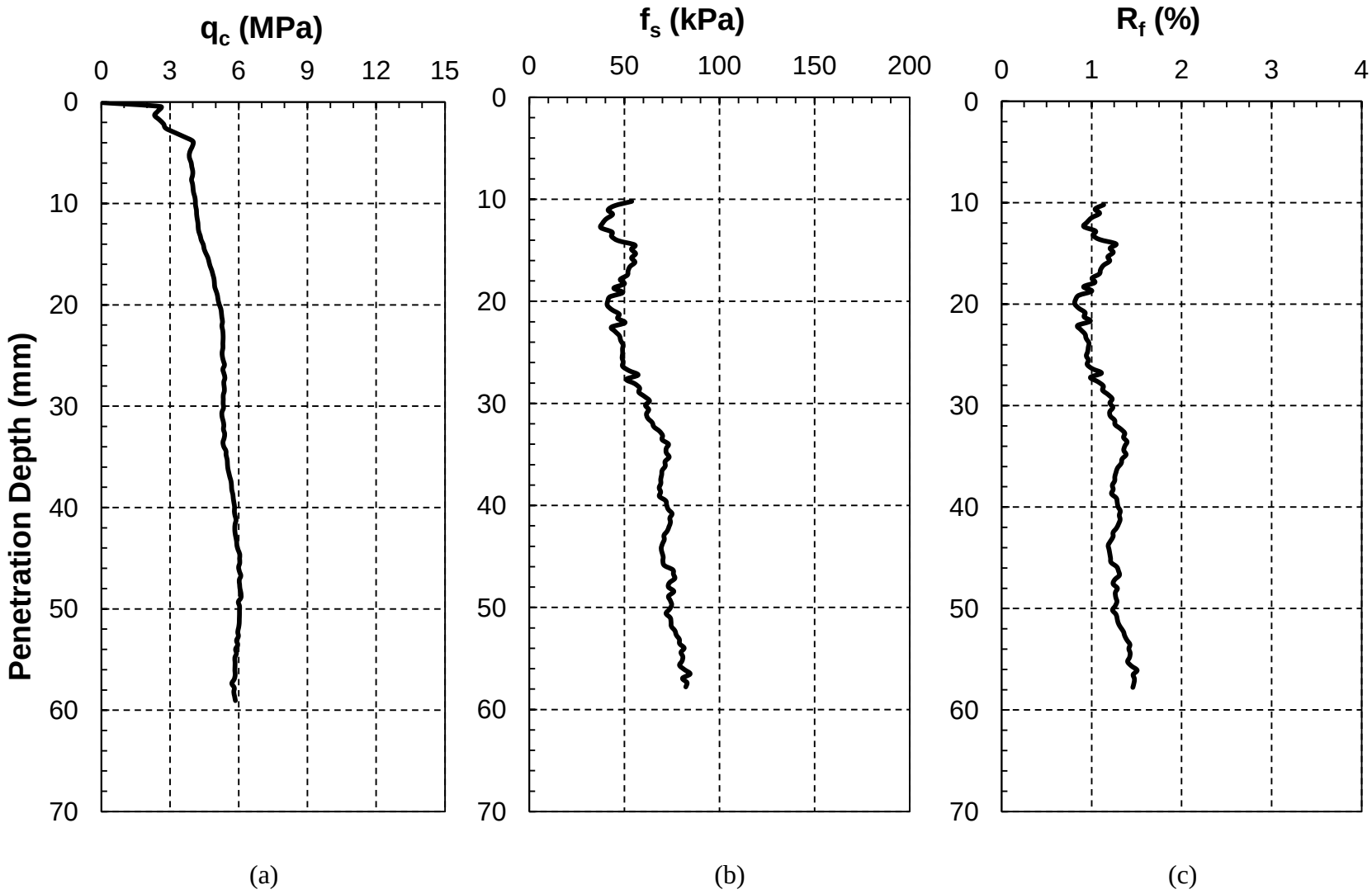

Figure 2-21: Cone penetration resistances mobilized in Test No. 10: (a) q_c, (b) f_s, and (c) R_f

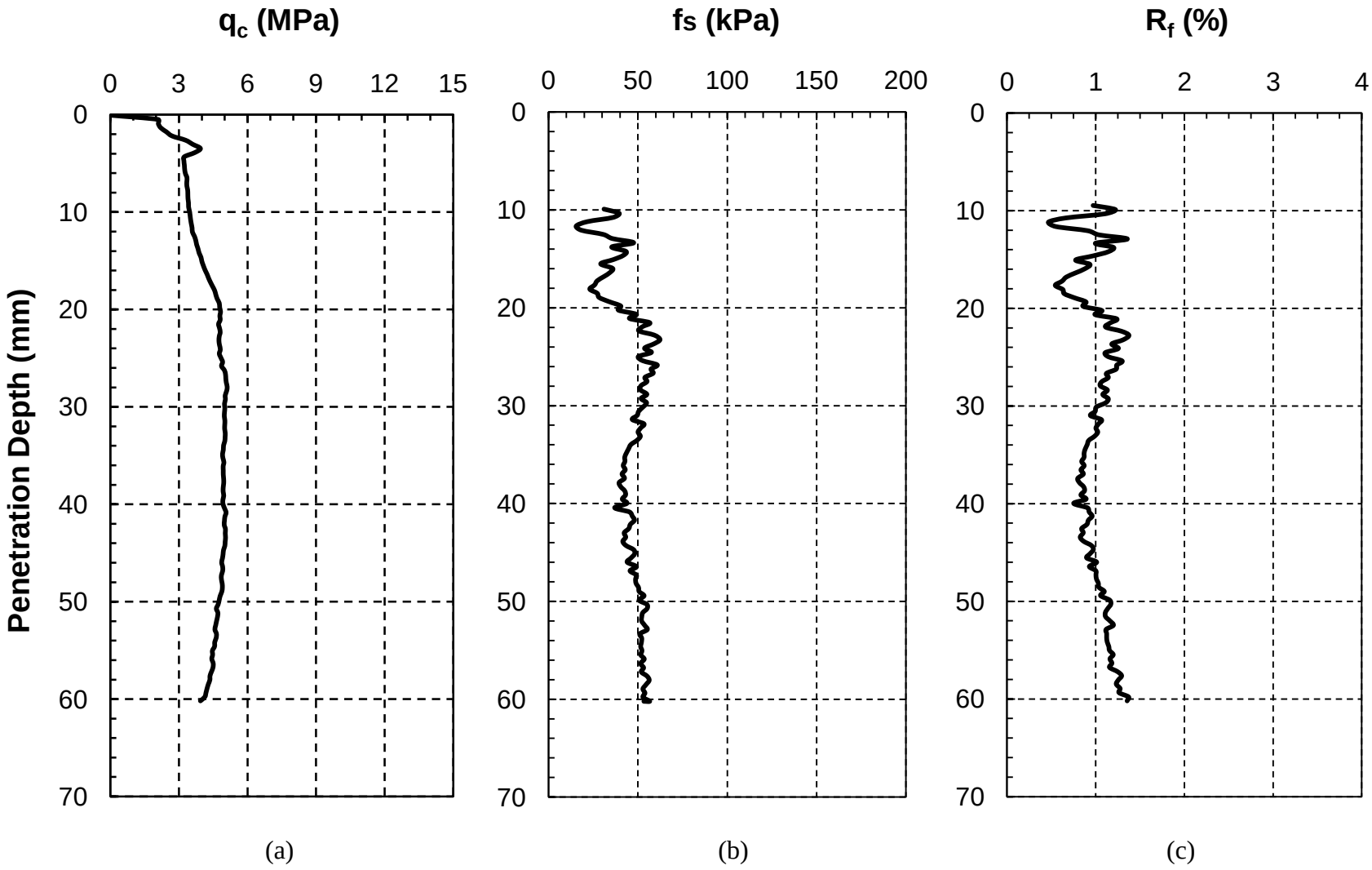

Figure 2-22: Cone penetration resistances mobilized in Test No. 11: (a) q_c, (b) f_s, and (c) R_f

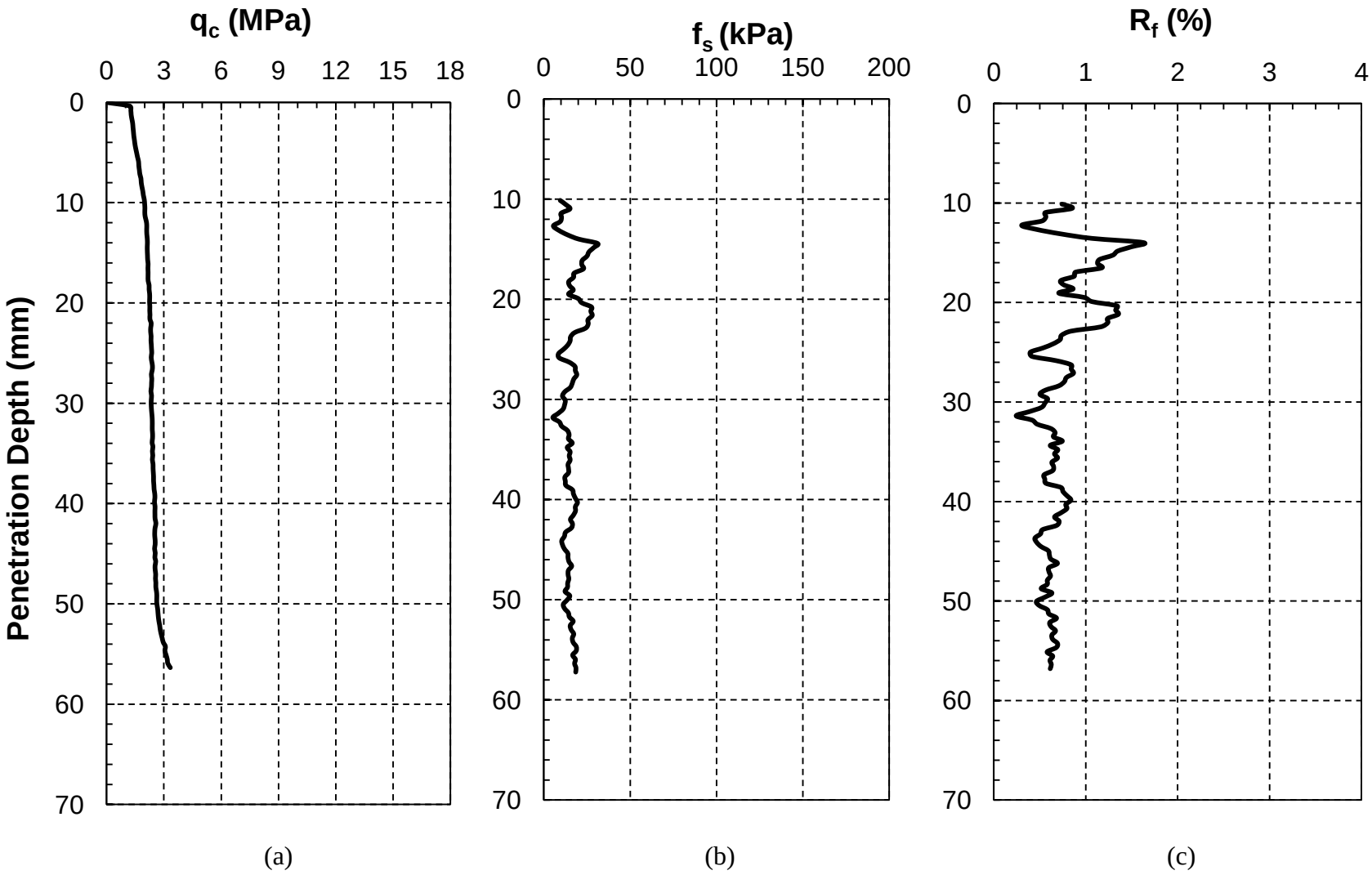

Figure 2-23: Cone penetration resistances mobilized in Test No. 12: (a) q_c, (b) f_s, and (c) R_f

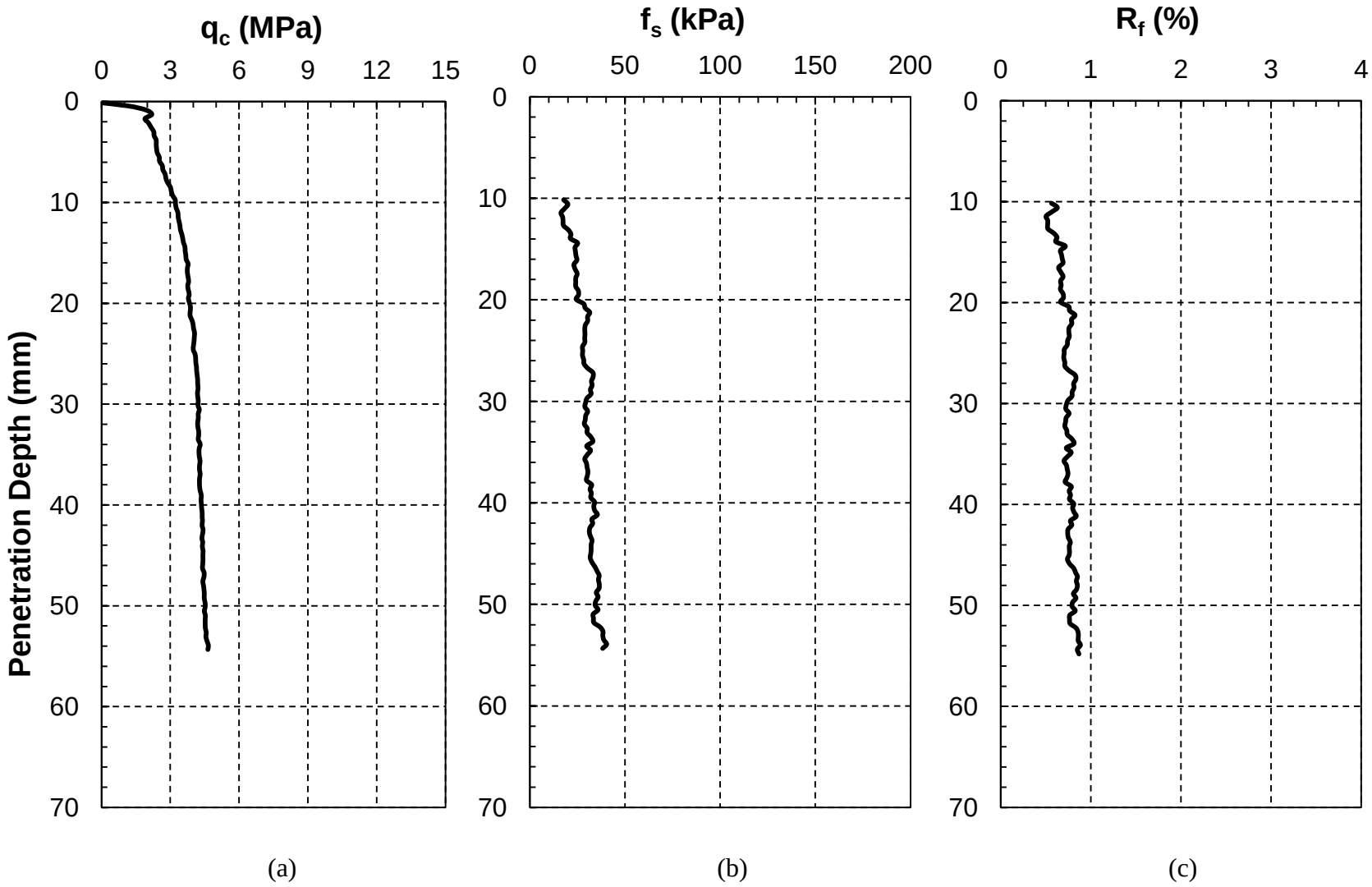

Figure 2-24: Cone penetration resistances mobilized in Test No. 13: (a) q_c, (b) f_s, and (c) R_f

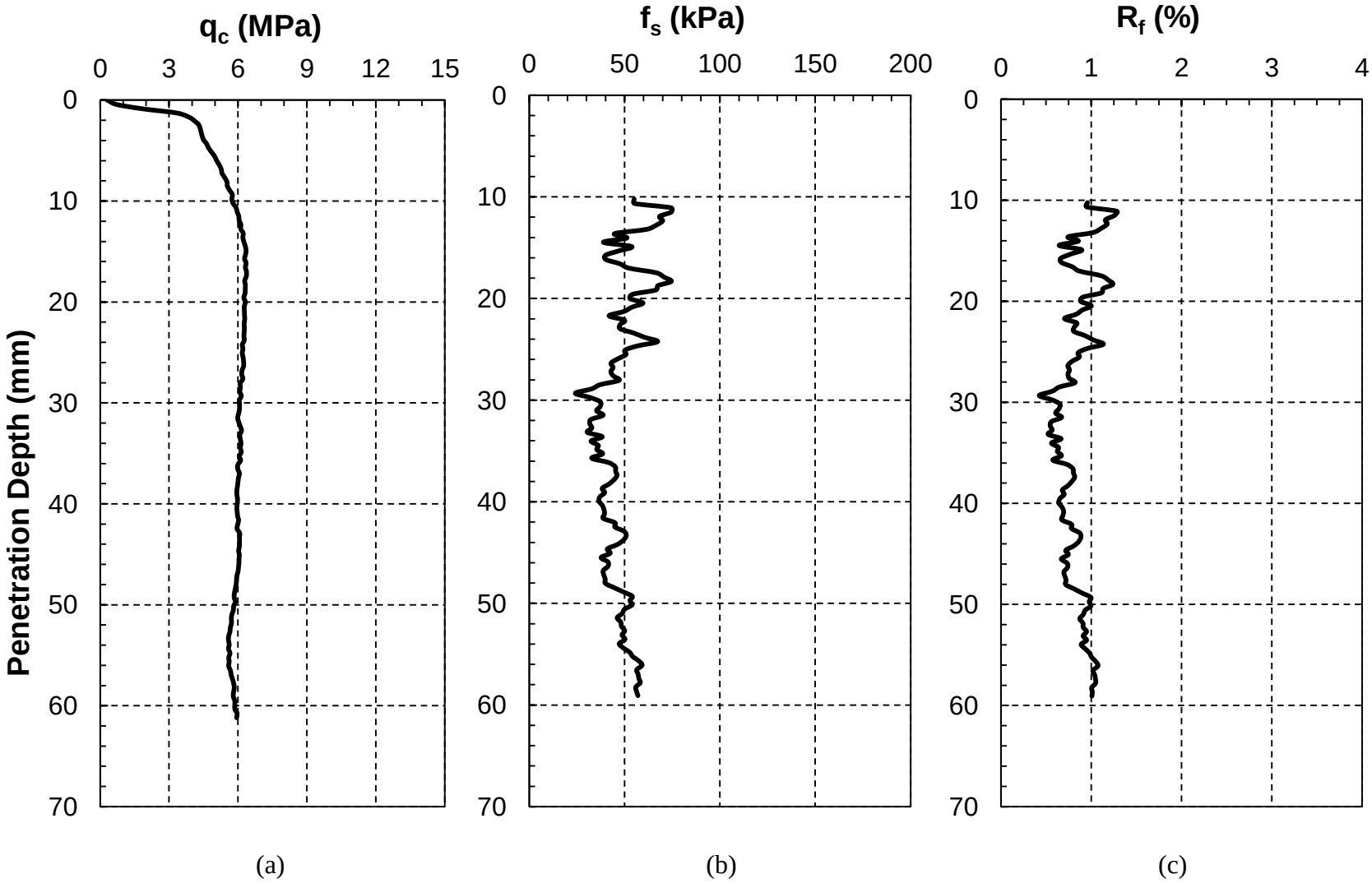

Figure 2-25: Cone penetration resistances mobilized in Test No. 14: (a) q_c, (b) f_s, and (c) R_f

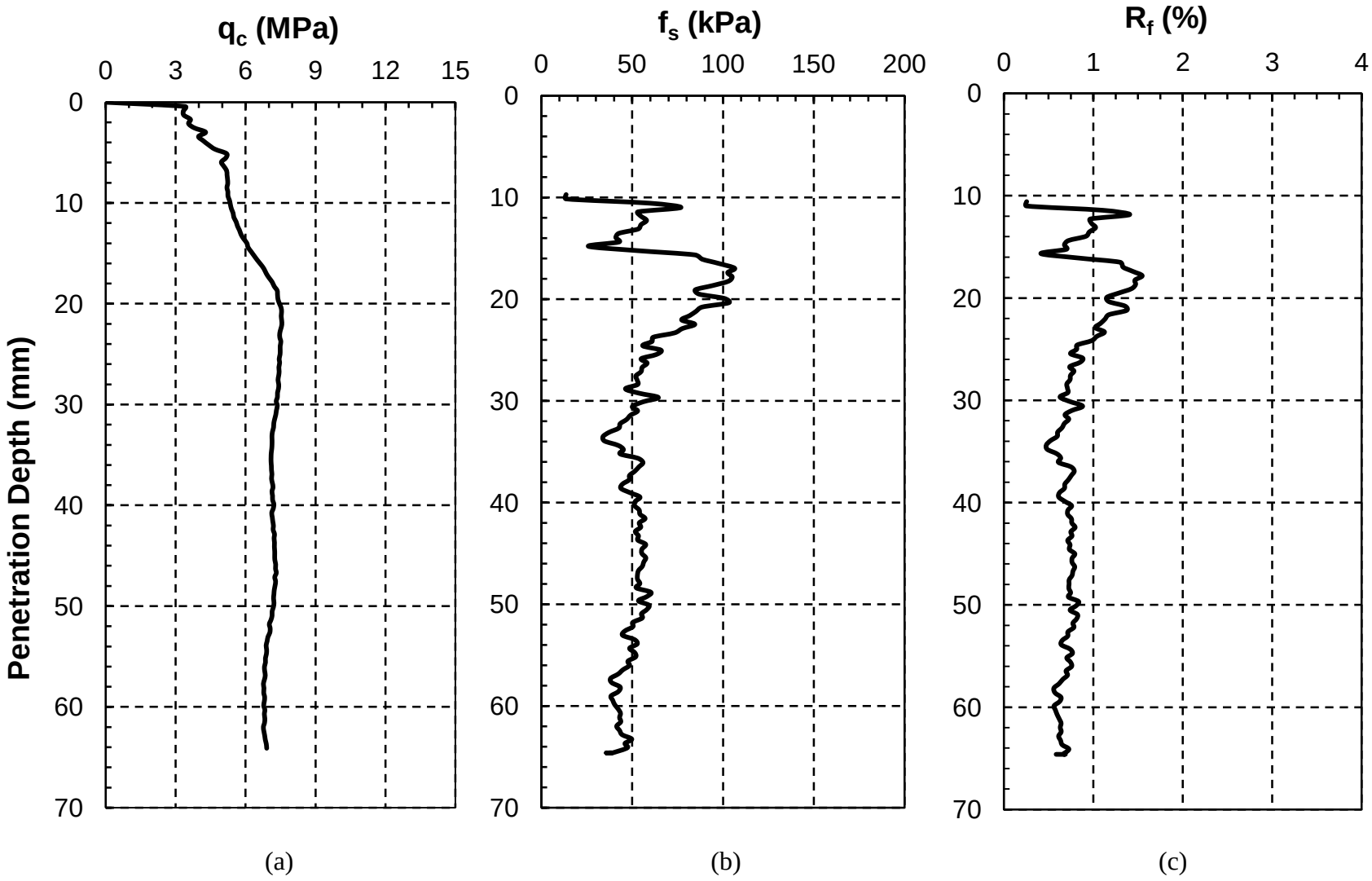

Figure 2-26: Cone penetration resistances mobilized in Test No. 15: (a) q_c, (b) f_s, and (c) R_f

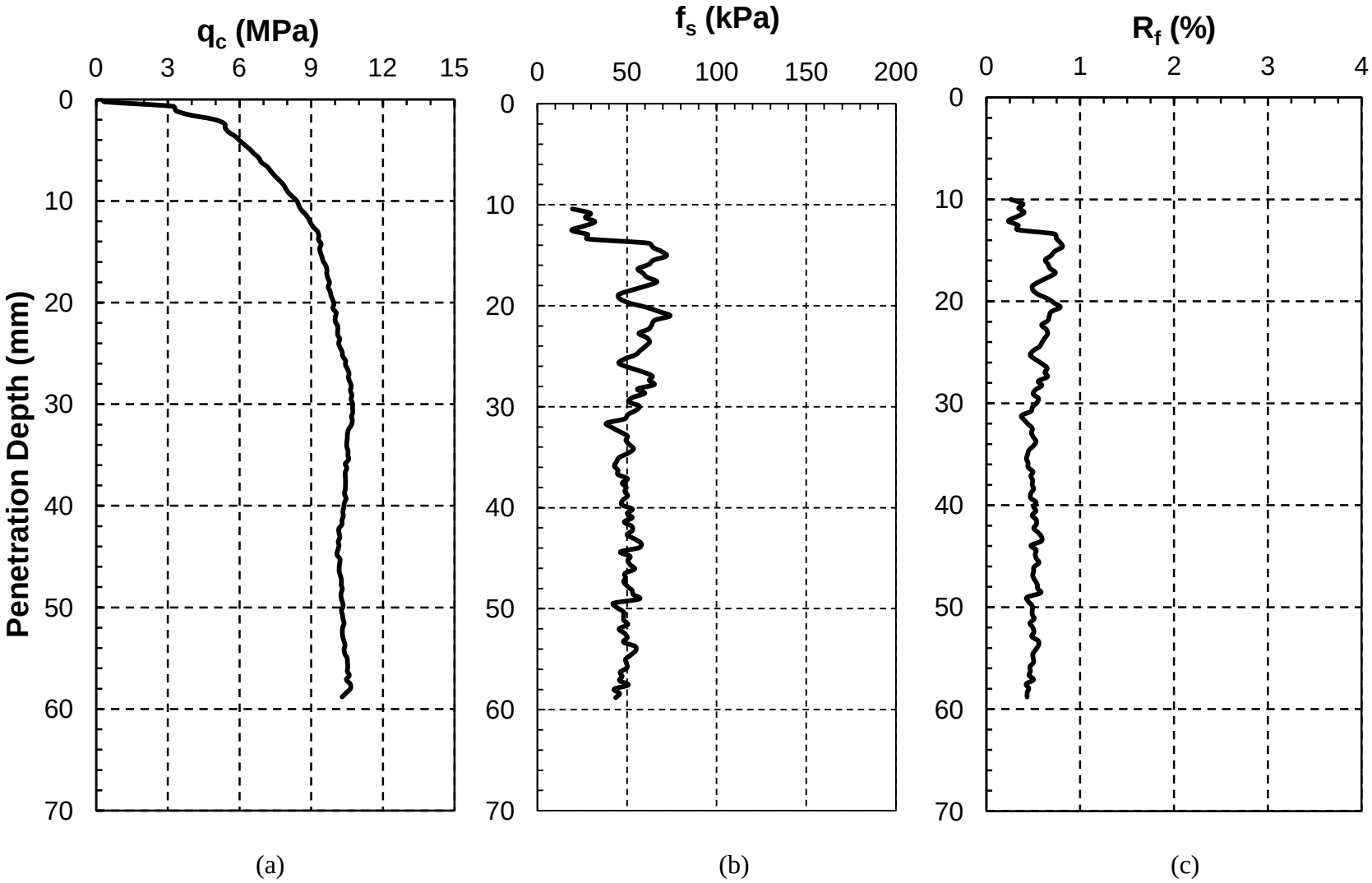

Figure 2-27: Cone penetration resistances mobilized in Test No. 16: (a) q_c, (b) f_s, and (c) R_f

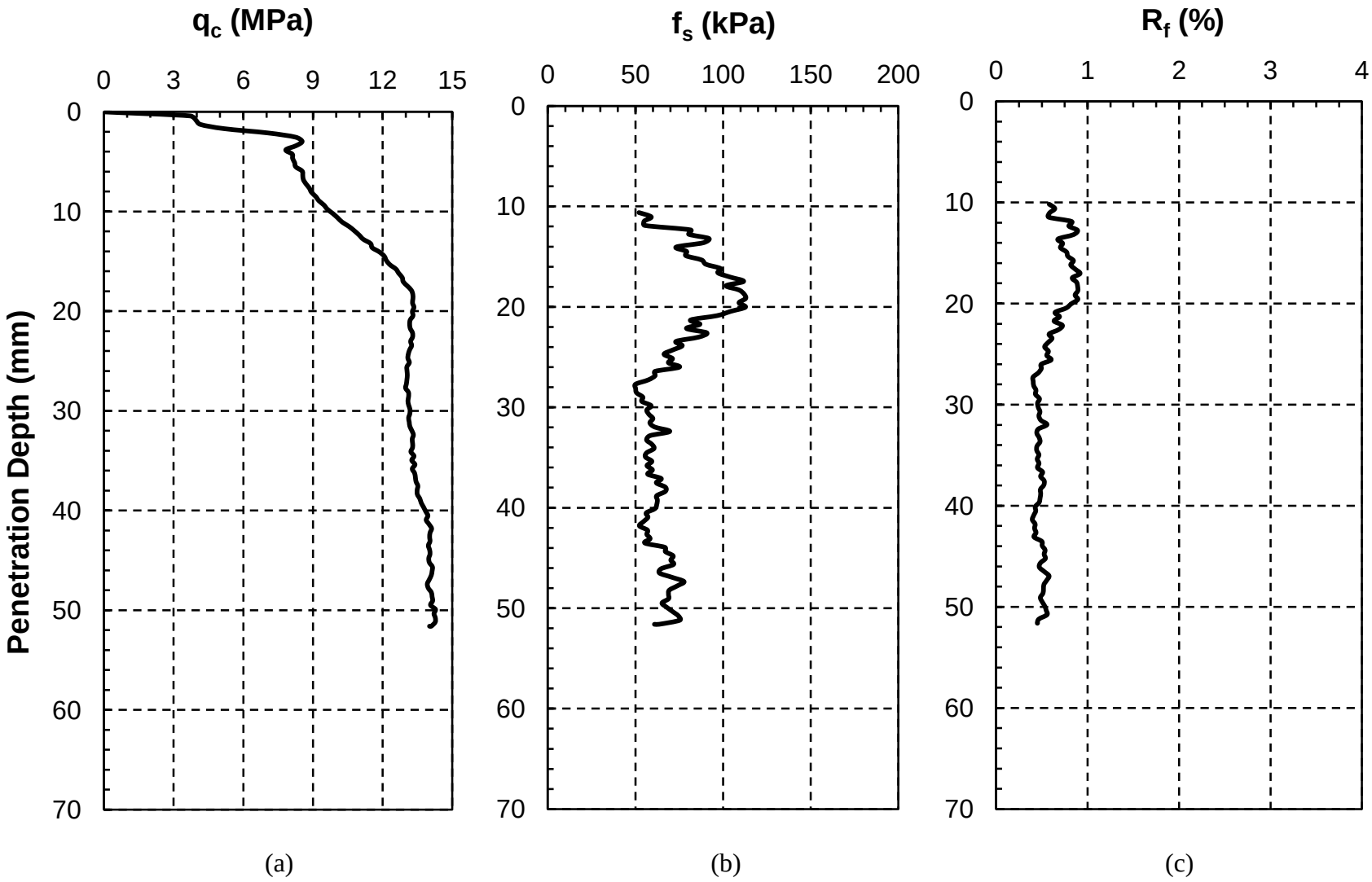

Figure 2-28: Cone penetration resistances mobilized in Test No. 17: (a) q_c, (b) f_s, and (c) R_f

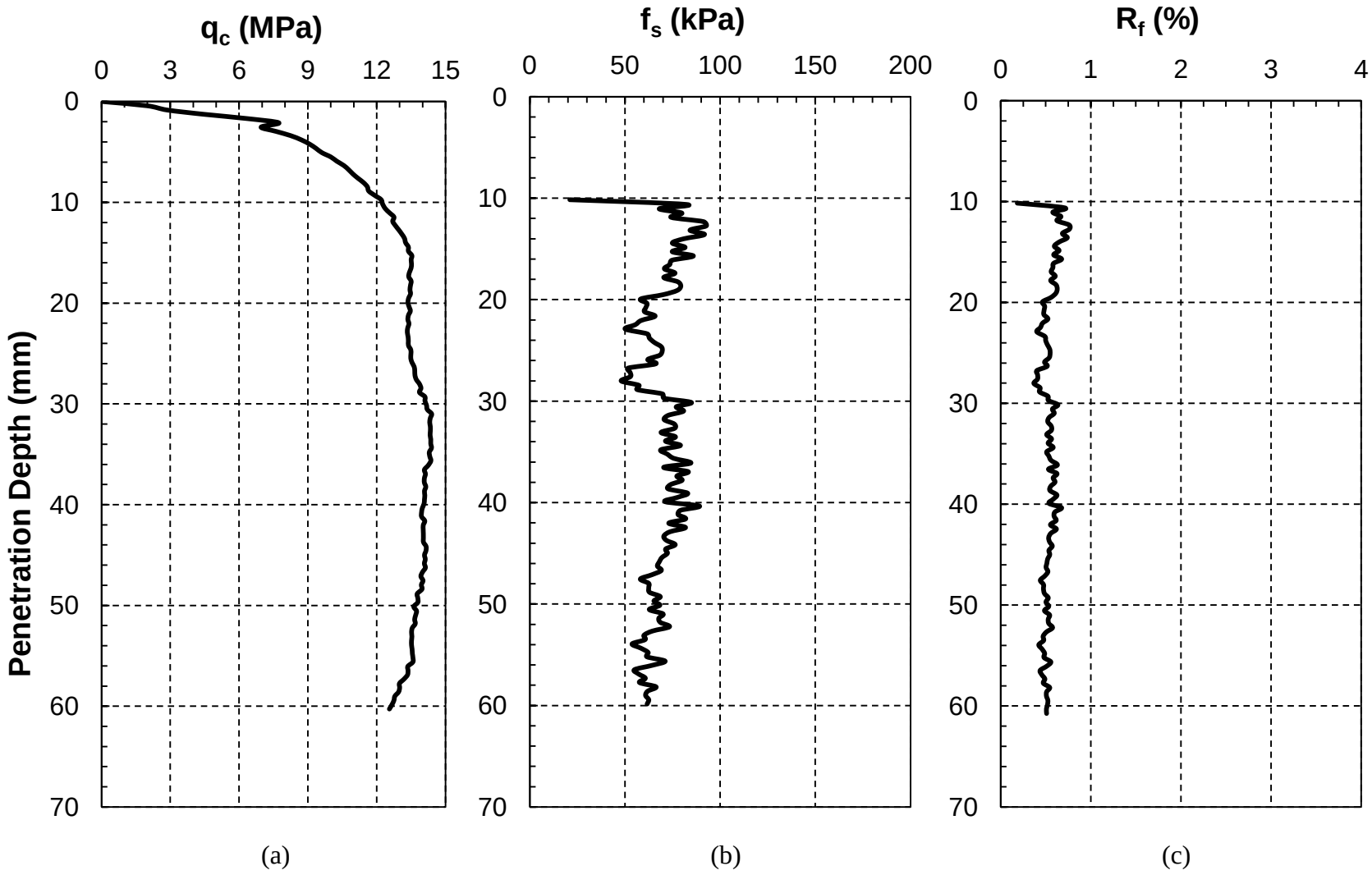

Figure 2-29: Cone penetration resistances mobilized in Test No. 18: (a) q_c, (b) f_s, and (c) R_f

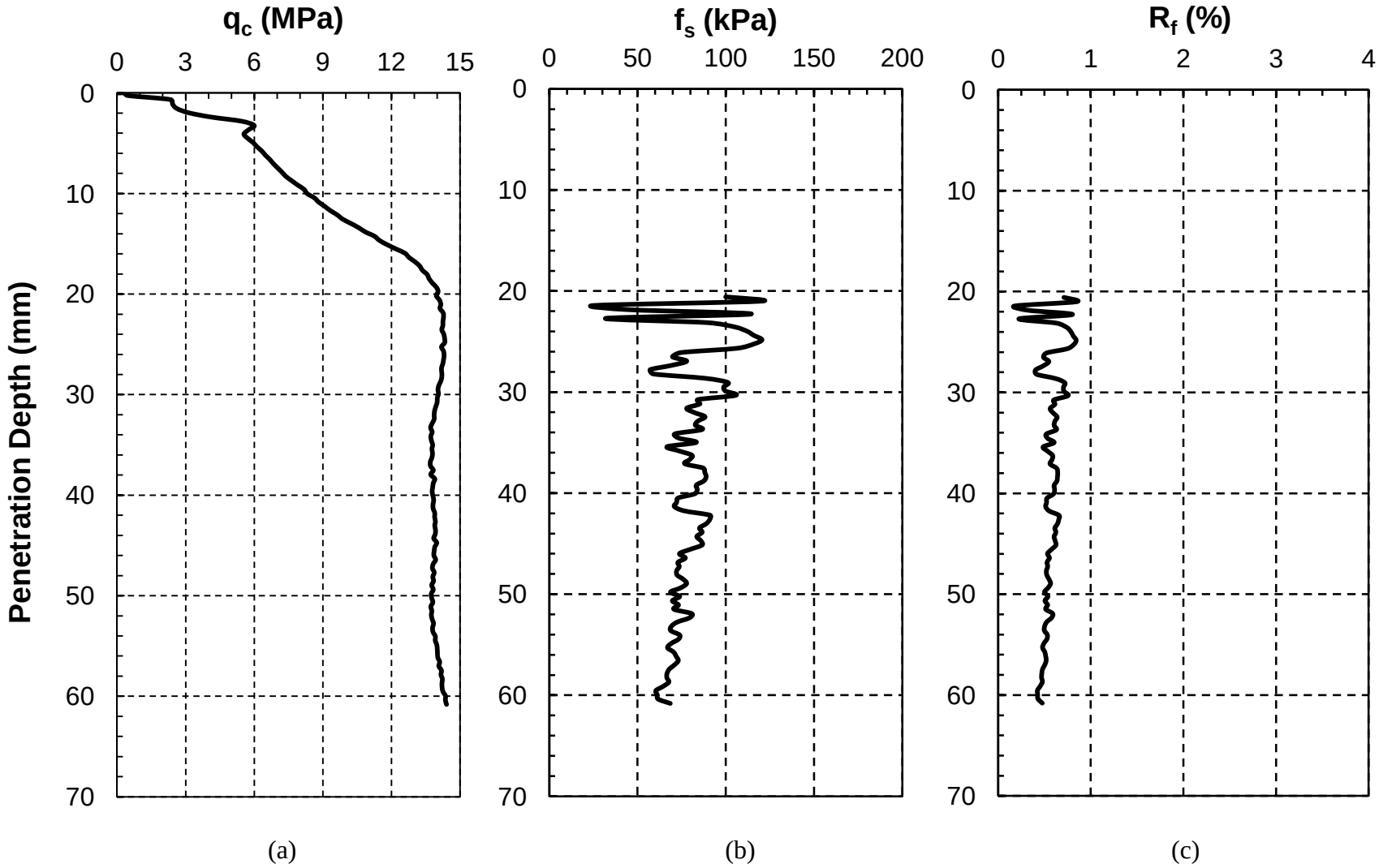

Figure 2-30: Cone penetration resistances mobilized in Test No. 19: (a) q_c, (b) f_s, and (c) R_f

2.4.1 Repeatability

Repeatability of test results under the same conditions is one of the major requirements of any reliable experiment, including the reduced-scale CPT of this study. In order to evaluate the repeatability of the CPT results, 5 tests were repeated with same D_{rc} and p'_c conditions. As compared in the Table 2-4, the repeated experiments show very similar average penetration resistances (q_c, f_s) after a depth of 20 mm, and therefore confirm the repeatability of the experiments. The small differences in q_c and in particular f_s measurements are inevitable and are associated with variations in specimen uniformity. Penetration resistances' profiles with depth for the 5 repeated tests are presented in Appendix C.

Table 2-4: Repeatability tests results

Test No		D_{ri} (%)	D_{rc} (%)	p'_c (kPa)	q_c (MPa)	f_s (kPa)
4	1st Trial	0	8	100	4.08	38.69
	2nd Trial				3.91	40.03
7	1st Trial	9	16	100	4.42	62.83
	2nd Trial				4.73	65.21
10	1st Trial	25	29	100	5.62	65.70
	2nd Trial				5.37	69.34
12	1st Trial	17	20	45	2.41	16.05
	2nd Trial				2.43	17.77
19	1st Trial	0	19	700	13.99	74.26
	2nd Trial				14.04	73.48

In the following paragraphs, the effect of specimen boundary conditions, scaling, penetration rate, particle crushing, overburden stress normalization, increase in the mean effective stress and increasing density are discussed with respect to the experiments of this study.

2.4.2 Specimen Boundary Conditions and Size Effect

Calibration chambers have a finite size while a field CPT is performed in a nearly infinite medium. Therefore, CPT carried out in a confined calibration chamber can be affected by the chamber boundaries in addition to the properties of the soil. Chamber boundary effect is often a major limitation for extending and comparing the results of CPT in a calibration chamber to field conditions and several researchers have investigated this issue (Parkin et al. 1980; Parkin and Lunne 1982; Jamiolkowski et al. 1985; Been et al. 1987; Harman 1976; Holdern 1971).

The different boundary conditions that can be developed in the calibration chamber tests are presented in Table 2-5. The experiments of this study were subjected to a constant isotropic stress, corresponding to the BC1 condition. The actual boundary condition in the field lies somewhere in between the BC1 and BC3 boundary conditions (Harman 1976; Holdern 1971).

Table 2-5: Boundary conditions in calibration chamber tests (Parkin et al. 1980)

Boundary condition	**Side restraint**	**Base restraint**
BC1	Constant stress	Constant stress
BC2	Constant volume	Constant volume
BC3	Constant volume	Constant stress
BC4	Constant stress	Constant volume

Parkin and Lunne (1982) investigated BC1 and BC3 boundary conditions using flexible-walled chambers. In their study, cone penetration tests were performed using different cone (d_c) and chamber (D_c) diameters. They found that the effect of chamber boundary conditions was negligible in loose sands ($D_{rc} < 30\%$) for $D_c/d_c \geq 20$. While, for dense sands (with $D_{rc} \approx 90\%$), the influence of chamber size was significant for $D_c/d_c < 50$.

Accordingly, many researchers have tried to correct laboratory CPT results for the effects of chamber size and boundary conditions.

For example, Jamiolkowski et al. (1985) studied calibration chamber CPT data on Ticino and Hokksund sands under BC1 and BC3 boundary conditions and proposed the following equation to correct for sample size and boundary effects. In this equation, $q_{c,cc}$ is the cone tip resistance measured in a calibration chamber test, and $q_{c,field}$ is the equivalent cone tip resistance which would be measured in the field. Based on this Equation 2-1, the effect of boundary conditions is observed for $D_{rc} \geq 30\%$ and increases with increasing D_{rc}.

$$\frac{q_{c,field}}{q_{c,cc}} = \left(1 + \frac{0.2(D_{rc}(\%)-30)}{60}\right) \geq 1.0 \qquad (2\text{-}1)$$

Been et al. (1987) developed the following graph to correct for chamber size and boundary effects. According to Figure 2-31, the effect of boundary conditions decreases with increasing the void ratio difference of the specimen from the critical state void ratio of the sand at the same effective stress level (i.e. state parameter, ψ_{cs}). In particular, boundary effects become negligible for $\psi_{cs} > -0.1$.

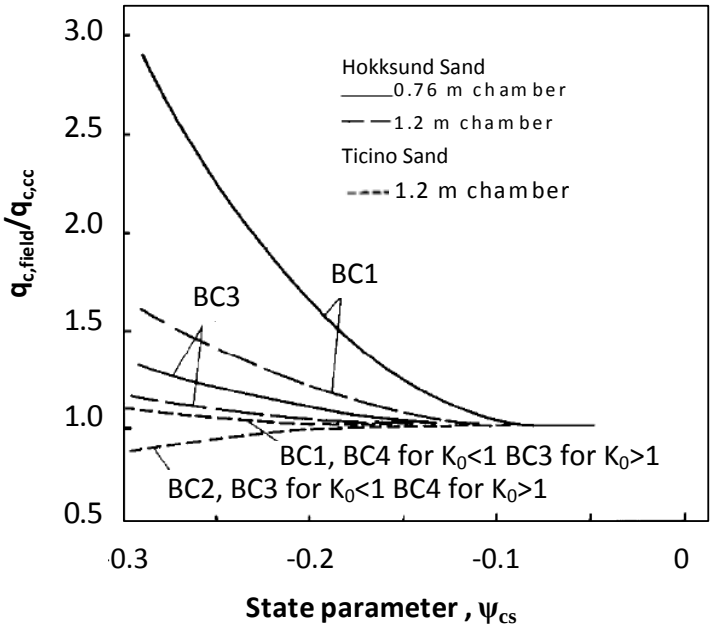

Figure 2-31 : Correction factor for calibration chamber size and boundary conditions (Been et al. 1987)

In summary, the effect of specimen size and boundary conditions is negligible for the experiments of this study which are conducted at D_{rc} < 30%.

2.4.3 Scale Effect

Scale effect is the influence of cone diameter (d_c) with respect to particle size (e.g. D_{50}) on the penetration resistance. For example, an ASTM standard cone (with a cone area of about 3003 mm^2) would be in direct contact with about 15,560 particles of the Barco 71 sand (D_{50} = 0.193 mm) used in this study, while the miniature cone is in contact with about 440 particles during penetration. A number of studies have investigated scale effect. For example, Schmertmann (1978) reported no significant variation in the measured penetration resistance of cones with different projected areas (5 to 20 cm^2) for different soil types. Canou et al. (1988) presented reduced-scale CPTs in a triaxial cell

with a diameter of 18 cm. Their experiments were conducted on a number of saturated sands with D_{50} = 0.3 to 0.7 mm, corresponding to d_c/D_{50} = 32 to 18. They observe no differences between their tests when compared to a standard-size CPT, suggesting no scale effect. Similar results were also obtained by Jacobs and Couts (1992). Parkin (1988) analyzed the scale effect using a theoretical approach by considering Terzaghi's bearing capacity analysis for a circular footing. He suggested that the relationship between cone size and the size of sand particles was unlikely a significant practical limitation for CPT. Ovesen (1981) reported that size effects are observed when the ratio of d_c/ D_{50} is less than 30.

Eid (1987) performed 47 CPT calibration chamber tests on three types of Monterey sand with D_{50} = 0.45, 0.75 and 0.32 mm using cones with 4.23, 10 and 15 cm^2 projected areas and concluded that a miniature cone could be more sensitive to small variations in soil conditions because of the relatively smaller ratio of cone diameter to sand particle sizes.

Gui and Bolton (1998) studied the grain size effect with a series of mini-cone penetration tests executed in a centrifuge. The tests were carried out using Leighton Buzzard sand of different grain sizes (in fine sand d_{50} = 0.225 mm, medium sand d_{50} = 0.4 mm and coarse sand d_{50} = 0.9 mm). Three different size mini-cones were used (19.05 mm, 10 mm and 6.35 mm). In case of Leighton Buzzard fine sand, no particle size effect was reported using the 6.35 mm cone (d_c/ D_{50} = 28).

Bałachowski (2007) also studied the size effect using mini-cone penetration tests in a centrifuge and reported no particle size effect in cone penetration tests when (d_c/ D_{50}) ratio exceeds 20. Bałachowski (2007) suggested that the results of penetration tests should be corrected for the grain size effect if the ratio model diameter to the mean grain size (d_c/ D_{50}) falls below 20.

More recently, Sharp et al. (2010) performed miniature cone penetration tests in a centrifuge on fine Nevada sand (with D_{50} = 0.13 mm) and reported no grain size effects for the d_c/ D_{50}= 30.7. Table 2-6 presents a summary of the studies in which d_c/ D_{50} ratio has been reported.

In the current study, a miniature cone with a diameter of 6 mm was pushed into a quartz sand with an average particle size, D_{50} = 0.193 mm, which corresponds to d_c/D_{50} = 31. Based on the above studies, scale effect is expected to be negligible for the combination of cone diameter and D_{50} used in this study. Confirming the previous studies, we did not observe significant fluctuations or erratic load cell readings indicating grain size effects.

Table 2-6: Summary of previous studies on the scale effect

Reference	d_c/D_{50}	Scale effect observed?
Canou et al. (1988)	18 to 32	No
Ovesen (1981)	< 30	Yes
Gui and Bolton (1998)	28	No
Bałachowski (2007)	< 20	Yes
Sharp et al. (2010)	30.7	No

2.4.4 Effect of Penetration Rate

The standard penetration rate, suggested by the ASTM D5778-2012, is 20 mm/s. However, similar to several other reduced-scale cone penetration experiments (Abedin 1995; Kokusho et al. 2003), the maximum penetration rate was limited by the rate of the uniaxial loading frame to 0.423 mm/s in this study. In order to investigate the effect of penetration rate on cone resistances, Test No.3. was repeated at a rate of 0.085 mm/s (about 5 times slower). According to Figure 2-32, the results of this experiment are comparable to those in a similar sample at the maximum penetration rate, which indicates negligible effect of penetration rate. This is somewhat expected for the drained CPT tests of this study with zero excess pore water pressure during penetration. Similarly, Dayal and Allen (1975) performed a series of tests on uniformly graded medium to fine sand at various penetration rates in the range of 0.13 to 81.14 cm/s and also observed negligible effect of penetration rate on cone resistance in a uniformly-graded fine sand. Therefore, although the CPTs of this study were conducted at a rate of about 47 times slower than

the standard rate, we expect that similar results would be obtained if the standard penetration rate was used.

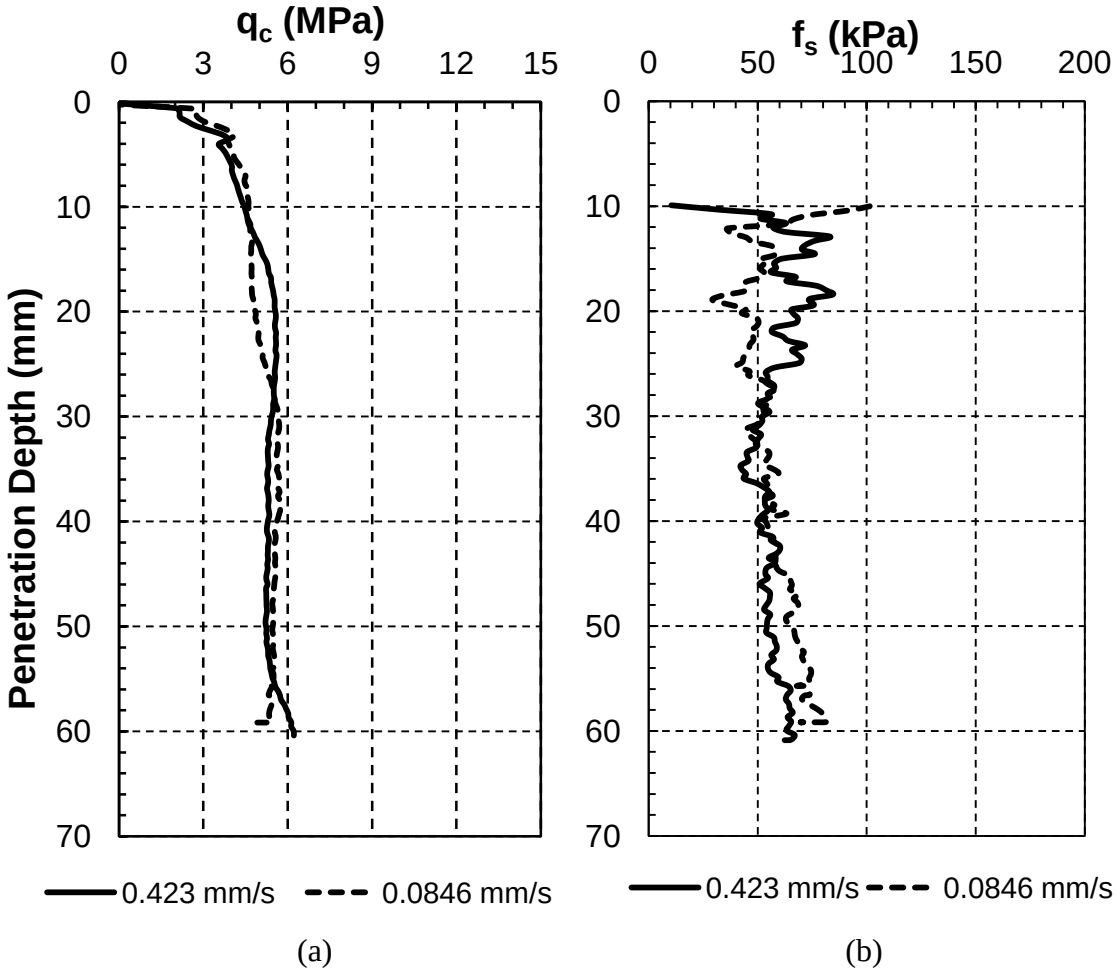

Figure 2-32: Effect of cone penetration rate on: (a) q_c, and (b) f_s in samples with D_{rc} = 11% at p'_c = 200 kPa (Test No. 3.)

2.4.5 Particle Crushing

Crushing of sand particles adjacent to the cone has been reported often for CPT in carbonate sands (Belloti and Pedroni 1991) or discrete element analysis (Ma 1994). However, we did not observe any particle crushing in our CPT experiments, likely because of the hard mineralogy of the quartz Barco 71 sand.

2.4.6 Overburden Stress Normalization

The comparison of cone penetration resistances at different depths can be misleading if the effect of overburden stress is not properly taken into account. Besides soil density, q_c and f_s increase with increasing effective stress, and therefore in order to compare soil characteristics from different depths, cone resistances should be normalized to a common effective overburden stress (typically 100 kPa). A number of methods (Wroth 1984; Houlsby 1988; Been et al. 1987; Robertson and Wride 1998; Olsen and Mitchell 1995; Kayen et al. 1992; Moss et al. 2006; Boulanger and Idriss 2004) are suggested for normalizing cone penetration resistance in cohesionless soils, which are summarized in Table 2-7 following by detailed definition of parameters used in each method.

Table 2-7: CPT overburden stress normalization methods

Cone tip resistance	**Sleeve friction**	**Reference**
$Q_t = (q_c - \sigma'_{v0})/\sigma_{v0}$	F_R (%) = $f_s/(q_t-\sigma_{vo})\times 100$	Wroth (1984); Houlsby (1988)
$Q_t = (q_c - p')/p$	-	Been et al. (1987)
$Q = \left(\frac{q_c - \sigma_{v0}}{P_{a2}}\right)\left(\frac{P_a}{\sigma'_{v0}}\right)^n$	F_R (%) = $f_s/(q_t-\sigma_{vo})\times 100$	Robertson and Wride (1998)
$q_{c,1} = C_q.q_c \quad , \quad C_q = \left(\frac{P_a}{\sigma'_v}\right)^c$	$f_{s,1} = C_f.f_s \quad , \quad C_f = \left(\frac{P_a}{\sigma'_v}\right)^s$	Olsen and Mitchell (1995)
$q_{c,1} = \frac{1.8}{0.8 + \sigma'_v/P_a}\ q_c$	-	Kayen et al. (1992)
$q_{c,1} = C_q.q_c \quad , \quad C_q = \left(\frac{P_a}{\sigma'_v}\right)^c$	$f_{s,1} = C_f.f_s \quad , \quad C_f = \left(\frac{P_a}{\sigma'_v}\right)^s$	Moss et al. (2006)
$q_{c,1} = C_q.q_c \ , \ C_q = \left(\frac{P_a}{\sigma'_v}\right)^{0.784-0.521D_R}$	-	Boulanger and Idriss (2004)

Been et al. (1987) used normalized tip resistance, Q_t, to correct for the effect of overburden pressure using equation (2-2).

$$Q_t = (q_c - p')/p \tag{2-2}$$

Where;

Q_t = normalized tip resistance

q_c = cone resistance, MPa,

p' = effective mean stress, MPa,

p = total mean stress, MPa,

Later, Robertson and Wride (1998) used an improved normalization method for cone tip resistance to define the soil identification index as bellow:

$$Q = \left(\frac{q_c - \sigma_{v0}}{P_{a2}}\right)\left(\frac{P_a}{\sigma'_{v0}}\right)^n \quad (2\text{-}3)$$

Where;

σ_{v0} and σ'_{v0} are the total and effective overburden stresses, respectively.

P_a is the reference pressure in the same units as σ'_{v0} (i.e. $P_a = 100kPa$ if σ'_{v0}in kPa)

P_{a2} is the reference pressure in the same units as q_c and σ_{v0} (i.e. $P_{a2} = 0.1\ MPa$ if q_c and σ_{v0}in MPa)

The exponent *n* varies from 0.5 for sands (when soil identification index is less than 2.6) to 1.0 for clays (when soil identification index is higher than 2.6) (Robertson and Wride 1998).

Olsen and Mitchell (1995) proposed a soil profiling chart, plotting "normalized cone resistance,$q_{c,1}$,"versus the friction ratio, R_F. The normalized cone resistance is determined as follows:

$$q_{c,1} = C_q . q_c \quad (2\text{-}4)$$

$$C_q = \left(\frac{P_a}{\sigma'_v}\right)^c \quad (2\text{-}5)$$

Where;

$q_{c,1}$= normalized cone resistance,

q_c= raw tip resistance,

σ'_v= effective overburden stress,

P_a = the reference pressure in the same units as σ'_{v0} (i.e. $P_a = 100kPa$ if σ'_{v0}in kPa)

c = tip normalization exponent for that particular soil state (0.75-1.0 for loose sands)

Later, Moss et al. (2006) proposed the following equations to find the exponents c and s:

$$c = s = f_1(\frac{R_f}{f_3})^{f_2} \tag{2-6}$$

$$f_1 = 0.78\ {q_c}^{-0.33} \tag{2-7}$$

$$f_2 = -(-0.32\ {q_c}^{-0.35} + 0.49) \tag{2-8}$$

$$f_3 = abs\ [\log(10 + q_c)]^{1.21} \tag{2-9}$$

$$R_f = \frac{f_s}{q_c} \times 100 \tag{2-10}$$

Kayen et al. (1992) proposed the following equation to correct cone resistance for the overburden pressure:

$$q_{c,1} = C_q . q_c = \frac{1.8}{0.8 + \frac{\sigma'_v}{P_a}}\ q_c \tag{2-11}$$

The framework by Boulanger and Idriss (2004) included normalizations to the same equivalent relative density. This relationship was derived from calibration chamber data of several sands tested in calibration chambers and from theoretical analyses of CPT tip resistance (Salgado et al. 1997a,b).

The following equation was proposed to correct cone resistance for the overburden pressure:

$$q_{c,1} = C_q . q_c = \left(\frac{P_a}{\sigma'_v}\right)^{0.784 - 0.521 D_R} \times\ q_c \tag{2-12}$$

Reviewed methods were applied to the data obtained from the current study to evaluate whether they fully correct the effect of overburden pressure.

In the current study, isotropic pressures were applied to the sample therefore equations suggested by Wroth (1984), Houlsby (1988) and Been et al (1987) will end up with the same results. Table 2-8 shows the normalized tip resistance for the data obtained from the current study in tests No. 11 to 19. To evaluate the proposed methods, tests at the same relative density (after consolidation) should be compared to each other. Here, tests No. 11 to 19 have almost the same relative densities but different stress levels.

Data shows that the equation proposed by Olsen and Mitchell (1995) (for exponent c=0.75) and Boulanger and Idriss (2004) and Kayen et al. (1992) predicted close values for the test No.11 to 19 and eliminated the effect of stress level much better than other methods as the variation between the normalized values is less.

Table 2-8: Normalized tip resistance

Test No.	D_{rc} (%)	q_c (Mpa)	Stress level (kPa) ($P = \sigma_v$)		Wroth (1984) / Houlsby (1988) / Been et al. (1987)	Robertson and Wride (1998)	Olsen and Mitchell (1995)		Moss et al. (2006)	Kayen et al. (1992)	Boulanger and Idriss (2004)
			P	P'			c=0.75	c=1			
11	20	4.80	225	100	45.76	45.76	4.84	4.85	4.80	4.80	4.84
12	20	2.41	200	45	49.01	32.87	4.41	5.40	3.28	3.46	4.18
13	20	4.23	200	75	53.74	46.54	5.29	5.70	4.66	4.91	5.19
14	19.6	6.10	300	150	38.64	47.33	4.53	4.10	5.39	4.77	4.66
15	20	7.06	400	200	33.32	47.13	4.23	3.57	5.69	4.54	4.45
16	19.4	10.40	450	300	33.16	57.44	4.60	3.50	7.19	4.93	4.95
17	20	13.54	650	450	28.64	60.75	4.41	3.04	8.38	4.60	4.91
18	19.4	13.74	800	600	21.57	52.84	3.61	2.31	7.83	3.64	4.08
19	19	13.99	800	700	18.85	49.86	3.28	2.02	7.76	3.23	3.72

The methods suggested by Olsen and Mitchell (1995), Moss et al. (2006) and Kayen et al. (1992) normalize the cone tip resistance with respect to the atmospheric pressure (≅ 100 kPa). Here the coefficient of normalization, C_q, is calculated and plotted for the mentioned methods as well as the data from the current study in figure 2-33. In this figure the trend line for each method is drawn based on the proposed equations and the data points for the current study are calculated assuming the measured q_c for test No.11, with the effective mean stress of 100 kPa, as q_{c1} and calculating the coefficient of normalization, C_q, using equation (2-4). As shown in figure 2-33, the C_q values suggested by Olsen and Mitchell (1995) (for exponent c=0.75) and Boulanger and Idriss (2004) and Kayen et al. (1992) are in a very good agreement with the measured data from the current study.

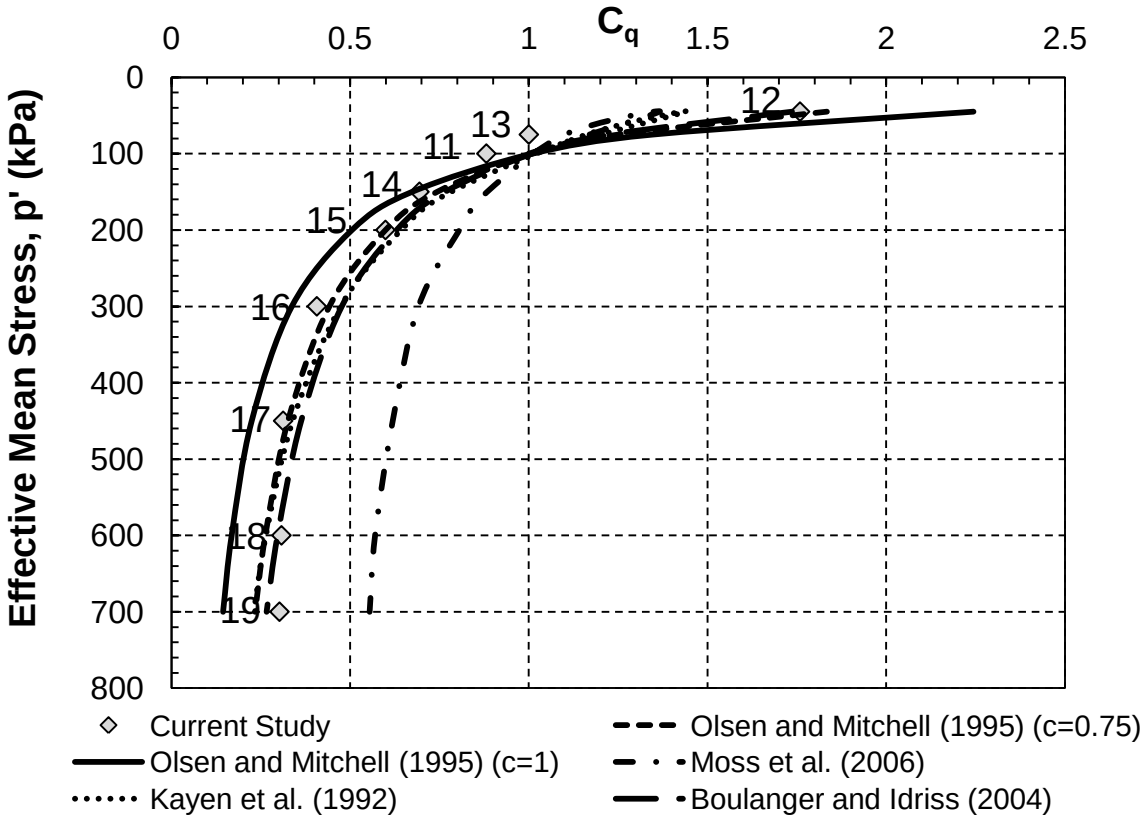

Figure 2-33: Comparison of the Coefficient of Normalization using different methods with data from tests No 11-19 (Numbers next to the data points show the Test. No.).

2.4.7 The Effect of Increase in Mean Effective Stress on q_c and f_s

Many researchers argued that the penetration resistances are a function of both soil's void ratio and stress level (Been et al. 1987; Konrad 1997; Fear and Robertson 1995; Been and Jefferies 1992). Here, the effect of increase in mean effective stress has been studied in tests No. 11 to 19 which were performed at the same relative densities. Figures 2-34 and 2-35 show the cone tip resistance and sleeve friction measured in tests No. 11 to 19 versus mean effective stress. These figures confirm that penetration resistances increase with increasing stress level at a constant void ratio. The equation of trend lines can be used to describe the relationship between stress level and penetration resistances for the tested sand. Note that this relationship will be different for other soils with different critical satate parameters (Been et al. 1987; Konrad 1997).

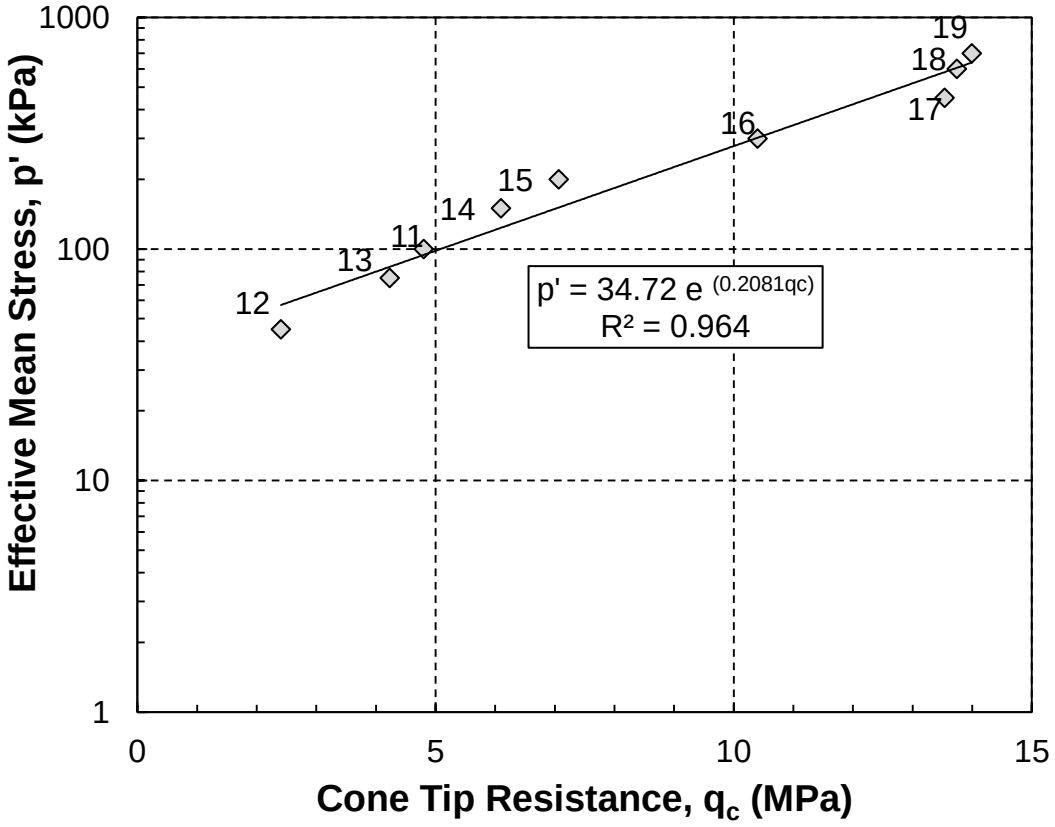

Figure 2-34: Cone tip resistance versus effective mean stress for tests No 11-19. (Numbers next to the data points show the Test. No.)

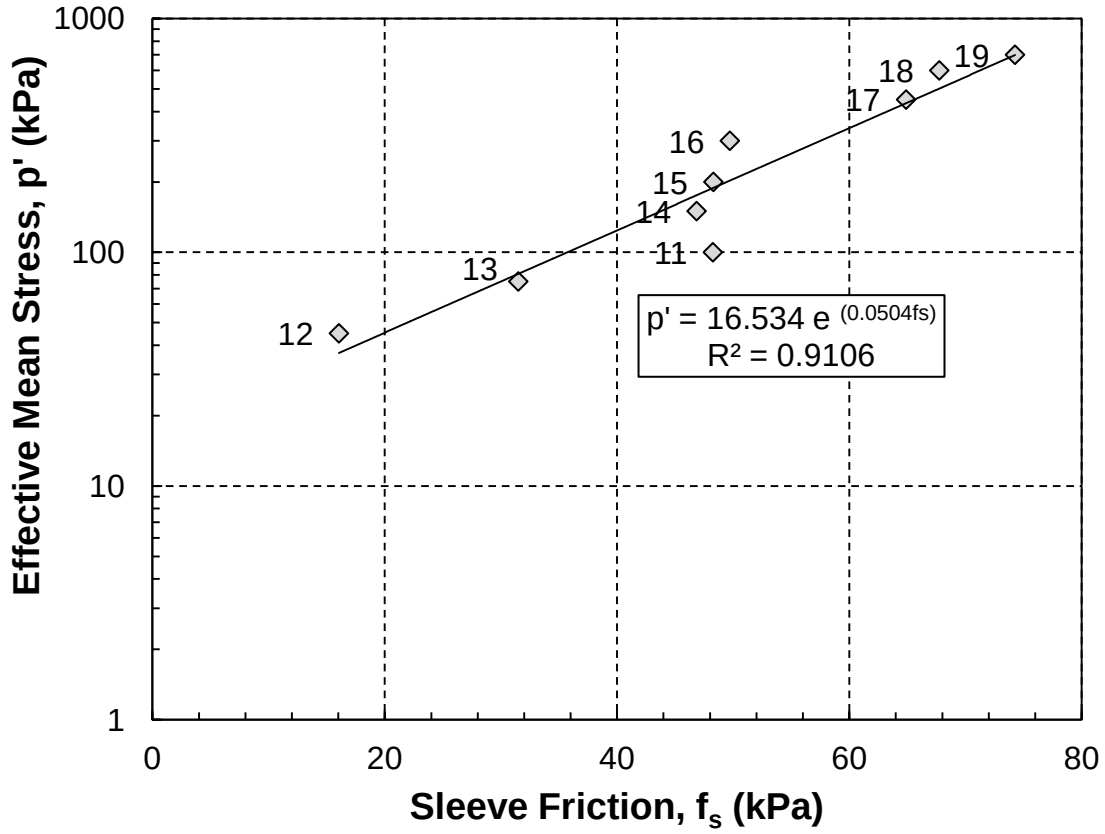

Figure 2-35: Sleeve friction versus effective mean stress for tests No 11-19.
(Numbers next to the data points show the Test. No.)

2.4.8 The Effect of Increase in Relative Density on q_c and f_s

The effect of increase in relative density has been studied in tests No. 4 to 11 which were performed at the same stress levels. Figures 2-36 and 2-37 show the cone tip resistance and sleeve friction measured in tests No. 4 to 11 versus consolidated relative density. Cone tip resistance and sleeve friction both increase with increasing the relative density. Figure 2-36 shows that there is a unique relationship between relative density and cone tip resistance. While, the scatter in the data presented in figure 2-37 is higher.

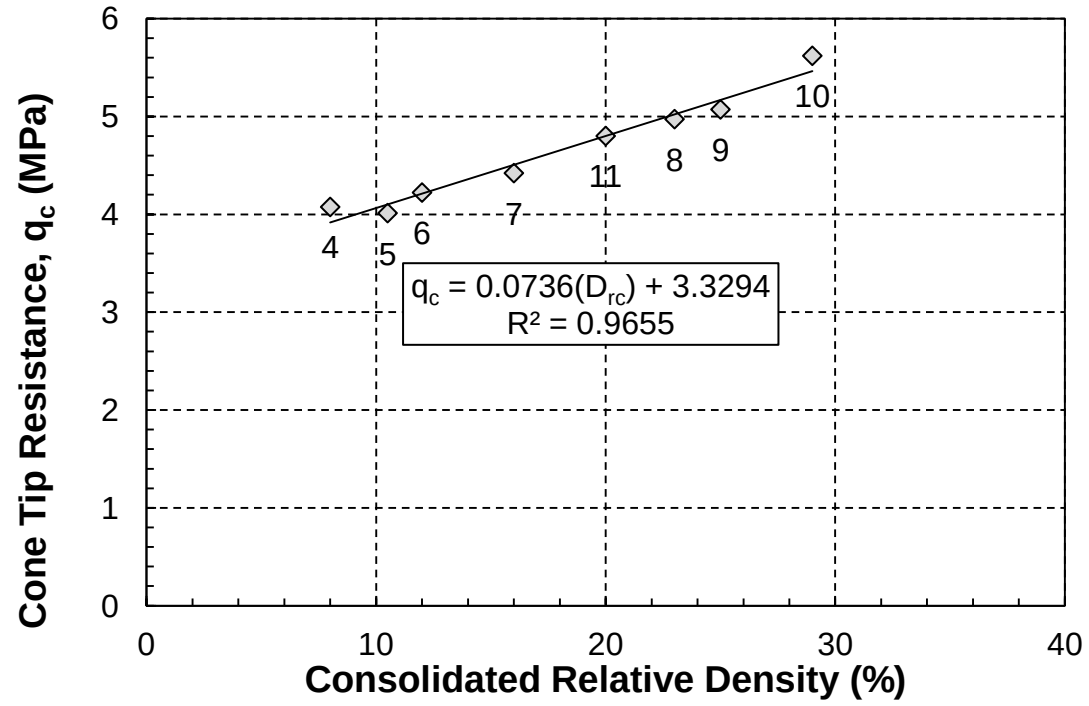

Figure 2-36: Cone tip resistance versus consolidated relative density for tests No. 4 to 11. (Numbers next to the data points show the Test. No.)

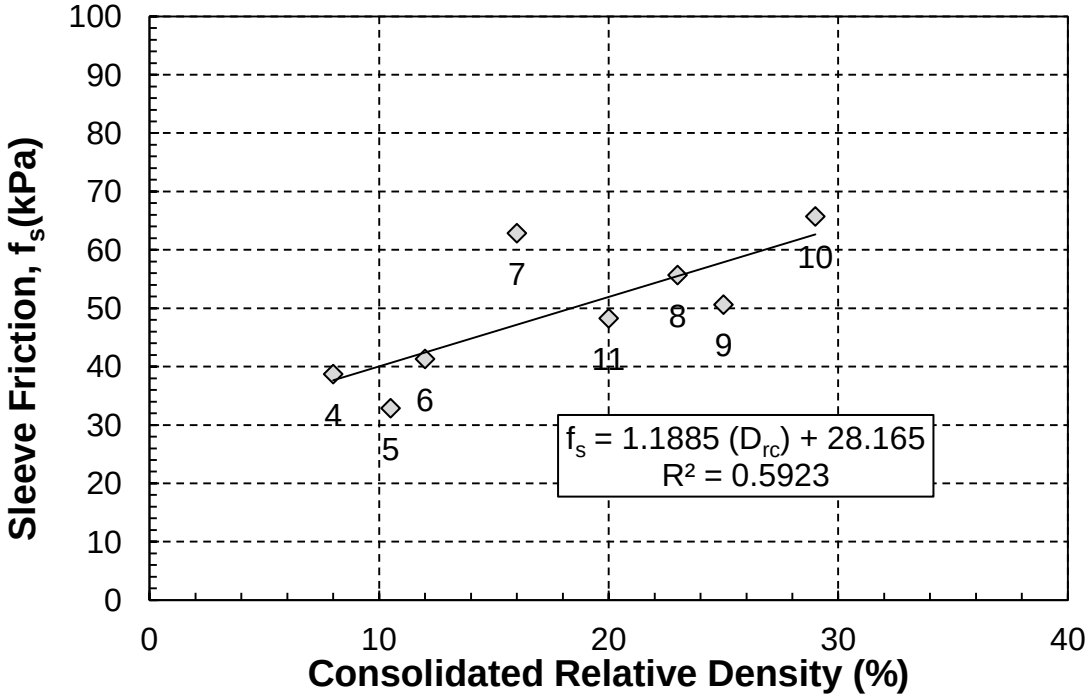

Figure 2-37: Sleeve friction versus consolidated relative density for tests No. 4 to 11. (Numbers next to the data points show the Test. No.)

2.5 Verification of CPT Measurements

The cone tip resistances measured in this study are within the range of q_c = 4-14 MPa (except for test No. 12), and Q = $(q_t-\sigma_v)/\sigma'_{vo}$ = 19 – 58.9 which are close to the range of typical q_c (> 5 MPa, Mayne 2007) and Q (> 20, Schneider et al. 2008) for sands. The lower values are measured in very loose specimens (D_{rc} = 8%) and are also due to the very fine gradation of Barco 71 sand, measured q_c value for test No. 12 is lower than the suggested rate which is due to the very low mean effective stress in that test. The CPT measurements of this study are further verified in the following paragraphs by comparison with calibration chamber miniature CPT on similar sands and evaluating the data for soil classification.

2.5.1 Comparison with Previous Studies

Past investigators have generally carried out calibration chamber CPT tests on medium dense to dense sands (Baldi et al. 1982, Huang and Hsu 2005, Harman 1976, Lhuer 1976). However, Triangale (1983) and Huntsman (1985) present very few CPT calibration chamber tests on loose Monterey sand, and Bonita (2000) presents some few data on Light Castle sand. Table 2-9 compares the CPT values from these studies with the experiment results of this study at similar D_{rc}. Note that because of the differences in stress level, the comparison is made based on q_{c1}.

Table 2-9: Comparison with the available data in the literature.

Test No	D_{rc} (%)	σ'_v (kpa)	σ'_h (kpa)	p' (kpa)	q_c (Mpa)	Kayen et al. (1992)	Olsen and Mitchell (1995)(c=0.75)	reference
03/26/99	20.1	99	43	61.67	3.05	3.88	4.41	Bonita (2000)
15	20	200	200	200	7.06	4.54	4.23	Current Study
19	19	700	700	700	13.99	3.23	3.28	Current Study

Harman (1976) performed a comprehensive cone penetration testing program on Ottawa sand using the University of Florida calibration chamber. The state parameter, ψ_{cs} (Been

and Jefferies 1985) can be used to combine the effect of D_{rc} and p'_c on sand behavior. Since the critical state line was also established by Harman (1976), ψ_{cs} is used for comparing the CPT results of Harman (1976) with those from this study. According to Figure 2-38, the results of the current study are in a very good agreement with data from Harman (1976) for $\psi_{cs} > -0.05$.

Omar (2013) performed comprehensive triaxial testing on Barco 71 and reported the slope of the critical state line, λ, and the intercept of critical state line, Γ, for this sand as presented in Table 2-10 which were used in this study to estimate the state parameter.

To ensure the validity of using the data reported by Omar (2013) and combining them with the results of the current study the tested material, preparation method and test procedure used by Omar (2013) have been compared with the current study. Omar (2013) reported the same gradation curve and very close values for e_{max} and e_{min} of the tested soil confirming that the soil tested in both studies is the same. Moreover, sample preparation method was checked and found to match the specimen preparation method used in the current study. The same as the procedure used in the current study, Omar (2013) used moist tamping method with an initial moisture content of 5 percent and a maximum under compaction ratio of 10 percent. The same Triaxial apparatus was also used by Omar (2013) and saturation and consolidation of the specimens were performed following the same stages.

Table 2-10: Critical State parameters of Barco 71 (Omar 2013).

Property	**value**
λ (in natural log scale)	0.0231
Γ	0.887

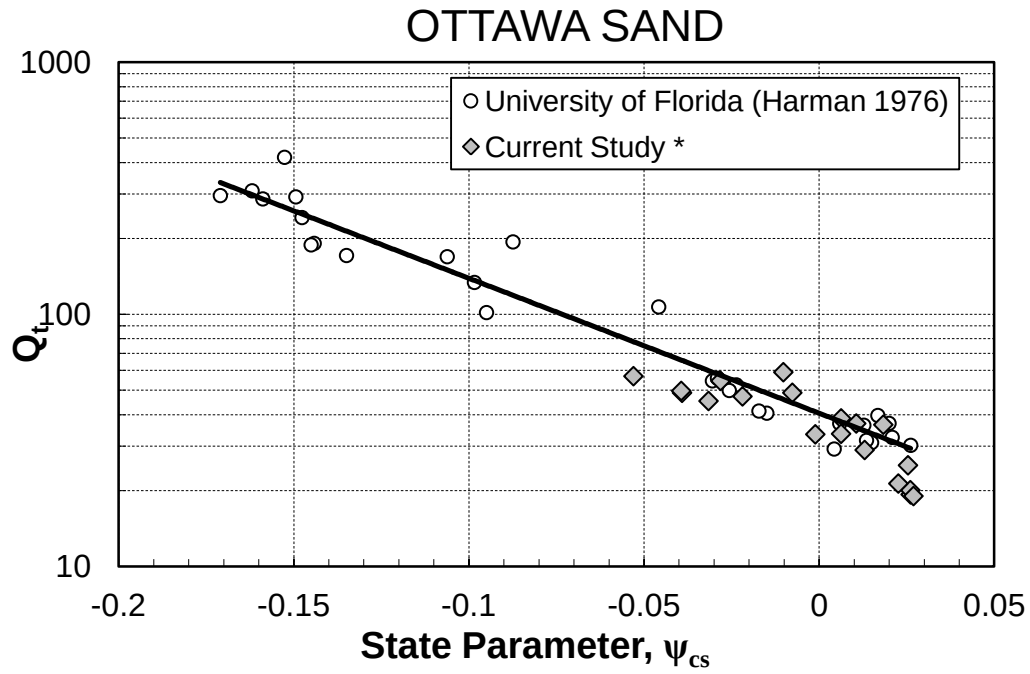

Figure 2-38: Comparison of normalized cone tip resistances of this study with those of Harman (1976) based on ψ_{cs}. (* Note that the state parameters were calculated based on the critical state parameters reported by Omar (2013) for Barco 71)

2.5.2 Evaluation for soil classification

Several studies have proposed empirical plots or correlations for soil classification based on CPT measurements (Robertson 1990; Eslami and Fellenius 1997; Mayne 2006; Schneider et al. 2008). For example, Eslami and Fellenius (1997) proposed a generalized plot for sands, silts, and clays based on 106 load tests from both driven and bored pile foundations. Mayne (2006) compiled CPT data from a series of well-documented geotechnical experimental test sites in clays, silts and sands and developed Figure 2-40 for CPT-based soil classification. Schneider et al. (2008) developed a framework for classifying soil based on piezocone test results, using the cone tip resistance and pore-water pressure at the cone shoulder, u_2. Figures 2-39 to 2-42 compare the data from this study with the soil type boundaries or zone of these studies. According to to Figures 2-39

to 2-42, the CPT results of this study plot around or within the boundary for sands and silty sands, which reflect the very fine nature of Barco 71 sand. These data indicate a drained sand behavior in Figure 2-42, conforming the zero excess pore water pressure measured during cone penetration.

The data from the current study plot at the boundary between sands and silts, which again indicate the very fine gradation of Barco 71 sand.

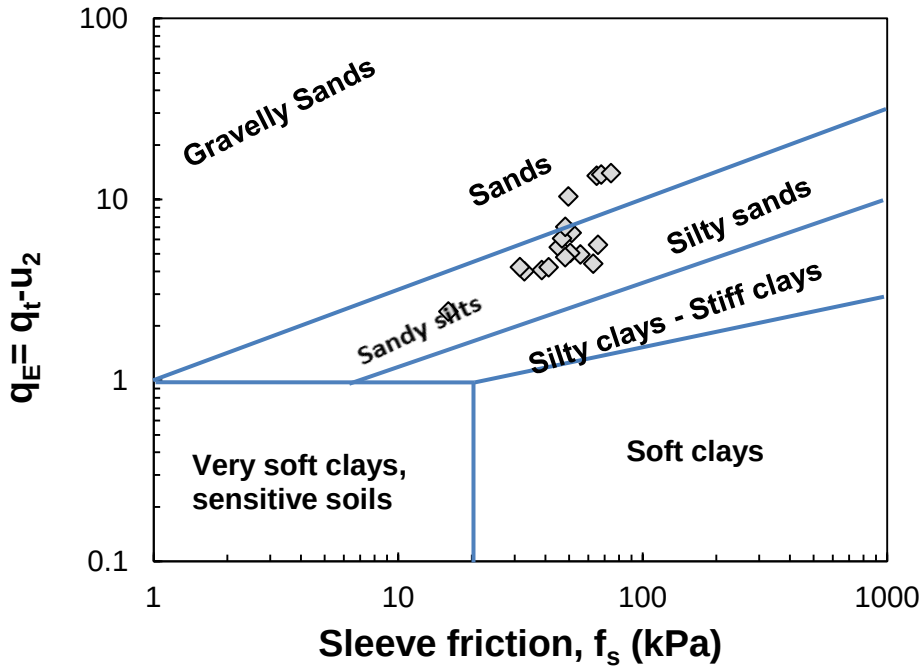

Figure 2-39: Comparison of CPT data of this study with soil type boundaries of Eslami and Fellenius (1997)

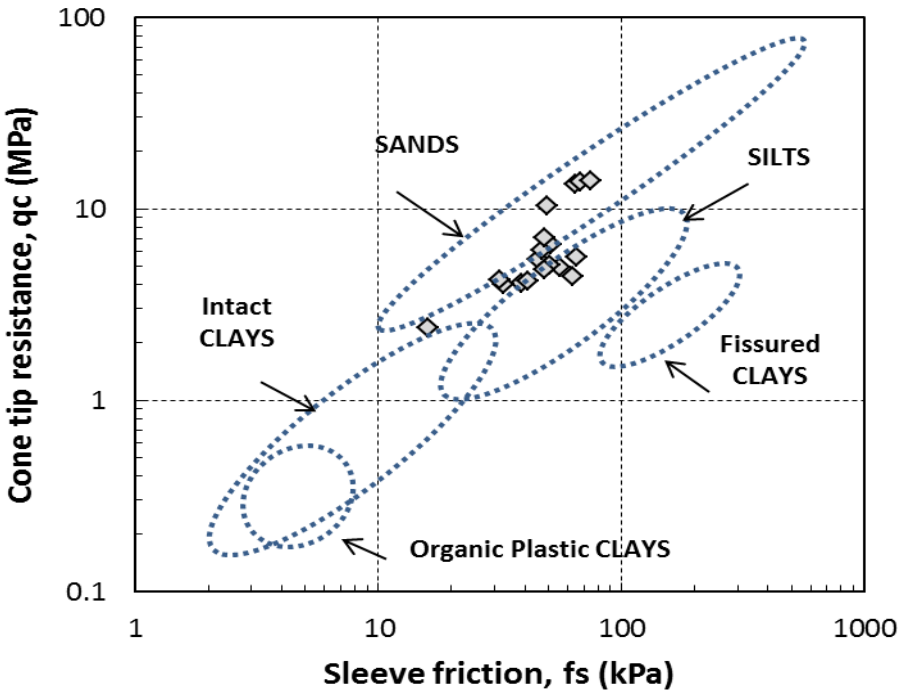

Figure 2-40: Comparison of CPT data of this study with soil identification zones of Mayne (2006)

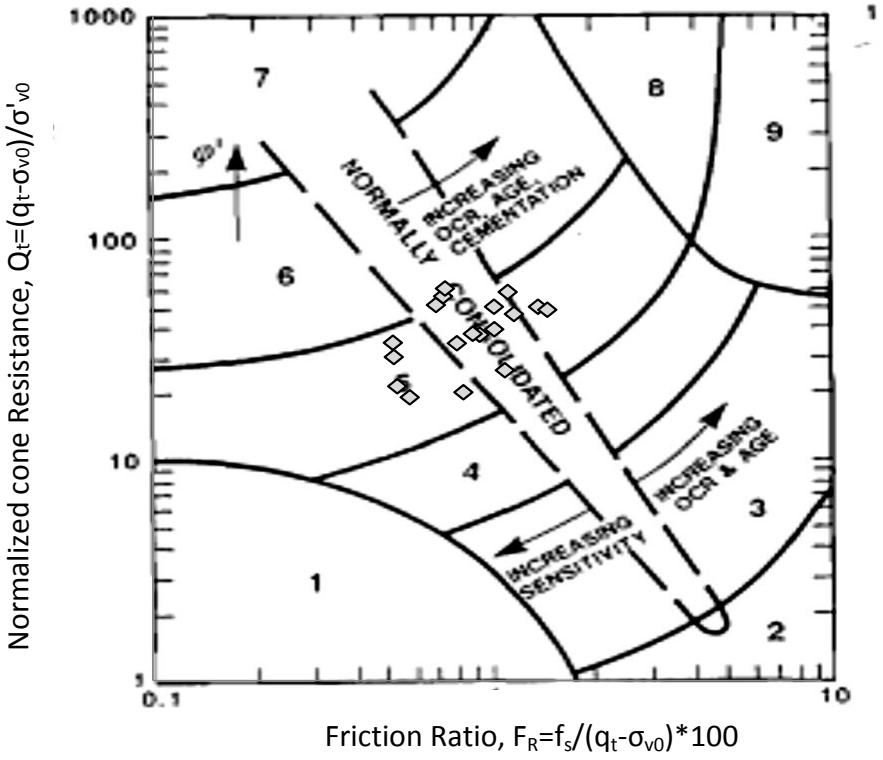

1. Sensitive fine grained
2. Organic Soils
3. Clays – clay to silty clay
4. Silt Mixtures – clayey silt to silty clay
5. Sand Mixtures – silty sand to sandy silt
6. Sands – clean sands to silty sands
7. Gravelly sand to sand
8. Very stiff sand to clayey sand
9. Very stiff fine grained

Figure 2-41: Comparison of CPT data of this study with soil identification zones of Robertson (1990)

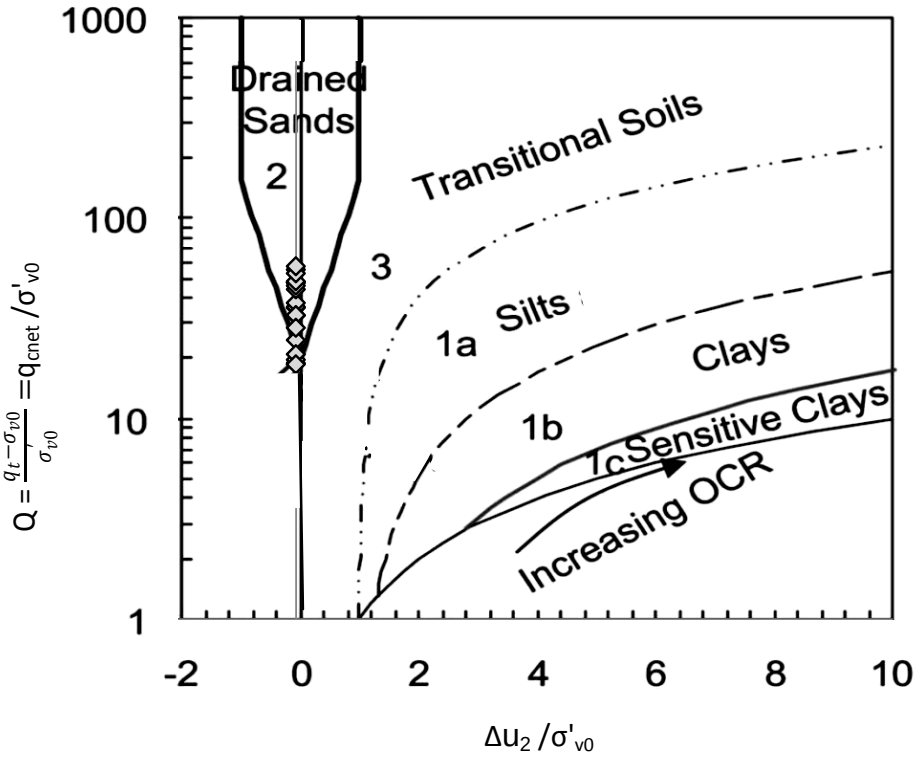

Figure 2-42: Comparison of CPT data of this study with soil type zones of Schneider et al. (2008)

2.6 Conclusions

Considering the difficulties associated with preparing loose sand samples in large calibration chambers and wide area of research on the behavior of loose sands, a miniature cone calibration chamber has been designed and developed in this study. The largest possible specimen that could be accommodated by the available load frame and the smallest cone that could be made by the university machine shop were designed. Therefore the cone diameter to sample diameter was increased to a value of 25 which has been demonstrated to exhibit negligible boundary condition effects in loose sands. Flexible latex membrane was used around the sample and the cell fluid surrounding the sample was pressurized to apply isotropic pressures to the sample. Therefore, constant stress boundary condition, BC1, was simulated. A pressure transducer was connected to the cone through the hollow shaft and a small tube welded to the cone probe which was used to measure the pore water pressure generated at the tip of the cone during penetration.

Nineteen CPT tests were performed on Ottawa sand and the results were compared to the available data in the literature. The accuracy of the results was validated by comparing the results with the suggested rate for the cone resistance in sands in literature. More specifically, results were compared with the results of the large calibration chamber tests performed on the same soil at University of Florida. Results were in a very good agreement with the literature and data available from large calibration chambers. Different soil identification systems were used to further validate and compare the results.

Repeatability of the data obtained from the developed device was evaluated by repeating one of the tests. Results of the two tests were in a close agreement despite some minor differences due to the possible sample density nonuniformity. The effects of boundary conditions on the data were comprehensively discussed and it was concluded that boundary conditions were not affecting the results for the developed assembly when testing loose sands. The effect of cone penetration rate on the cone tip and sleeve friction was studied by performing two tests on the sample with same properties at the same

stress level but with different penetration rates. Results indicated that penetration rate has no effect on the results of the tests performed on sand which was backed up with the available literature as well. The possibility of particle crushing for the tested material was studied by taking samples from the soil adjacent to the cone probe and performing sieve analysis. No particle crushing was observed for the tested material.

Based on the results of the miniature CPT experiments, available methods for overburden stress normalization were evaluated and compared to find the method with the best performance. The effect of increase in relative density and stress level on penetration resistances was also studied. Both tip resistance and sleeve friction increased with increasing density or stress level.

The advantages of the developed miniature cone calibration chamber could be summarized as bellow:

- Use of the hydraulic pumps enables the researcher to monitor the precise change in the void ratio of the specimen during saturation, consolidation and the penetration stages.
- Minimizing the boundary condition effect by carefully designing the miniature penetrometer size compared to the specimen size and designing the specimen height in a manner that the cone does not sense the lower boundary of the specimen.
- Simplifying the design in order to measure all the data produced by CPT (q_c,f_s and u) while using the existing equipment and obtaining verified results same as the results produced in large calibration chambers.

References

ASTM Standard D4253, (2006), "Standard Test Methods for Maximum Index Density and Unit Weight of Soils Using a Vibratory Table," ASTM International,West Conshohocken, PA. DOI: 10.1520/D4253-00R06. www.astm.org.

ASTM Standard D4254, (2006), "Standard Test Methods for Minimum Index Density and Unit Weight of Soils and Calculation of Relative Density," ASTM International,West Conshohocken, PA. DOI: 10.1520/D4254-00R06E01. www.astm.org.

ASTM Standard D5778, (2012), "Standard Test Method for Electronic Friction Cone and Piezocone Penetration Testing of Soils," ASTM International, West Conshohocken, PA. DOI: 10.1520/D5778-12. www.astm.org.

Abedin, M. Z., (1995), "The characterization of unsaturated soil behaviour from penetrometer performance and the critical state concept," PhD Thesis, The University of Newcastle upon Tyne, UK.

Abedin, M.Z., Hettiaratchi, D.R.P., (2002). "State parameter interpretation of the cone penetration tests in agricultural soils," *Biosystems Engineering* 83, 469-479.

Ahmadi, M. M., Byrne, P. M., Campanella R. G., (2005) "Cone tip resistance in sand: modeling, verification, and applications" *Canadian Geotechnical Journal*, 42(4): 977-993, 10.1139/t05-030

Bałachowski, L. (2007). "Size effect in centrifuge cone penetration tests". *Archives of Hydro-Engineering and Environmental Mechanics*, 54(3), 161-181.

Baldi, G. Bellotti, R. Ghionna, V. Jamiolkowski, M. and Pasqualini, E., (1982), "Design Parameters for Sands from CPT," *Proceedings of the 2nd European Symposium on Penetration Testing*, Amsterdam, 2: 425-432.

Baldi, G., Bellotti, R., Ghionna, V., Jamiolkowski, M. and Pasqualini, E. (1986). Interpretation of CPTs and CPTU's, 2nd Part. *Proceedings of the 4th International Geotechnical Seminar*, Nanyang Technological Institute, Singapore, 143–156.

Been, K. Jefferies, M.B. Crooks, J.H.A. and Rothenburg, L., (1987), "The cone penetration test in sands, part 2. General inference of state," *Géotechnique*, 37(3): 285–299.

Been, K. and Jefferies, M.G., (1992), "Towards systematic CPT interpretation," *In Proceedings of the Wroth Symposium*, Oxford, U.K. pp. 44–55.

Bellotti, R., Pedroni, S., (1991), "Design and development of a small calibration chamber for compressible sands." *Proceedings of the 1st International Symposium on Calibration Chamber Testing*, Elsevier, Potsdam, New York. pp. 91-100.

Belloti, R., Crippa, V., Pedroni, S. and Ghionna, V.N. (1988), "Saturation of Sand Specimen for Calibration Chamber Tests," *Proceedings of the ISOPT-1*, Orlando, Vol.2, pp.661-672.

Boulanger, R. W. and Idriss, I. M. (2004). State normalization of penetration resistances and the effect of overburden stress on liquefaction resistance, *in Proceedings, 11th International Conference on Soil Dynamics and Earthquake Engineering, and 3rd International Conference on Earthquake Geotechnical Engineering,* D. Doolin et al., eds., Stallion Press, Vol. 2, pp. 484–91.

Bonita, J. A., (2000), "The Effects of Vibration on Penetration Resistance and Pore Water Pressure in Sands," Civil Engineering. Virginia Polytechnic Institute, Blacksburg, VA.

Butlanska, J., Arroyo M., Gens, A., O'Sullivan, C., (2014) "Multi-scale analysis of cone penetration test (CPT) in a virtual calibration chamber" *Canadian Geotechnical Journal*, 51(1): 51-66, 10.1139/cgj-2012-0476

Canou, J., El Hachem, M., Kattan, A., Juran, I., (1988). "Mini piezocone (M-CPTU) investigation related to sand liquefaction analysis, *Proceedings of the 1st International Symposium on Penetration Testing, ISOPT-1,* Orlando, Florida, pp 699-706.

Chen, C. C., (2000), "Shear Induced Evolution of Structure in Water-Deposited Sand Specimens," School of Civil and Environmental Engineering. Georgia Institute of Technology. Atlanta, GA, Ph.D. Dissertation: 497pp

Dayal, U. and Allen, J. H., (1975), "The Effect of Penetration Rate on the Strength of Remoulded Clay and Sand Samples," *Canadian Geotechnical Journal*, Vol. 12, pp. 336–347.

Eid, W.K., (1987), "SCALING EFFECT IN CONE PENETRATION TESTING IN SAND". Virginia Polytechnic Institute and State University.

Eslami, A. and B.H. Fellenius, (1997), "Pile Capacity by Direct CPT and CPTu Methods Applied to 102 Case Histories", *Canadian Geotechnical Journal*, Vol. 34, No. 6, pp. 880-898.

Fear, C. E. Robertson, P. K., (1995), "Estimating the undrained strength of sand: a theoretical framework," *Canadian Geotechnical Journal* 32: 859-870

Franzen, J. H., (2006), "Cone penetration resistance in silt," M.S. Thesis, University of Rhode Island.

Ghionna V.N., and Jamiolkowski M. (1991). "A Critical Appraisal of Calibration of Calibration Chamber Testing of Sands." *Proceedings of the 1st International Symposium on Calibration Chamber Testing, ISOCCT 1*, Potsdam, New York, 13-39.

Gui M. W. and Bolton M. D. (1998). "Geometry and scale effects in CPT and pile design", *Proceedings of International Conference Geotechnical Site Characterization, Eds.* P. Robertson and P. Mayne, Balkema, Rotterdam, 1063–1068.

Harman, D.E. (1976), "A Statistical Study of Static Cone Bearing Capacity, Vertical Effective Stress, and Relative Density of Dry and Saturated Fine Sands in a Large, Triaxial Test Chamber," Master of Engineering Thesis, University of Florida, 181 pp.

Holden, J. (1971), "Laboratory Research on Static Cone Penetrometers," University of Florida, August, 91 pp.

Houlsby, G. (1988), "Discussion session contribution". Penetration Testing in the U.K., Birmingham.

Huang, A. B. (1992), "Calibration chamber testing," Clarkson University, Postdamn New York .13699.

Huang, A. B. and Hsu, H. H., (2005), "Cone Penetration Tests under Simulated Field Conditions," *Géotechnique*, 55(5): 345-354.

Huntsman, S.R. (1985). Determination of in situ lateral pressure of cohesionless soils by static cone penetrometer. PhD Thesis, University of California at Berkeley.

Idriss, I. M., and Boulanger, R. W. (2007). "SPT- and CPT-based relationships for residual shear strength of liquefied soils." *Proceedings of the 4th Int. Conf. on Earthquake Geotechnical Engineering*, K. D. Pitilakis, ed., Springer, New York, 1–22.

Jacobs, P.A., Coutts, J.S., (1992). "A comparison of electric piezocone tips at the Bothkennar test site." *Géotechnique,* 42, 369-375.

Jamiolkowski, M. Ladd, C. C. Germaine, J.T. and Lancellotta, R., (1985), "New Developments in Field and Laboratory Testing of Soils," *Proceedings of the 11th ICSMFE*, San Francisco, CA, 1: 54-154

Jang, D.-J. (1997). "Quantification of Sand Structure and Its Evolution During Shearing Using Image Analysi"s. School of Civil and Environmental Engineering. Georgia Institute of Technology. Atlanta, Ph.D. Dissertation: 259pp

Jasinski, J. D. (2008), "Mini cone chamber testing of silt," M.S. Thesis, University of Rhode Island.

Jefferies, M.G. and Been, K., (2006), "Soil liquefaction , a critical state approach," Published by Taylor & Francis

Kayen, R.E., Mitchell, J.K., Seed, R.B., Lodge, A., Nishio, S., and Coutinho, R. (1992). "Evaluation of SPT-, CPT-, and shear wavebased methods for liquefaction potential assessments using Loma Prieta data". *In Proceedings of the 4th Japan–U.S. Workshop on Earthquake Resistant Design of Lifeline Facilities and Countermeasures for Soil Liquefaction*, Honolulu, Hawaii. Vol. 1, pp. 177–192.

Kokusho, T. Murahata, K. Hushikida, T. and Ito, N., (2003), "Introduction of miniature cone in triaxial apparatus and correlation with liquefaction strength," *Proceedings of the Annual Convention of Japan Society of Civil Engineers (JSCE),* Tokyo, Japan, III-96, Japan Society for Civil Engineers, 191–192 (in Japanese).

Konrad, J. M., (1997), "In situ sand state from CPT: evaluation of a unifed approach at two CANLEX sites," *Canadian Geotechnical Journal*, 1: 120-130.

Kumar, J. and Raju, K.V.S.B., (2008), "Correlation between miniature cone tip resistance and shear strength parameters of clean and silty sand using a conventional triaxial setup," *Geotechnical Testing Journal*, 31(3): 206–216.

Ladd, R. S., (1987), "Preparing Test Specimens Using Undercompaction," *Geotechnical Testing Journal*, 1(1): 16-23.

Lhuer, J.-M. (1976); "An experimental study of quasi-static cone penetration in saturated sands." MSc Thesis, University of Florida.

Löfroth, H., (2008), "Undrained shear strength in clay slopes – Influence of stress conditions, A model and field test study," Thesis. Chalmers University of Technology. Gothenburg.

Lunne,T. Robertson, P.K. and Powell, J.J.M.,(1997), "Cone Penetration Testing in Geotechnical Practice," Routledge, Blackie Academic & Professional. London.

Ma, M.Y., (1994). "A numerical Study of cone penetration test in granular assemblies." Clarkson University.

Mayne, P.W., (2006), "In-Situ Test Calibrations for Evaluating Soil Parameters" Overview Paper on In-Situ Testing - Singapore Workshop, Nov. 29- Dec. 01, 2006

Mayne, P.W., (2007), "Cone Penetration Testing State-of-Practice" NCHRP Project 20-05, Topic 37-14.

Mitchell, J. K., Chatoian, J. M. and Carpenter, G. C. (1976). "The Influence of Sand Fabric on Liquefaction Behavior." Report to U.S. Army Corps of Engineers of Engineers Waterways Experiment Station. Vicksburg, Miss.

Moss; R. E. S. Seed; R. B. and Olsen R. S., (2006) . "Normalizing the CPT for Overburden Stress." *Journal of Geotechnics and Geoinvironment* 132, pp. 378-387.

Mulilis, J. P., Seed, H. B., Chan, C. K., Mitchell, J. K. and Arulanandan, K. (1977). "Effects of Sample Preparation on Sand Liquefaction." *Journal of Geotechnical Engineering Division, ASCE,* 103(GT2): 91-107.

Olsen, R. S. and Mitchell, J. K. (1995). "CPT stress normalization and prediction of soil classification." *Proceedings of the Int. Symp. on Cone Penetration Testing, CPT 95,* Linkoping, Sweden, 257–262.

Olson, S. M., and Stark, T. D. (2003). "Yield strength ratio and liquefaction analysis of slopes and embankments." *Journal of Geotechnical and Geoenvironmental Engineering,* 129_8_, 727–737.

Omar, Tarek., (2013), "Specimen Size Effect on Shear Behavior of Loose Sand in Triaxial Testing," University of Western Ontario - Electronic Thesis and Dissertation Repository. Paper 1755.

Park, J. Y. (1999). “A Critical Assessment of Moist Tamping and Its Effect on the Initial and Evolving Structure of Dilatant Triaxial Specimens.” School of Civil and Environmental Engineering. Georgia Institute of Technology. Atlanta, Ph.D. Dissertation: 384pp

Parkin, A.K. (1988), "The Calibration of Cone Penetrometers," *Proceedings of the First International Symposium on Penetration Testing, ISOPT-1,* Orlando, Florida, 20-24 March, Vol. 1, pp. 221-243

Parkin, A. Holden, J. Aamot, K. Last, N. and Lunne, T., (1980), “Laboratory investigations of CPT's in sand,” Norwegian Geotechnical Institute, Report 52108-9.

Parkin, A. and Lunne, T., (1982), “Boundary Effects in the Laboratory Calibration of a Cone Penetrometer in Sand,” *Proceedings of ESOPT II,* Balkema, Amsterdam, The Netherlands, 2: 761-768.

Peterson, R.W., (1988). “Laboratory investigation of the penetration resistance of fine cohesionless materials,” *Proceedings of the First International Symposium on Penetration Testing,* Orlando, Florida, pp. 895-901.

Pournaghiazar, M., Russel, A.R., Khalili, N., (2011). “Development of a new calibration chamber for conducting cone penetration tests in unsaturated soils.” *Canadian Geotechnical Journal* 48, 314-321.

Robertson, P.K., (1990), “Soil Classification Using the Cone Penetration Test,” *Canadian Geotechnical Journal,* 27(1): 151-158. Doi:10.1139/t90-014.

Robertson P.K., and Wride C.E. (1998). “Evaluating Cyclic Liquefaction Potential Using the Cone Penetration Test.” *Canadian Geotechnical Journal,* 35(3): 442-459.

Russell, A. R. and Khalili, N., (2002), “Drained cavity expansion in sands exhibiting particle crushing,” *International Journal for Numerical and Analytical Methods in Geomechanics,* 26: 323–340 (DOI: 10.1002/nag.203).

Salgado, R., Boulanger, R. W., and Mitchell, J. K. (1997a). "Lateral stress effects on CPT liquefaction resistance correlations," *Journal of Geotechnical and Geoenvironmental Engineering*, ASCE 123(8), 726–35.

Salgado, R., Mitchell, J. K., and Jamiolkowski, M. (1997b). Cavity expansion and penetration resistance in sands *Journal of Geotechnical and Geoenvironmental Engineering*, ASCE 123(4), 344–54.

Schmertmann, J.H. (1976) " An Updated Correlation between Relative Density D_R and Fugro-Type Electric Cone Bearing, qc." Contract Report DACW 39-76 M 6646 WES, Vicksburg, Miss., 1976.

Schmertmann, J.H. (1978), "Guidelines for Cone Penetration Test, Performance and Design," Federal Highway Administration, Report FHWA-TS-78-209, Washington, July 1978, 145 pp.

Schneider, J.A., Randolph, M.F., Mayne, P.W., and Ramsey, N. (2008). "Analysis of factors influencing soil classification using normalized piezocone tip resistance and pore pressure parameters," *Journal of Geotechnical and Geoenvironmental Engineering*, 134(11): 1569-1586.

Seher, N.V., (2008). "Mini-cone chamber testing and liquefaction potential of silts," M.S. thesis. University of Rhode Island.

Sharp, Michael K., Ricardo Dobry, and Ryan Phillips. (2010). "CPT-based evaluation of liquefaction and lateral spreading in centrifuge." *Journal of geotechnical and geoenvironmental engineering*. 136.10: 1334-1346.

Shuttle, D. and Jefferies, M., (1998), "Dimensionless and unbiased CPT interpretation in sand," *International Journal for Numerical and Analytical Methods in Geomechanics*, 22: 351-391.

Sivathayalan, S., (1994), "Static. cyclic and post liquefaction simple shear response of sands". M.A.Sc. Thesis. University of British Columbia. Vancouver. BC. Canada. 139p.

Skempton, A.W., (1954). "The pore pressure coefficient A and B." *Géotechnique* 4. pp. 143-147.

Wroth, C.P. (1984). Interpretation of In situ soil test, *24th Rankine Lecture*, *Géotechnique*, 34: 449-489.

Yang, C.-T. (2002). "Boundary Condition and Inherent Stratigraphic Effects on Microstructure Evolution in Sand Specimens." School of Civil and Environmental Engineering. Georgia Institute of Technology. Atlanta, GA, Ph. D. Dissertation: 522pp

Yang, X. (2005). "Three-dimensional characterization of inherent and induced sand microstructure" PhD Dissertation, Georgia Institute of Technology, School of Civil and Environmental Engineering, Atlanta.

Chapter 3

3 CPT-based Static Liquefaction Evaluation

3.1 Introduction

Soil liquefaction is the main issue when constructing structures on or using saturated sandy soils especially for large soil structures such as mine tailings impoundments and earth dams (Robertson 2010). Liquefaction due to undrained strain softening of loose (or contractive) cohesionless soils which results in loss of shear strength by monotonically increasing loads is known as static or flow liquefaction (e.g., Jefferies and Been 2006, Lade and Yamamuro. 2011, Wanatowski and Chu 2007, Yamamuro and Lade 1997, McRoberts, and Sladen 1992). Moreover, flow liquefaction may follow liquefaction if the static driving shear stress is greater than the post-liquefaction shear strength (Poulos et al. 1985). Examples of flow liquefactions triggered by static loads include the failures of Calaveras Dam (Hazen 1918) and Fort Peck Dam (Casagrande 1965). Failures of the Lower San Fernando Dam, following the 1971 San Fernando earthquake (Castro et al. 1989; Seed et al. 1989) and Sheffield Dam, following the 1925 Santa Barbara earthquake (Seed et al. 1969) are examples of flow liquefactions induced by seismic loads.

3.2 Background

Flow liquefaction is a major geotechnical challenge when designing large soil structures, such as mine tailings impoundments and earth dams, which requires a liquefaction analysis to estimate the residual or liquefied shear strength of cohesionless soils.

A version of this chapter will be submitted to the Canadian Geotechnical Journal.

A liquefaction analysis for sloping ground where soil is subjected to a static driving shear stress consists of three steps. (1) a susceptibility analysis which determines if the soil deposit is susceptible to undrained strain-softening behavior and flow failure, (2) evaluation of liquefaction triggering and (3) post-triggering stability analysis using liquefied strength (Olson and Stark 2002, 2003).

In this study, the CPT based static liquefaction analysis procedures are reviewed and evaluated using the data from miniature laboratory CPT experiments and corresponding undrained shear strengths reported by Omar (2013) covering the three steps mentioned above.

3.2.1 Flow Liquefaction Susceptibility Analysis

Flow liquefaction requires a strain-softening soil response and strength loss. Therefore, evaluation of susceptibility to flow liquefaction involves evaluation of the potential for a saturated cohesionless soil to strain soften in undrained shear.

The concepts for strength loss and liquefaction in sands were first put forward by Casagrande (1940). Later, Schofield and Wroth (1968) developed the framework of critical state soil mechanics and, Castro (1969) employed critical state to define the post-liquefaction strength, s_u(liq) by expanding the critical void ratio concept. The concept of a critical void ratio and critical state soil mechanics are both based on the assumption that the behavior of cohesionless soil is controlled by both void ratio and effective stress.

The state parameter (ψ_{cs}), which is the difference between the initial void ratio of a soil from the void ratio on the critical state line (CSL) at the same effective stress level, has been suggested to combine the effects of void ratio (density) and effective stress for soil behavior characterization (Taylor 1948; Been and Jefferies 1985). The definition of ψ_{cs} is demonstrated in Figure 3-1.

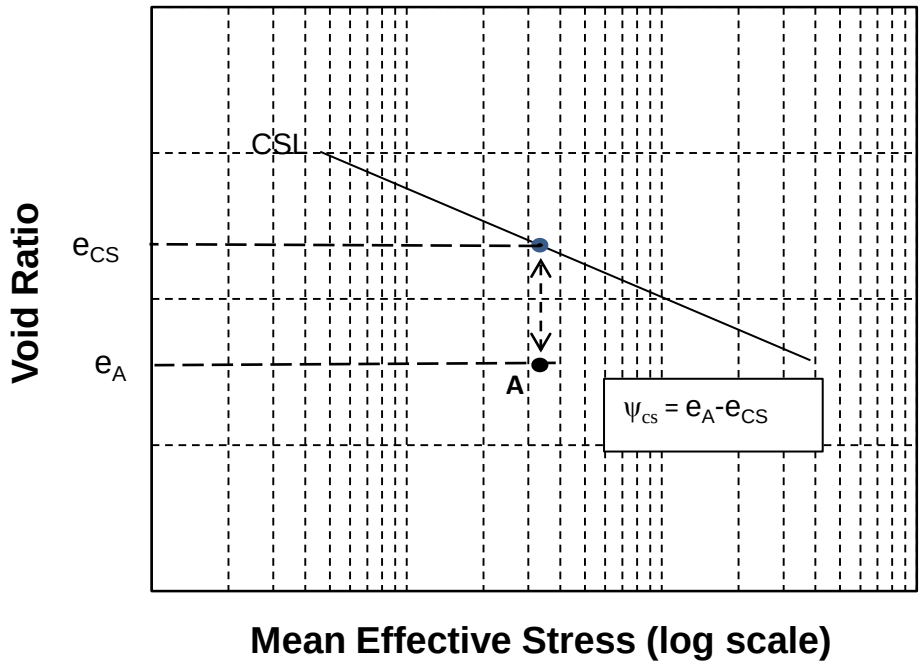

Figure 3-1: Definition of state parameter, ψ_{cs}

Jefferies and Been (2006) and Shuttle and Cunning (2007) suggested that for cohesionless soils with $\psi_{cs} > -0.05$, strain softening and strength loss in undrained shear can be expected. Hence, identifying soils based on this criterion is helpful as a screening technique to determine the susceptibility for flow liquefaction.

Some researchers have proposed susceptibility boundary lines between penetration resistance and effective confining stress to separate contractive from dilative soil states. For example, Fear and Robertson (1995) suggested an approximate boundary between the liquefiable and non-liquefiable soil response for Ottawa sand based on a proposed framework that can be used to estimate the in situ ultimate undrained steady state shear strength of sands.

Later, Robertson (2010) identified a zone on the soil behavior type plot, based on normalized cone tip resistance and friction ratio, that represents the approximate boundary between strain-hardening and strain-softening soil response based on the works

of Plewes et al. (1992), Jefferies and Been (2006), and Shuttle and Cunning (2007), combined with the test results from frozen samples (Robertson et al. 2000).

3.2.2 Liquefaction Triggering Analysis Using s_u(yield)

Static liquefaction triggering analysis involves evaluating whether the combined initial static and monotonic triggering shear stresses are sufficient to overcome pre-liquefaction mobilized undrained shear strength, s_u(yield) (Terzaghi et al. 1996, Poulos et al. 1985).

The yield strength ratio which is the undrained yield strength, presented as s_u(yield), normalized by the pre-failure vertical effective stress, σ'_{vo}, has been used to evaluate the triggering of liquefaction in contractive, sandy soils (Olson 2001; Sadrekarimi 2014; Olson and Stark 2003).

There has been a considerable interest in correlating s_u(yield)/σ'_{vo} with in-situ standard penetration (SPT) or cone penetration (CPT) resistances as obtaining undisturbed samples in cohesionless soils is very difficult and expensive. In fact, cohesionless soils cannot be properly reconstituted for laboratory tests as the information on consolidation and ageing history of in-situ cohesionless soil deposits is not readily available. Empirical correlations with in-situ SPT blow count, $(N_1)_{60}$, or CPT tip resistance, q_{c1}, are often used for estimating the in-situ triggering strength because of their simplicity, convenience, lower cost and continuous measurements.

Olson (2001) proposed a procedure to evaluate the triggering of liquefaction in ground subjected to a static shear stress using the yield strength ratio back calculated from liquefaction flow failures. Olson (2001) presented a range of back-calculated strength ratio and measured (or estimated) penetration resistance for each case history and plotted the best estimates of yield and mobilized strength ratios and mean q_{c1} values as shown in Figure 3-2.

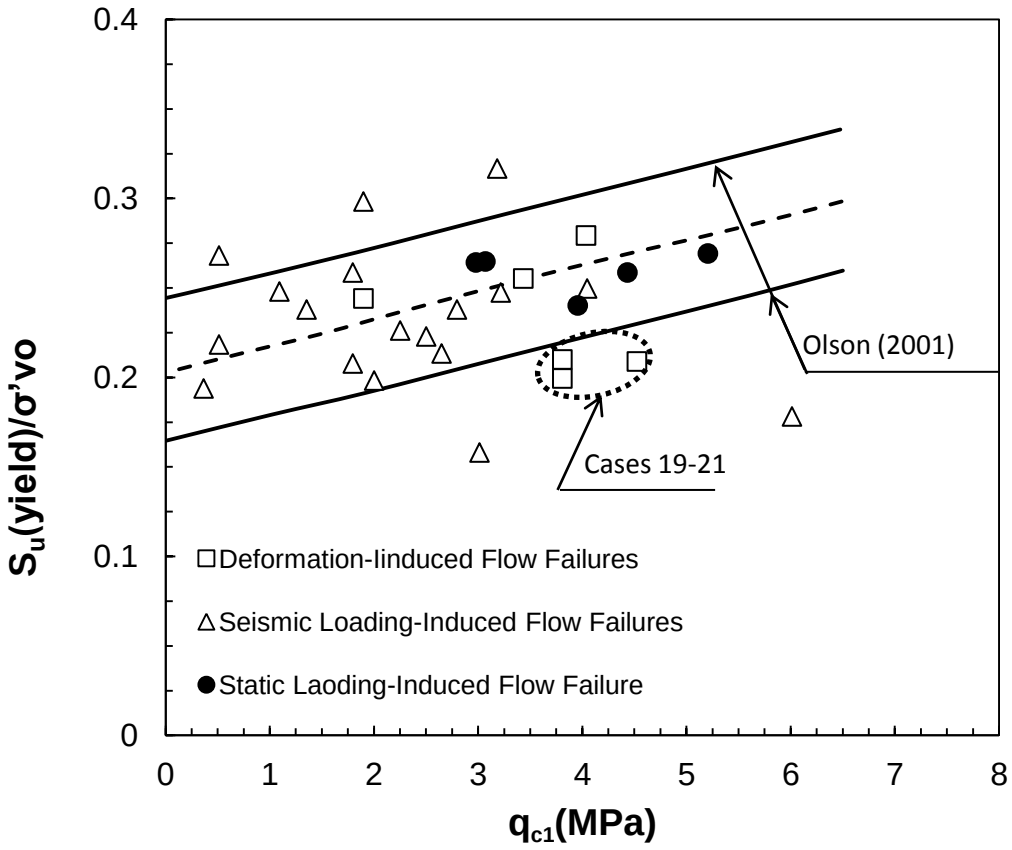

Figure 3-2: Comparison of yield strength ratios and corrected CPT tip resistance for liquefaction flow failures (Olson 2001)

Olson (2001) observed a trend of increasing yield strength ratio with increasing penetration resistance for the static loading and deformation-induced failures, excluding the Nerlerk berm cases (cases 19-21 in Figure 3-2). Considering the few data point above the trend line, it was concluded that there may be greater variability in the relationship between yield strength ratio and penetration resistance than that indicated by the static loading-induced cases. As a result, the upper and lower bound trend lines were positioned conservatively as follow:

$$\frac{S_u(yield)}{\sigma'_{v0}} = 0.205 + 0.0143\ (q_{c1}) \mp 0.04 \ \text{ for } \ q_{c1} \leq 6.5\ MPa \qquad (3\text{-}1)$$

Where, σ'_{v0} is pre-failure vertical effective stress and, $q_{c,1}$ is the normalized cone tip resistance calculated as follow:

$$q_{c,1} = C_q . q_c \tag{3-2}$$

Where;

q_c= raw tip resistance (MPa),

And, C_q is calculated using the following equation proposed by Kayen et al. (1992).

$$C_q = \frac{1.8}{0.8 + \frac{\sigma'_{v0}}{P_a}} \tag{3-3}$$

Sadrekarimi (2014) developed improved correlations for estimating undrained triggering shear strengths of cohesionless soils based on the most reliable field liquefaction data from past cases of liquefaction flow failures and soil shearing behavior in a large database of 893 laboratory shear tests for different modes of shear.

The proposed method by Sadrekarimi (2014) accounts for the variations in the mode of shear and anisotrpic consolidation, K_c in providing estimates of the undrained triggering strengths mobilized in static liquefaction flow failures.

Sadrekarimi (2014) compared the r_u-I_B trend lines associated with different K_c values considering different modes of shear and suggested empirical relationships between I_B and r_u for cohesionless soils. Sadrekarimi (2014) suggested to calculate s_u(yield) using the definition of I_B (Equation 3-4) and with an estimation of s_u(liq) based on in situ test measurements such as SPT or CPT (Equation 3-5).

$$I_B = \frac{\frac{s_u(\text{yield})}{\sigma'_{1c}} - \frac{s_u(\text{liq})}{\sigma'_{1c}}}{\frac{s_u(\text{yield})}{\sigma'_{1c}}} \tag{3-4}$$

According to Sadrekarimi (2014), $s_u(liq)/\sigma'_{1c}$ can be estimated using Equation (3-5):

$$\frac{S_u(liq)}{\sigma'_{1c}} = 0.022 + 0.017\,(q_{c1}) \;\text{ for }\; q_{c1} \leq 8\,MPa \tag{3-5}$$

And, I_B is calculated using the following equations:

$$I_B^* = \propto (r_u^*)^2 + \beta r_u^* + \gamma \tag{3-6}$$

In which:

$$I_B^* = I_B - A\frac{1-K_c}{K_c{}^{0.5}} \tag{3-7}$$

$$r_u^* = \frac{r_u}{1-B(1-K_c)} \tag{3-8}$$

Where; parameters A and B are used to take into account the effect of mode of shearing (A=1.0 and B=0.60 for TxC), and parameters α, β, and γ characterize the level of anisotropic consolidation (K_c) and are equal to 0.9768, 0.997 and -1.0318 respectively for TxC.

r_u is calculated using the following equation for triaxial compression tests:

$$r_u = K_c - \frac{2s_u(\text{liq})}{\sigma'_{1c}\cos\varphi'_{cs}(tan^2\left(45+\frac{\varphi'_{cs}}{2}\right)-1)} \tag{3-9}$$

Note that $\sigma'_{1c} = P'$ in isotropic consolidation, and, $K_c = 1$, therefore $r_u^* = r_u$ and $I_B^* = I_B$.

3.2.3 Post-Liquefaction Strength of Soil, s_u(liq)

The undrained shear strength mobilized at large deformation by a saturated contractive soil following the triggering of a strain-softening response and liquefaction is referred to as the post-liquefaction shear strength, s_u(liq) (Olson and Stark 2002; Olson 2001). However, some researchers have also used other terms to describe the same phenomenon, for example the undrained residual shear strength (Seed and Harder 1990), undrained critical (Sadrekarimi and Olson 2011) or steady-state (Poulos et al. 1985) shear strength, or the ultimate stress (Verdugo and Ishihara 1996).

The liquefied strength ratio which is the post-liquefaction shear strength, presented as $s_u(liq)$, normalized by the pre-failure vertical effective stress, σ'_{vo}, has been used to evaluate the shear strength of soil after liquefaction in contractive, sandy soils (Olson 2001; Sadrekarimi 2014; Olson and Stark 2002).

Olson (2001) back calculated the liquefied strength ratio for 33 cases where flow failure had happened and plotted the best estimates of liquefied strength ratios and mean q_{c1} values as shown in Figure 3-3.

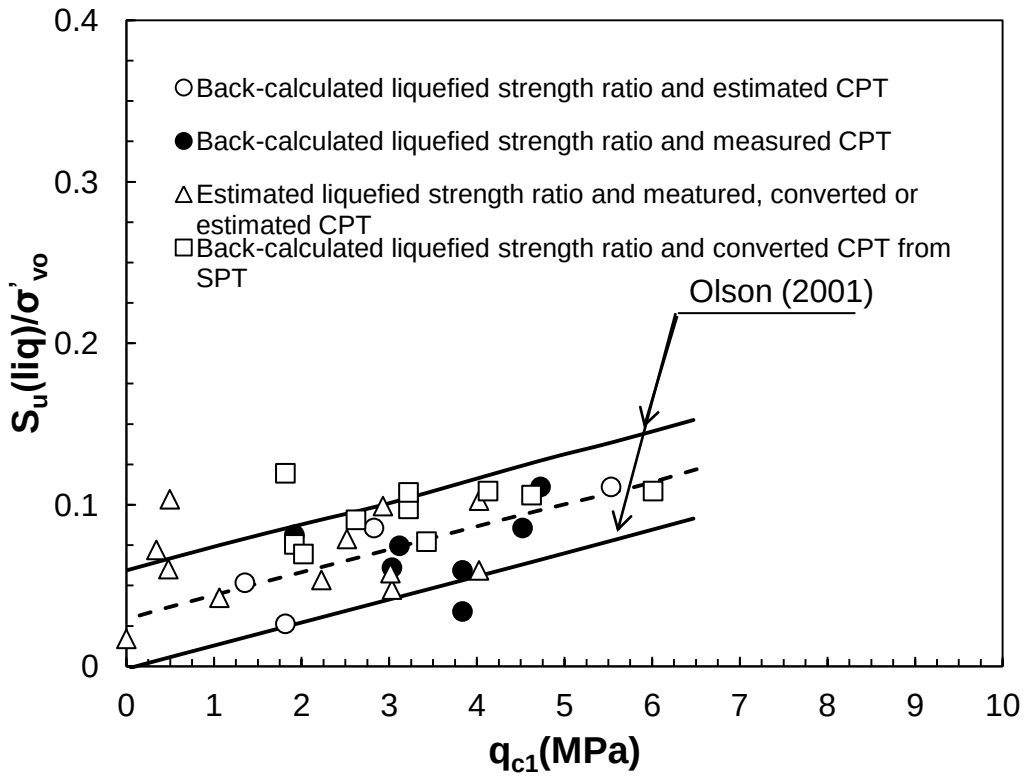

Figure 3-3: Comparison of $s_u(liq)/\sigma'_{vo}$ and corrected CPT tip resistance from the back-analyses of liquefaction flow failures (Olson 2001)

Despite some scatter, Olson (2001) observed a reasonable trend in the data shown in Figure 3-3, particularly for the cases where the most information is available. Upper bound, lower bound, and average trend lines suggested by Olson (2001) are shown in Figure 3-3. The average trend line was defined as follow:

$$\frac{S_u(liq)}{\sigma'_{v0}} = 0.03 + 0.0143\ (q_{c1}) \mp 0.03 \ \text{ for } \ q_{c1} \leq 6.5\ MPa \qquad (3\text{-}10)$$

The procedure suggested by Kayen et al. (1992) is used for the overburden stress normalization of q_c to obtain q_{c1}.

Sadrekarimi (2014) re-evaluated the database of liquefaction flow failures analyzed by Olson (2001) and Muhammad (2012) and used the cases with the highest level of confidence in backcalculating S_u(liq) with a direct measurement of SPT or CPT resistances. The penetration resistances indirectly predicted from the SPT blow counts, (Kulhawy and Mayne, 1990, Stark and Olson, 1995), inferred from relative density, or based on typical values in comparable soil types were avoided to minimize the level of uncertainties.

The following relationship was subsequently established based on CPT resistance.

$$\frac{S_u(liq)}{\sigma'_{v0}} = 0.022 + 0.017\ (q_{c1}) \ \text{ for } \ q_{c1} \leq 8\ MPa \qquad (3\text{-}11)$$

3.3 Evaluation of the available procedures for liquefaction analysis

3.3.1 Liquefaction susceptibility

Methods described at section 3.2.1 are evaluated and compared using the miniature laboratory CPT experiments performed in the current study. Table 3-1 summarizes the state parameter and stress characteristics of the miniature cone penetration tests conducted in this study. As presented in this table, all tests have a state parameter of larger than -0.05 except for test No. 10. Hence, According to Jefferies and Been (2006) and Shuttle and Cunning (2007), strength loss in undrained shear can be expected in all the tests except for test No. 10. Three triaxial compression tests have been performed on samples with the same test condition as tests No. 10, 11 and 12 to further evaluate the criteria suggested by Jefferies and Been (2006) and Shuttle and Cunning (2007).

Table 3-1: Summary of miniature CPT tests performed in this study

Test No	ψ_{cs}	p'_c (kPa)	q_{c1} (MPa)	Q_t	F_R(%)
1	0.0201	500	3.19	19.18	0.44
2	0.0200	300	3.10	19.99	0.85
3	0.0194	200	3.50	25.50	1.13
4	0.0123	100	4.08	38.00	0.95
5	0.0046	100	4.01	37.13	0.91
6	0.0003	100	4.22	38.73	1.05
7	-0.0137	100	4.42	41.71	1.42
8	-0.0376	100	4.97	47.23	1.20
9	-0.0452	100	5.07	47.72	1.05
10	-0.0590	100	5.62	54.20	1.15
11	-0.0279	100	4.80	45.76	1.52
12	-0.0454	45	3.46	49.01	0.70
13	-0.0342	75	4.91	53.74	0.74
14	-0.0162	150	4.77	38.64	0.75
15	-0.0071	200	4.54	33.32	0.81
16	0.0003	300	4.93	33.16	0.52
17	0.0070	450	4.60	28.64	0.53
18	0.0166	600	3.64	21.57	0.54
19	0.0209	700	3.23	18.85	0.59

Results of the triaxial compression tests are presented in figures 3-4 to 3-9. As shown in these figures strain hardening happened after soil yielded which suggests that the suggested criteria by Jefferies and Been (2006) and Shuttle and Cunning (2007) , $\psi_{cs} > -0.05$, for soils to strain soften underestimates the required state parameter at which the soil's behaviour changes from contractive to dilative.

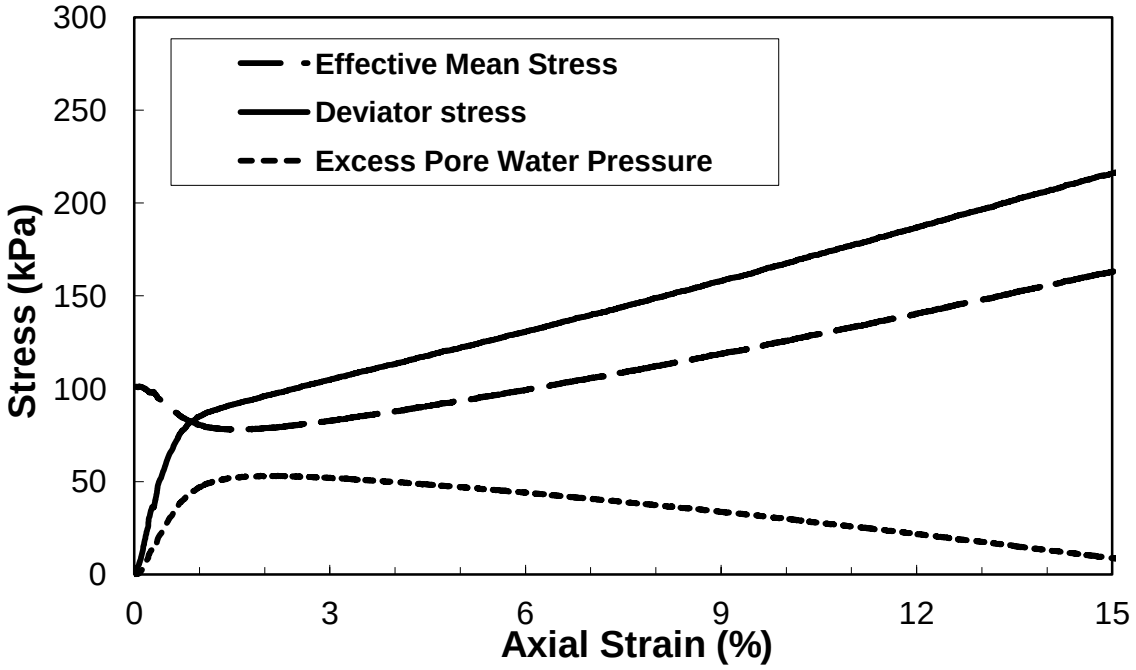

Figure 3-4: Stress-Strain response of undrained triaxial compression test on a sample with D_{rc} = 29% at p'_c = 100 kPa (Test No. 10.)

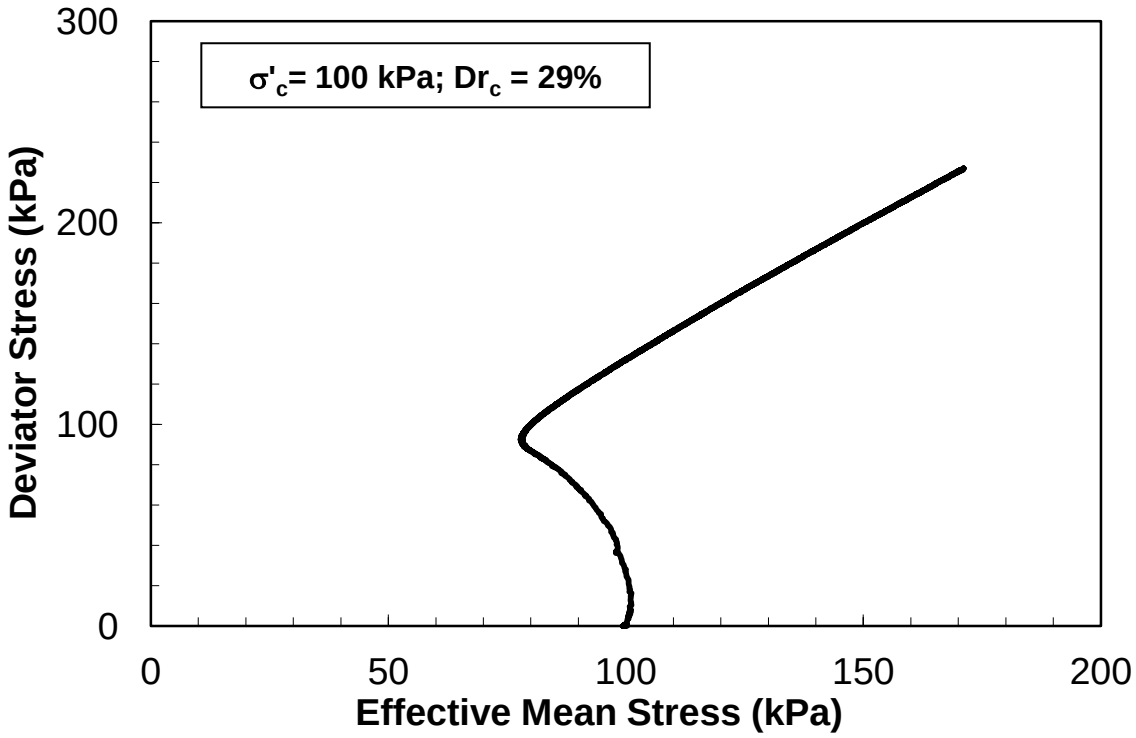

Figure 3-5: Effective stress path of undrained triaxial compression test on a sample with D_{rc} = 29% at p'_c = 100 kPa (Test No. 10.)

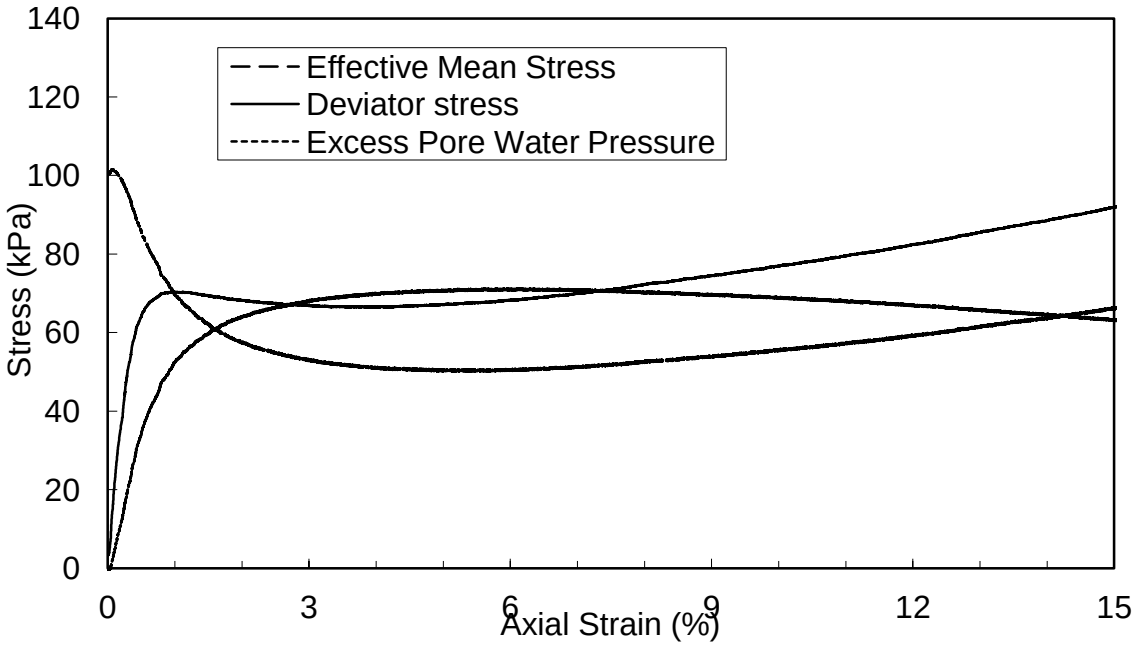

Figure 3-6: Stress-Strain response of undrained triaxial compression test on a sample with D_{rc} = 20% at p'_c = 100 kPa (Test No. 11.)

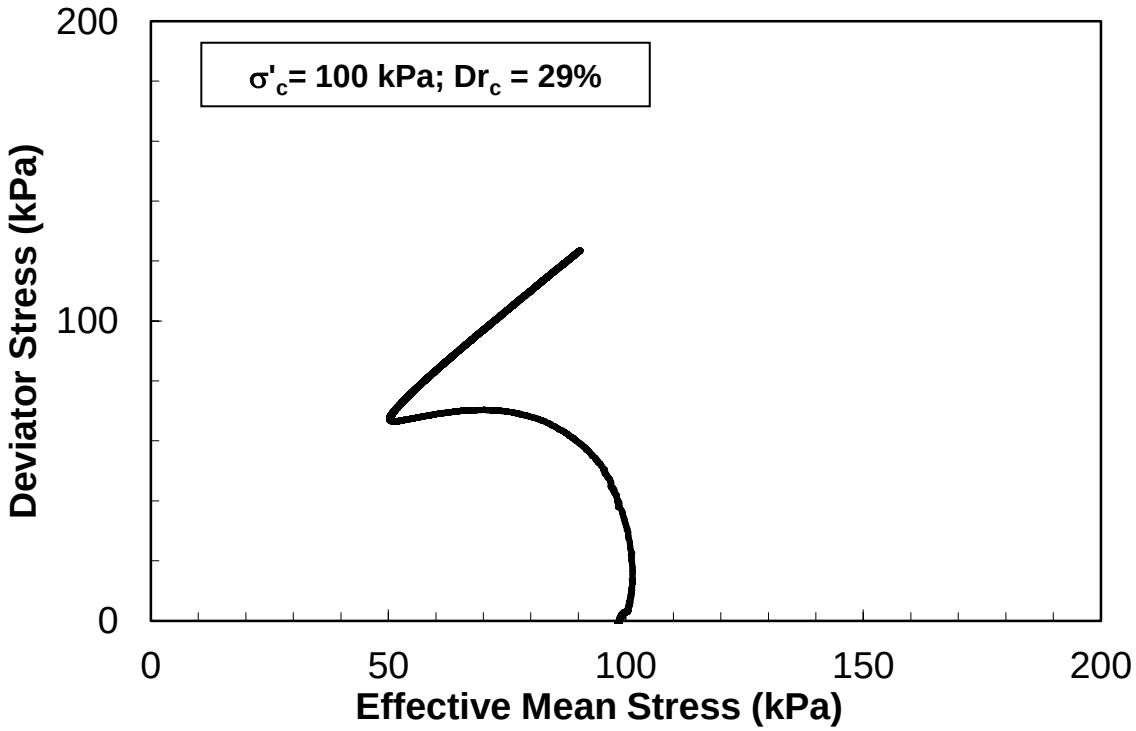

Figure 3-7: Effective stress path of undrained triaxial compression test on a sample with D_{rc} = 20% at p'_c = 100 kPa (Test No. 11.)

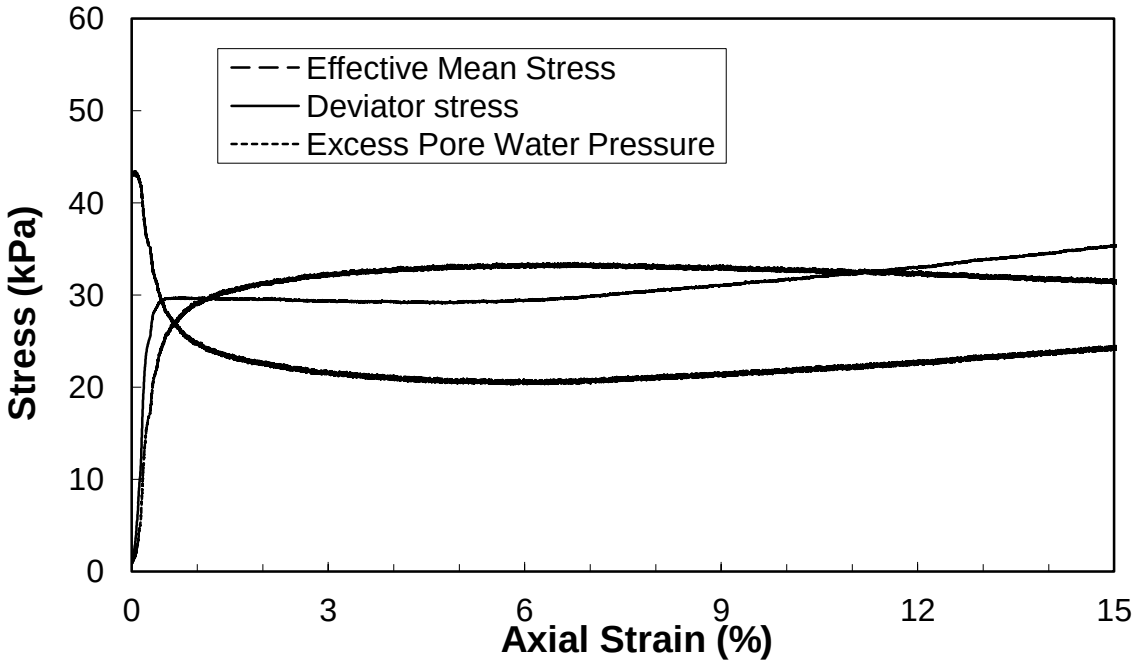

Figure 3-8: Stress-Strain response of undrained triaxial compression test on a sample with D_{rc} = 20% at p'_c = 45 kPa (Test No. 12.)

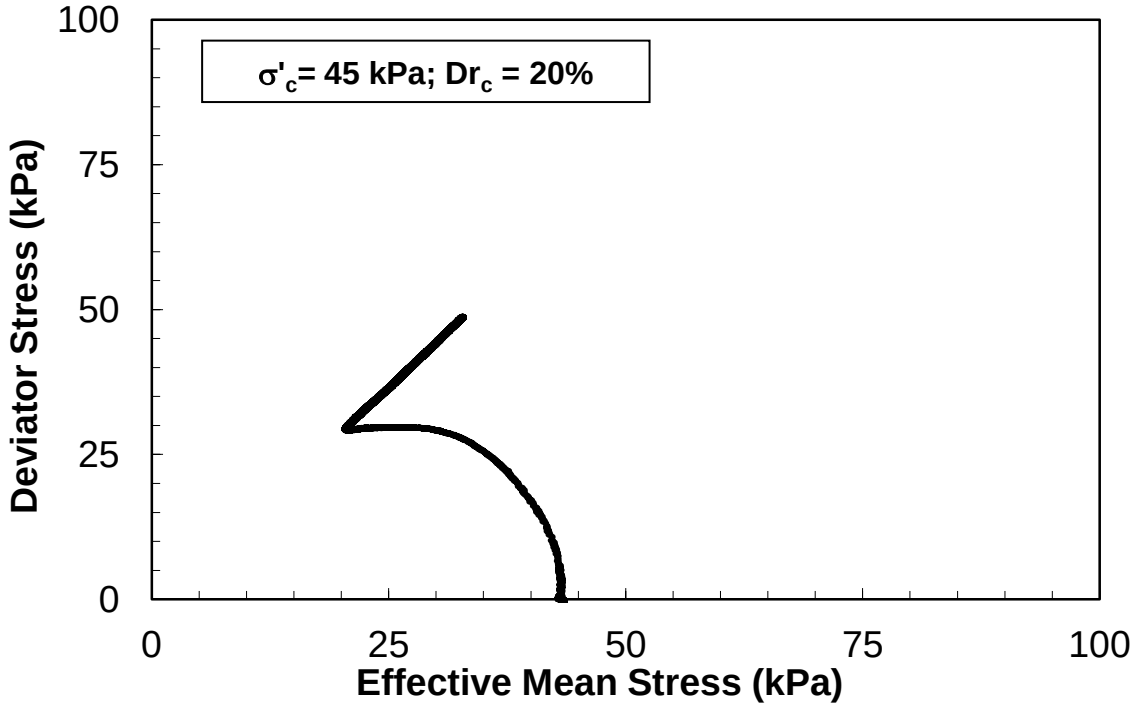

Figure 3-9: Effective stress path of undrained triaxial compression test on a sample with D_{rc} = 20% at p'_c = 45 kPa (Test No. 12.)

Figures 3-10 and 3-11 show the identification charts by Robertson (2010) and Fear and Robertson (1995), as well as the data from the current study. According to the chart suggested by Robertson (2010) almost half of the tests were not likely to liquefy but the boundary suggested by Olson and Stark (2003) (shown in figure 3-10), suggests that all the tests were likely to liquefy.

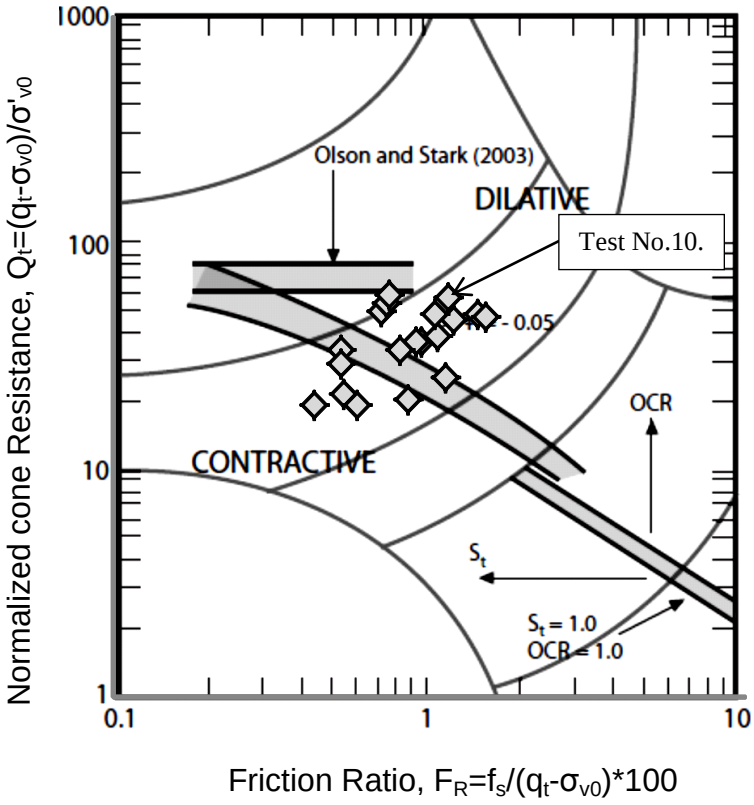

Figure 3-10: Approximate boundary between dilative and contractive soil response from Robertson (2010) and data from current study

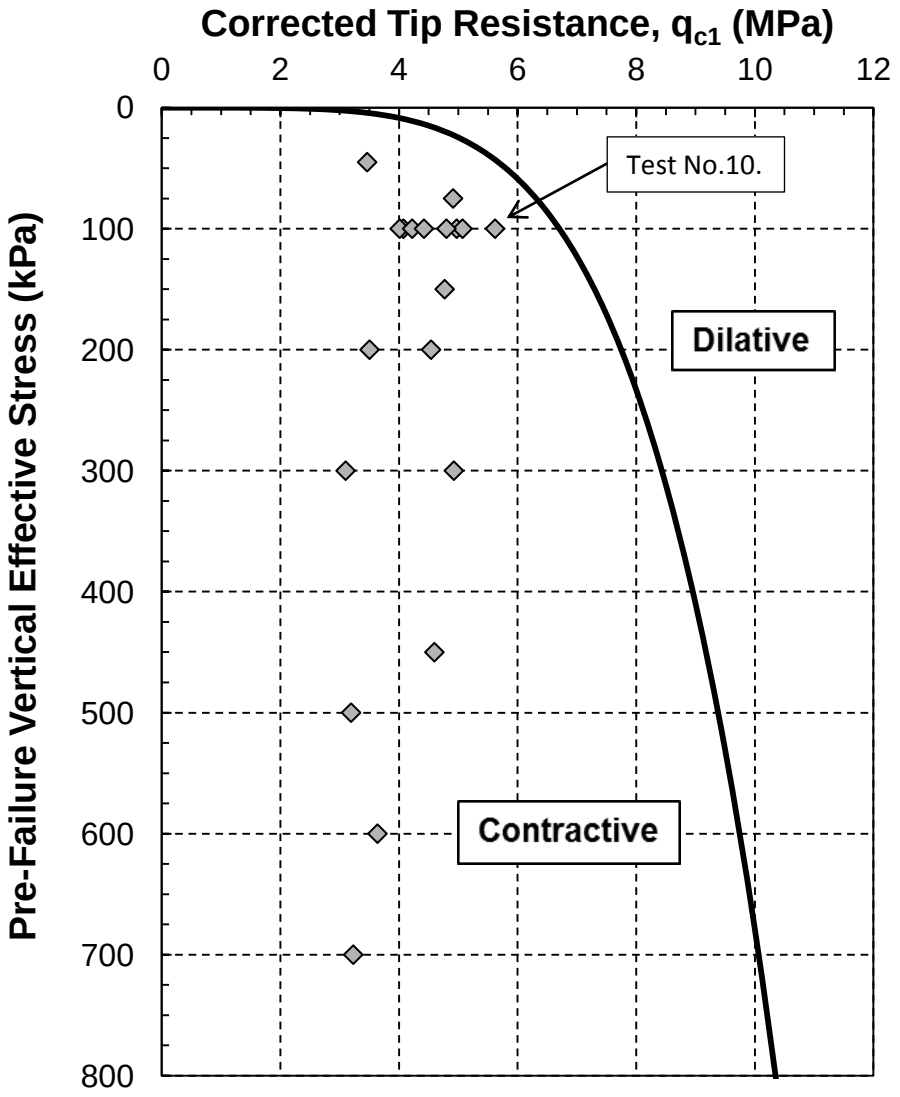

Figure 3-11: Boundary between dilative and contractive soil response from Fear and Robertson (1995) and data from current study

3.3.2 Liquefaction triggering analysis

Here, the correlations suggested by Olson (2001) and Sadrekarimi (2014) are evaluated using the cone tip resistances measured in the miniature CPT performed in the current study and the undrained shear strengths for Barco 71 reported by Omar (2013) and a number of triaxial test performed in the current study.

To ensure the validity of using the data reported by Omar (2013) and combining them with the results of the current study the tested material, preparation method and test procedure used by Omar (2013) have been compared with the current study. Omar (2013) reported the same gradation curve and very close values for e_{max} and e_{min} of the tested soil confirming that the soil tested in both studies is the same. Moreover, sample preparation method was checked and found to match the specimen preparation method used in the current study. The same as the procedure used in the current study, Omar (2013) used moist tamping method with an initial moisture content of 5 percent and a maximum under compaction ratio of 10 percent. The same Triaxial apparatus was also used by Omar (2013) and saturation and consolidation of the specimens were performed following the same stages.

Omar (2013) performed undrained triaxial compression tests on Ottawa sand specimens with an initial relative density of 0% and consolidation isotropic effective stresses of, p'_c = 100, 200, 300, and 500 kPa. Two other triaxial compression tests were performed in the current study on samples with an initial relative density of 20% and consolidation isotropic effective stresses of, p'_c = 300 and 450 kPa to cover the range of the q_{c1} values obtained in the current study.

Miniature cone penetration tests were performed at similar D_{rc} and p'_c and the obtained cone tip resistances are plotted versus the values of s_u(yield)/ σ'_{v0} from triaxial compression tests (from Omar (2013) and current study) on 70 mm diameter specimens. The cone tip resistances are normalized by the method proposed by Kayen et al. (1992). The undrained shear strengths and the corresponding cone tip resistance values are presented in Table 3-2. The stress-strain behaviour of the triaxial tests performed in the current study are presented in Appendix D. These data are used to evaluate the q_{c1} - s_u(yield)/σ'_{v0} correlations proposed by Olson and Stark (2003) and Sadrekarimi (2014).

Table 3-2: s_u(yield) and q_{c1} values used to evaluate the available correlations

CPT Test No	Stress level (kPa)	q_{c1} (MPa) (Current Study)	$S_u(yield)/\sigma'_{vo}$ (Omar 2013)	$S_u(yield)/\sigma'_{vo}$ (Current Study)	$S_u(yield)/\sigma'_{vo}$ (Olson 2001)	$S_u(yield)/\sigma'_{vo}$ (Sadrekarimi 2014)
4	100	4.08	0.219	-	0.263	0.242
3	200	3.50	0.194	-	0.255	0.216
2	300	3.10	0.165	-	0.249	0.198
1	500	3.19	0.142	-	0.251	0.202
16	300	4.93	-	0.235	0.271	0.265
17	450	4.60	-	0.226	0.275	0.280

Results of the comparisons are presented in Figures 3-12 and 3-13.

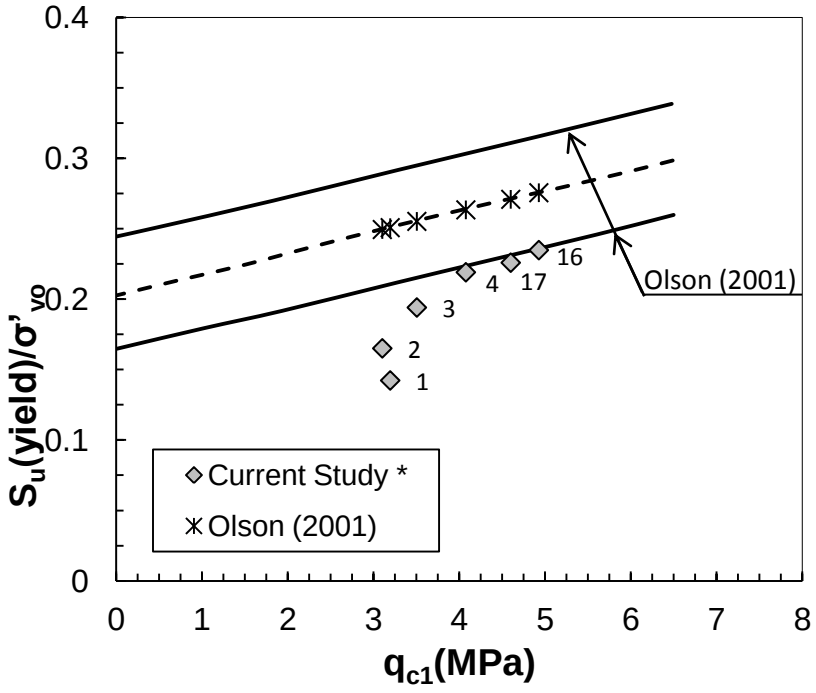

Figure 3-12: Comparison of yield strength ratios predicted by Olson (2001) and the data from the current study (Numbers next to the data points show the CPT Test. No. , * Note that the s_u values for Test No. 1,2,3 and 4 were reported by Omar (2013))

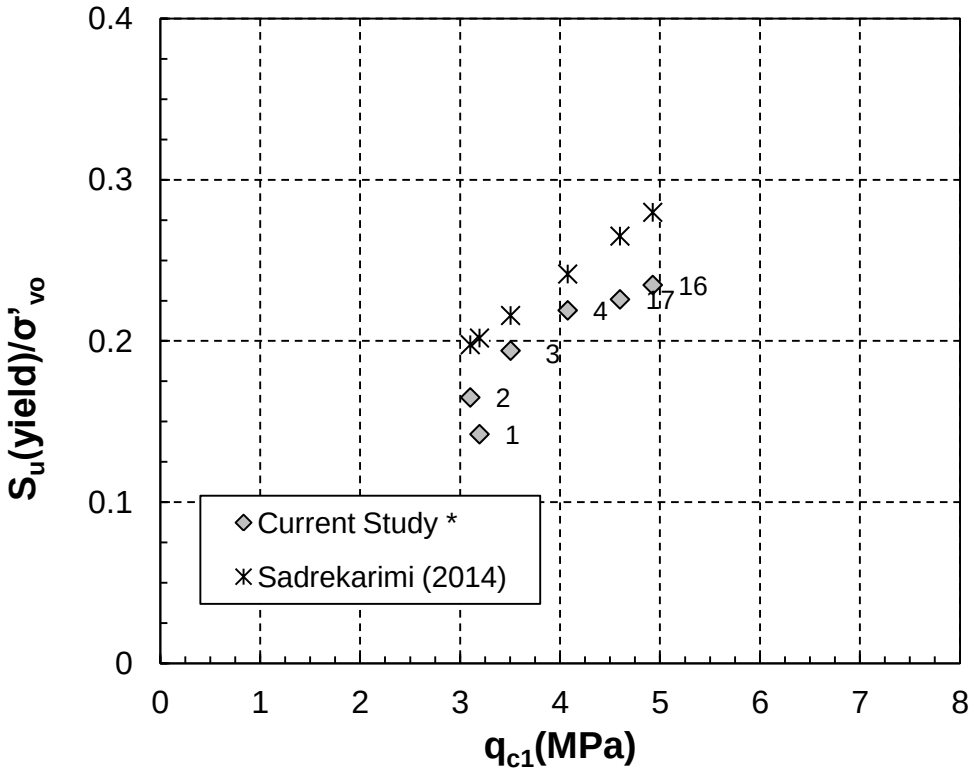

Figure 3-13: Comparison of the yield strength ratios predicted by Sadrekarimi (2014) and the data from the current study (Numbers next to the data points show the CPT Test. No, *Note that the s_u values for Test No.1,2,3 and 4 were reported by Omar (2013))

As shown in Figures 3-12 and 3-13, the predicted yield strength ratios by Olson (2001) are higher than the measured values. While, the method suggested by Sadrekarimi (2014) predicts the yield strength ratio close to what had been measured. This is associated with the difference in consolidation state of stress and anisotropic consolidation between data used for developing the empirical correlations and those obtained from the isotropically consolidated triaxial compression tests of Omar (2013) and current study.

The amount of anisotropic consolidation has a key influence on the undrained strain-softening behavior and s_u(yield) of cohesionless soils (Doanh et al. 1997, Finge et al. 2006). For example, Fourie and Tshabalala (2005) found that anisotropic consolidation under K_o conditions leads to a significantly higher values of s_u(yield) than isotropic consolidation.

3.3.3 Methods for estimating liquefied strength

Similar to Section 3.3.2, the correlations suggested by Olson (2001) and Sadrekarimi (2014) are evaluated using the cone tip resistances obtained from the miniature penetrometer developed in the current study $s_u(liq)/\sigma'_{vo}$ values reported by Omar (2013) and current study for the 70 mm diameter specimens.

These values are presented in Table 3-3 and compared in Figures 3-14 and 3-15.

Table 3-3: $s_u(liq)$ and q_{c1} values used to evaluate the available correlations

CPT Test No	Stress level (kPa)	q_{c1} (MPa) (Current Study)	$S_u(liq)/\sigma'_{vo}$ (Omar 2013)	$S_u(liq)/\sigma'_{vo}$ (Current Study)	$S_u(liq)/\sigma'_{vo}$ (Olson 2001)	$S_u(liq)/\sigma'_{vo}$ (Sadrekarimi 2014)
4	100	4.08	0.122	-	0.088	0.091
3	200	3.50	0.096	-	0.080	0.082
2	300	3.10	0.074	-	0.074	0.074
1	500	3.19	0.062	-	0.076	0.076
16	300	4.93	-	0.142	0.096	0.100
17	450	4.60	-	0.124	0.100	0.106

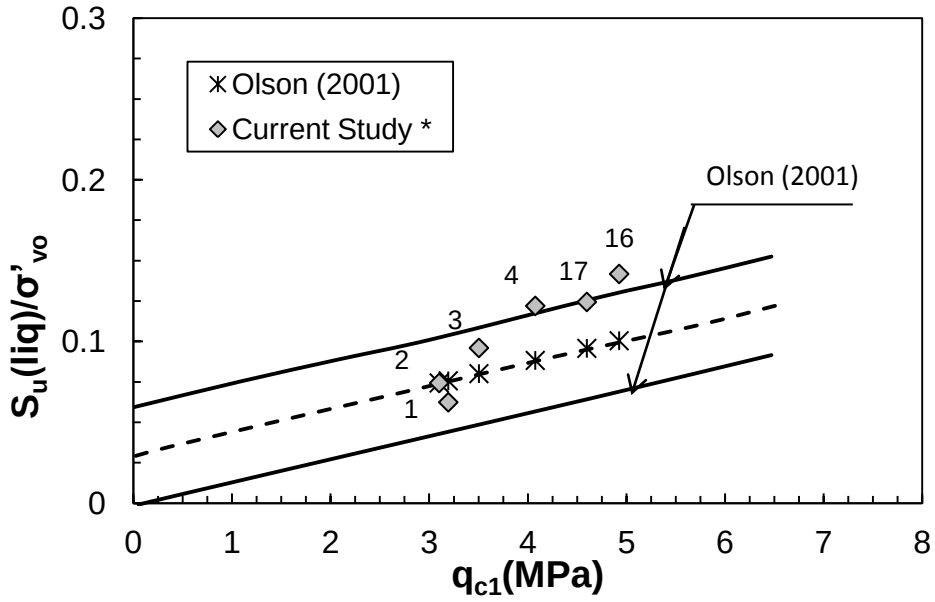

Figure 3-14: Comparison of the liquefied strength ratios predicted by Olson (2001) and the data from the current study (Numbers next to the data points show the CPT Test. No, *Note that the s_u values for Test No.1,2,3 and 4 were reported by Omar (2013))

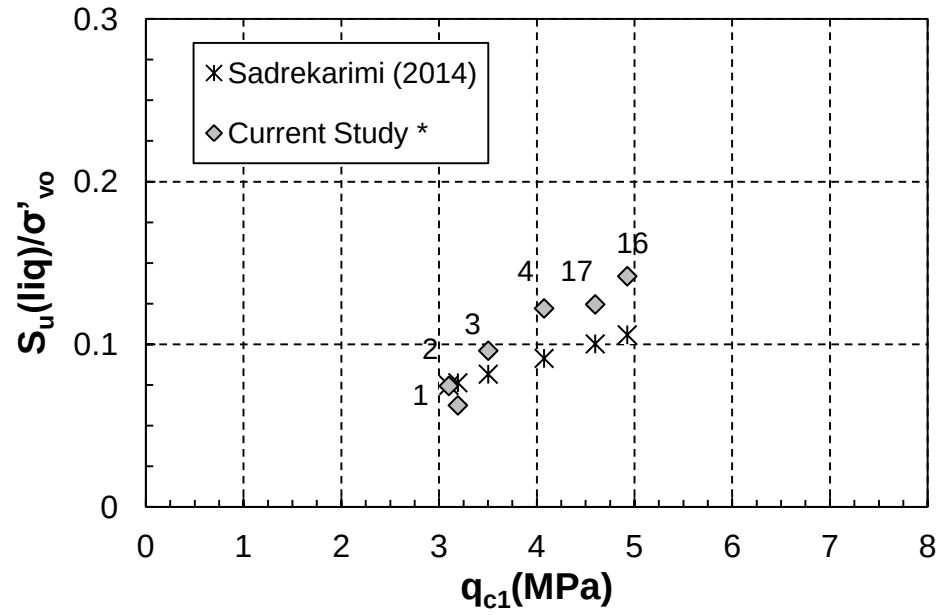

Figure 3-15: Comparison of the liquefied strength ratios predicted by Sadrekarimi (2014) and the data from the current study (Numbers next to the data points show the CPT Test. No, *Note that the s_u values for Test No.1,2,3 and 4 were reported by Omar (2013))

Predicted liquefied strength ratios by Olson (2001) and Sadrekarimi (2014) are in a very good agreement with the measured data in the current study. Isotropic consolidation has been suggested to have no effect on the liquefied shear strength of sands which further explains the reason why the proposed methods are in a good agreement with the measured liquefied strength and not with the measured yield shear strengths.

3.4 Estimation of Loose Sand Parameters from CPT

Besides ψ_{cs}, s_u(yield), and s_u(liq), a number of other parameters are also required for static liquefaction analysis, including soil unit weight and relative density (for effective stress stability analysis). Extensive research has been conducted to provide empirical correlations between CPT data and these soil properties. These correlations are typically developed using either laboratory calibration chamber CPT experiments, comparison with in-situ field tests, or numerical analyses (e.g., cavity expansion, finite element, or discrete element analyses). The experimental results of this study are compared with some of these correlations in the following paragraphs.

3.4.1 Estimation of Soil Unit Weight

The unit weight of each of the soil layers is one of the preliminary information required for geotechnical design and calculation of overburden stress. The unit weight is best calculated based on undisturbed thin-walled tube samples from borings. However, in clean sands, cohesionless silts, and gravels undisturbed samples are difficult to obtain. Therefore, indirect methods for assessing unit weight are preferred.

Mayne (2007) used results from large scale calibration chamber CPT tests to evaluate the dry unit weight (γ_d) of sands from normalized cone tip resistance (q_{c1}) and suggested a correlation to estimate the dry unit weight of uncemented unaged quartz to siliceous sands as bellow:

$$\gamma_d = 1.89 \log q_{c1} + 11.8 \quad (3\text{-}12)$$

In which, σ_{atm} is the atmospheric pressure (= 101 kPa), and q_{c1} is calculated using the following equation:

$$q_{c1} = \frac{q_t}{\sigma_{atm}} / (\frac{\sigma'_{v0}}{\sigma_{atm}})^{0.5} \quad (3\text{-}13)$$

Figure 3-16 shows the comparison between the dry unit weights of the samples in the current study for test No. 4-11 which were performed at the same consolidation pressure and those calculated based on normalized tip resistance as suggested by Mayne (2007). As shown in this Figure, the correlation suggested by Mayne (2007) slightly overestimates the dry unit weight of the soil but generally is in a good agreement with the measure values.

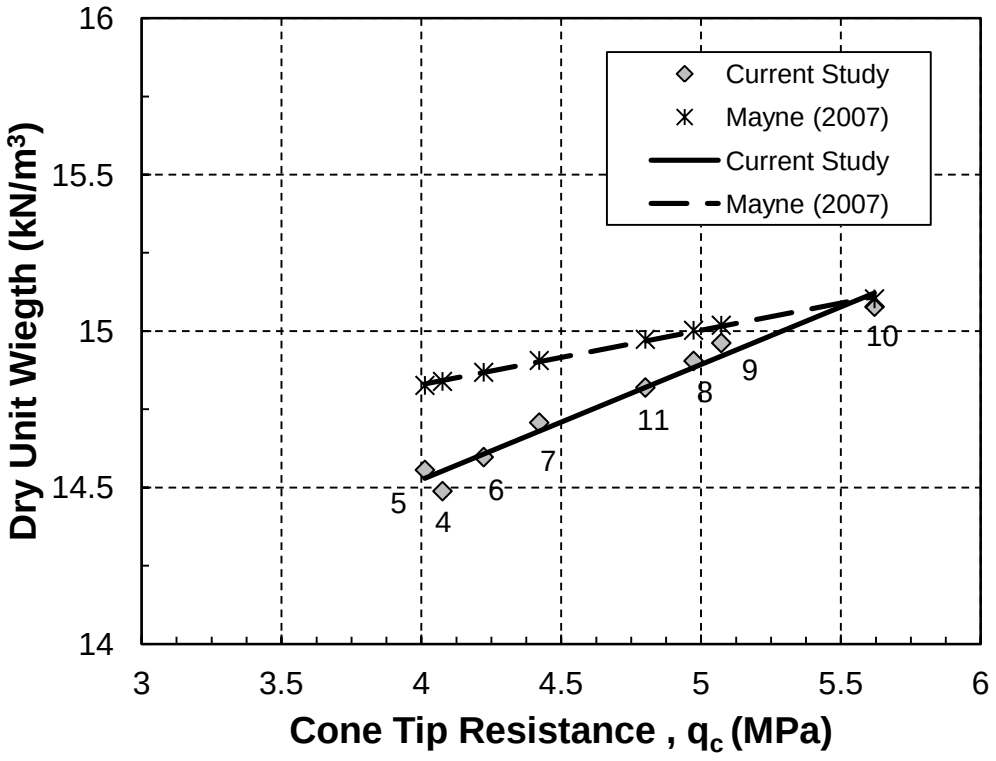

Figure 3-16: Comparison of the dry unit weights predicted by Mayne (2007) and the data from the current study (Numbers next to the data points show the Test. No.)

Mayne et al. (2010) proposed the following empirical relationship between total unit weight, γ_t and CPT readings by conducting a comprehensive series of multiple regression analyses on the data available for a wide range of soils including both clays and sands:

$$\gamma_t = 1.81\gamma_w \left(\frac{\sigma'_{v0}}{\sigma_{atm}}\right)^{0.05} . \left(\frac{q_t - \sigma_{v0}}{\sigma_{atm}}\right)^{0.017} . \left(\frac{f_s}{\sigma_{atm}}\right)^{0.073} . (B_q + 1)^{0.16} \quad (3\text{-}14)$$

Where B_q is the normalized pore water pressure parameter calculated as bellow:

$$B_q = \frac{(u_2 - u_0)}{(q_t - \sigma_{v0})} \quad (3\text{-}15)$$

Figures 3-17 shows the comparison between the total unit weights of the samples in the current study for test No. 4-11 which were performed at the same consolidation pressure and those calculated based on the above correlation.

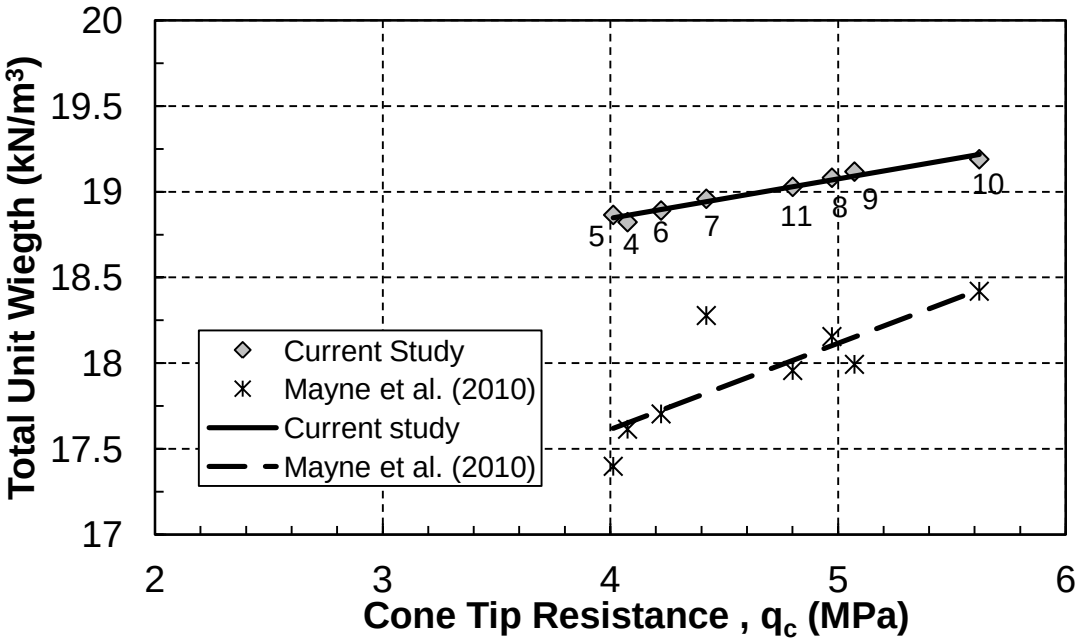

Figure 3-17: Comparison of the saturated unit weights predicted by Mayne et al. (2010) and the data from the current study

As shown in Figure 3-17, the correlation suggested by Mayne et al. (2010) in general underestimates the total unit weight of the soil.

3.4.2 Estimation of Soil Relative Density

Schemertmann (1976) presented the first comprehensive relationship between q_c and relative density on the basis of CPTs performed in the CPT calibration chambers at the University of Florida. The analytical expression suggested by Schemertmann (1976) is as follow:

$$D_r = \frac{1}{C_2}\ln\left(\frac{q_c.(\sigma'_{v0})^{C_1}}{C_0}\right) \quad (3\text{-}16)$$

Where C_0, C_1 and C_2 are the empirical correlation factors equal to 24.94, 0.46 and 2.96, respectively. The empirical correlation factors are discussed in details by Schemertmann (1976).

Later, based on extensive calibration chamber testing on Ticino sand, Baldi et al. (1986) suggested that there is a unique relationship between relative density, cone tip resistance and mean effective stress as shown in Figure 3-18.

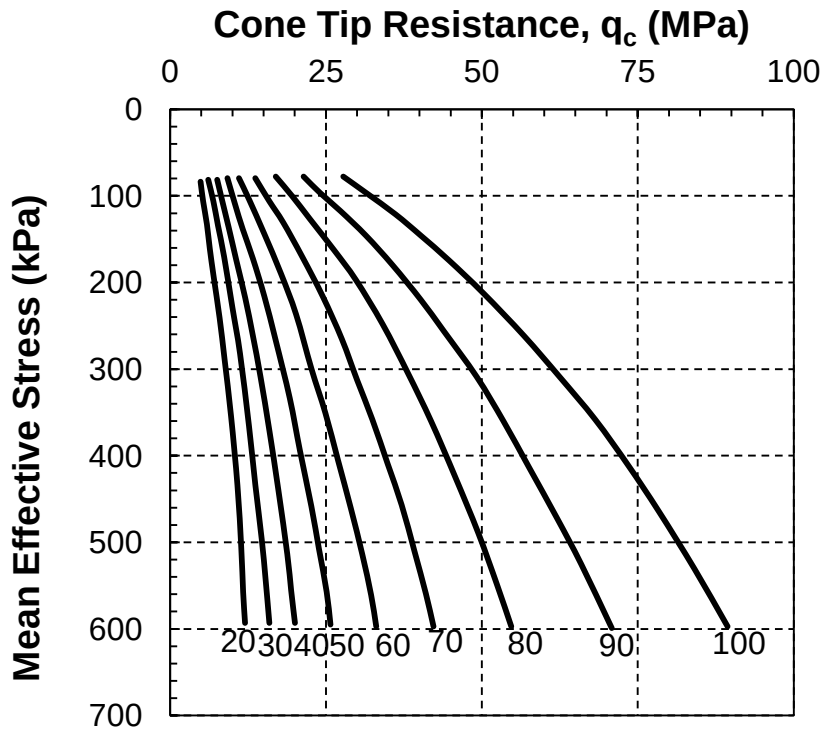

Figure 3-18: Relationship between soil relative density, cone tip resistance and mean effective stress (Baldi et al. 1986)

Figures 3-19 and 3-20 show the comparison between the relative density of the samples in the current study and those calculated based on correlation as suggested by Schemertmann (1976) and Baldi et al. (1986). As shown in Figures 3-19 and 3-20, both correlations overestimate the relative density of soil.

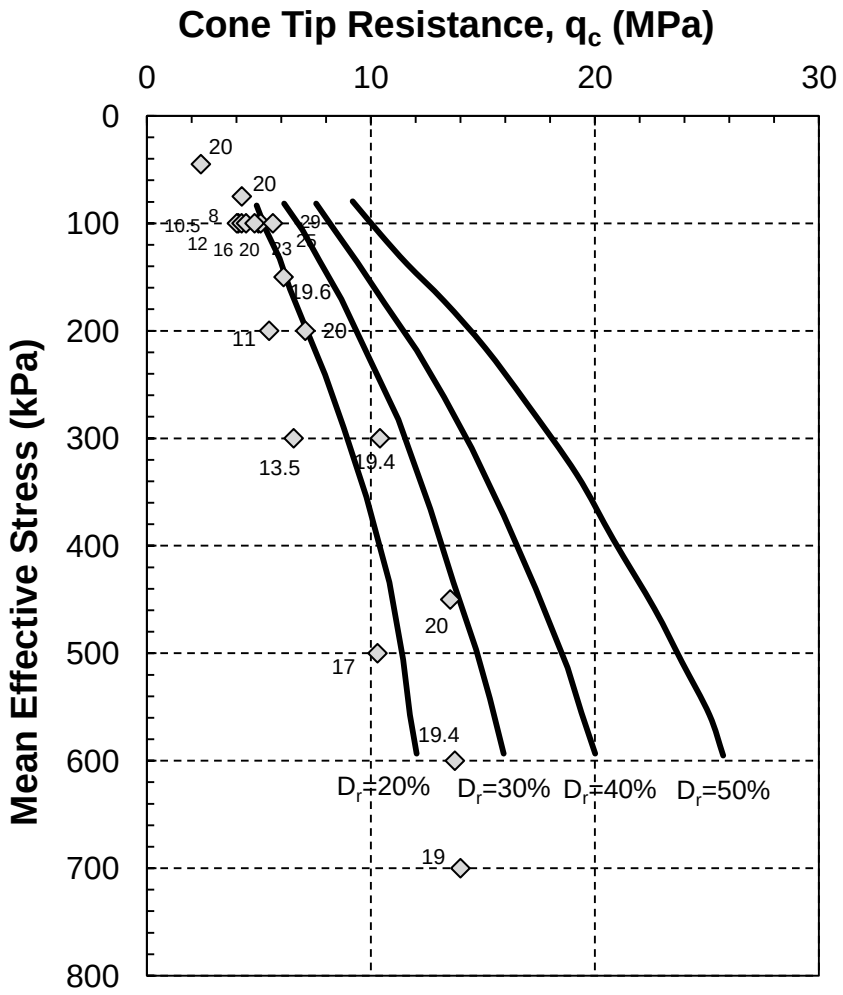

Figure 3-19: Comparison of the relative density predicted by Baldi et al. (1986) and the data from the current study (Numbers next to the data points show the tested relative density in percentage).

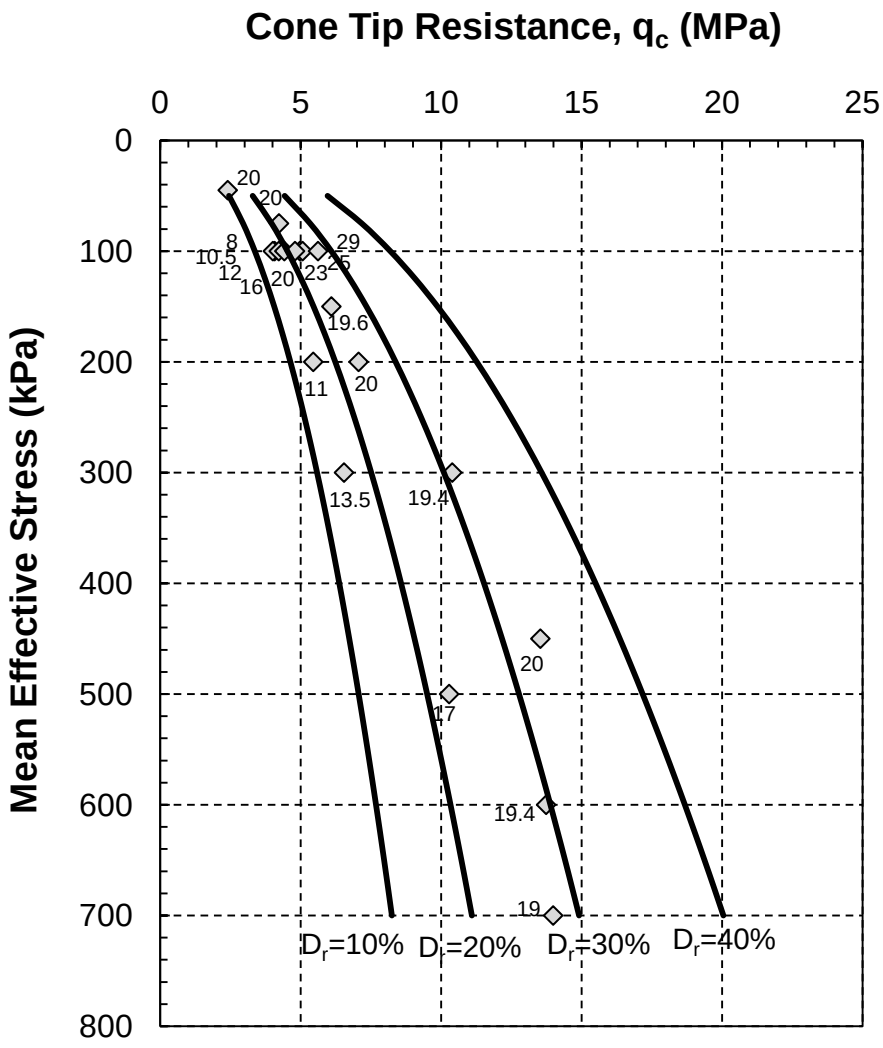

Figure 3-20: Comparison of the relative density predicted by Schemertmann (1976) and the data from the current study (Numbers next to the data points show the tested relative density in percentage).

Figures 3-21 shows the comparison between the measured cone tip resistances of the samples in the current study and those calculated based on correlation as suggested by Schemertmann (1976) and Baldi et al. (1986) for samples with a consolidated relative density of about 20%. As shown in this figure, both correlations underestimate the cone tip resistance for the given relative density.

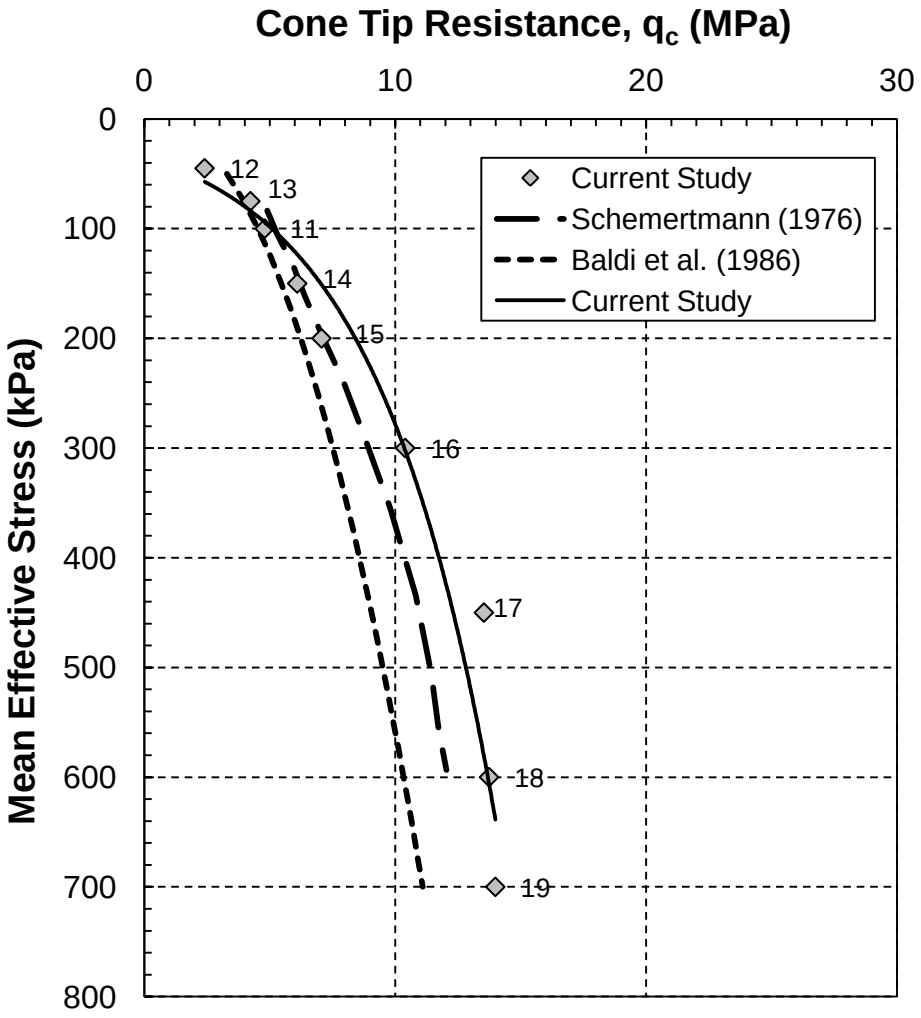

Figure 3-21: Comparison of the relative density predicted by Baldi et al. (1986), Schemertmann (1976) and the data from the current study (Number next to the data points is the Test. No.)

3.4.3 Estimation of in Situ State Parameter

Laboratory tests indicate that the behavior of cohesionless soil is controlled by both density and effective stress (Been and Jefferies 1985). The critical state parameter (ψ_{cs}), which is the difference between the initial void ratio of a soil from the void ratio on the critical state line (CSL) at the same effective stress level, has been suggested to combine the effects of void ratio (density) and effective stress for soil behavior characterization (Taylor 1948; Been and Jefferies 1985). Accordingly, soil response to cone penetration is also controlled by ψ_{cs} or alternatively ψ_{cs} could be inferred from CPT.

Here, some of the most well-established methods for estimating ψ_{cs} from CPT data are reviewed. These methods are evaluated by calculating ψ_{cs} for the cone tip resistance and critical state characteristics of the soil used in the miniature calibration chamber experiments performed in the current study, and comparison with the ψ_{cs} produced in the miniature calibration chamber experiments.

Both empirical and numerical/analytical methods have been used for CPT interpretation and the inference of $\psi_{cs.}$ The empirical methods are essentially based on CPT calibration chamber tests, while the numerical techniques simulate cone penetration as the expansion of a spherical cavity in finite element numerical analysis with an appropriate soil constitutive model. Table 3-4 summarizes these methods.

Table 3-4: State parameter interpretation methods from CPT

Empirical/Semi-empirical correlations	Numerical/Analytical solutions
Been et al. (1987)	Shuttle and Jefferis (1998)
Been and Jefferies (1992)	Russell and Khalili (2002)
Fear and Robertson (1995)	
Konrad (1997)	

3.4.3.1 Empirical Methods

The first empirical procedure for estimating ψ_{cs} from CPT resistance was developed by Been et al. (1987) based on CPT calibration chamber tests on Hilton Mines tailings, Hokksund, Monterey No. 0, Ottawa, Reid Bedford, and Ticino sands. The proposed relationship is a relatively simple semi-logarithmic function of CPT resistance, and the critical state line slope. As the CCTs were performed on dense sands ($\psi_{cs} < 0$), the empirical relationship suggested by Been et al. (1987) is anticipated to be only applicable for $\psi_{cs} < 0$, and it could underestimate ψ_{cs} of loose sands ($\psi_{cs} > 0$) leading to unsafe assessment of liquefaction potential and design. Later, Been and Jefferies (1992) added the CCT data on Ticino sand to their calibration database and suggested that besides the slope of CSL, CPT resistance also depends on the critical state friction angle, and thus proposed a new equation that included the critical state friction angle.

Understanding the significant stress concentration at the cone tip and the potential for particle crushing to occur at the vicinity of the cone, Konrad (1997) extended Been et al. (1987) empirical relationship to include the impact of particle crushing based on CCT results on Ticino sand. Particle crushing was included by employing a bilinear CSL. Konrad (1997) took into account the influence of the stress level by choosing a reference initial mean effective stress of 100 kPa and expressing the normalized CPT tip resistance at this reference stress level for Ticino sand. The effect of soil type was considered by normalizing ψ_{cs} with respect to the difference between the maximum and minimum void ratios of the sand.

Based on the strong framework developed from laboratory element tests for predicting shear wave velocity in cohesionless soils, Robertson et al. (1995) proposed a relationship to estimate ψ_{cs} from shear wave velocity measurements. This relationship was then extended to CPT tip resistance through an empirical correlation between shear wave velocity and CPT tip resistance (Fear and Robertson, 1995). The main drawback of this method is the number of empirical parameters (particularly for relating shear wave velocity to CPT resistance) which are only calibrated for a limited number of sands. This

limits the application of this method to sands with different composition, mineralogy, particle size distribution and fines content.

3.4.3.2 Numerical Methods

Most numerical methods of CPT interpretation are based on the analogy of cone penetration to the expansion of a spherical cavity in a uniform soil medium until the pressure required to expand the cavity stabilize at a limiting constant pressure (cavity limit pressure). The cavity limit pressure is computed as a function of effective stress (i.e. soil depth) using finite element analysis with a proper soil constitutive model. One of the main sources of uncertainty of these numerical methods is the additional correlation which is required to relate the cavity limit pressure to CPT tip resistance. Two of the most complete and recent analysis of cavity expansion presented by Shuttle and Jefferies (1998), and Russell and Khalili (2002) were evaluated in this study.

Shuttle and Jefferies (1998) performed a series of cavity expansion finite element analyses using the NorSand critical state model (Jefferies 1993) with the material properties of Ticino sand. There results indicated that soil shear modulus had significant impact on CPT resistance. Based on their numerical analyses, Shuttle and Jefferies (1998) suggested a relationship with 8 parameters (M, N, H, Γ, λ, ν, G/p_o, p_o) to estimate ψ_{cs}. These parameters were calibrated for Ticino sand only. Extensive laboratory triaxial testing is required for parameter calibration and the application of their relationship for other sands. The calibrated equation for Ticino sand has been used in this study.

More recently, Russell and Khalili (2002) used the cavity expansion analogy with the Mohr-Coulomb failure criterion. In their analysis, the sand state was defined in terms of a CSL which accounts for particle crushing particularly at high stresses. They suggested that for given values of initial mean stress and shear modulus ratio (G/G_{max}), the cavity limit pressure had logarithmic relationship with ψ_{cs}. Accordingly, they proposed series of equations, as a function of initial mean stress, to estimate ψ_{cs} from the cavity limit pressure at $G/G_{max} = 0.4$.

Similar to any other cavity expansion analysis, the main challenge in the application of the relationship developed by Russell and Khalili (2002) is the determination of the CPT resistance corresponding to the cavity expansion pressure. The following correlations were proposed and calibrated to relate cavity expansion pressure (σ'_c) to the CPT tip resistance (q_c):

$$\sigma'_c = a\, Q_t + b \tag{3-17}$$

$$Q_t = \frac{q_c - p}{p'} \tag{3-18}$$

Where;

Q_t is the normalized CPT tip resistance,

p' is the effective mean stress,

p is the total mean stresses,

And, a and b parameters are empirical constants determined by mathematical regression analysis of CCT data as below:

$$a = -8 * 10^{-5}\, p'^2 + 0.0939\, p' + 0.944 \tag{3-19}$$

$$b = -0.0185\, p'^2 + 19.568\, p' + 564.54 \tag{3-20}$$

Figure 3-22 presents the very good agreement and the validation of Q_t estimated using equation (3-17) in combination with the relationship developed by Russell and Khalili (2002), for calculating σ'_c, with that from CCT on Ticino sand. Therefore, for estimating ψ_{cs} equation (3-17) can be used to calculate the equivalent cavity expansion limit pressure from CCT results for input in the cavity expansion analysis relationship of Russell and Khalili (2002).

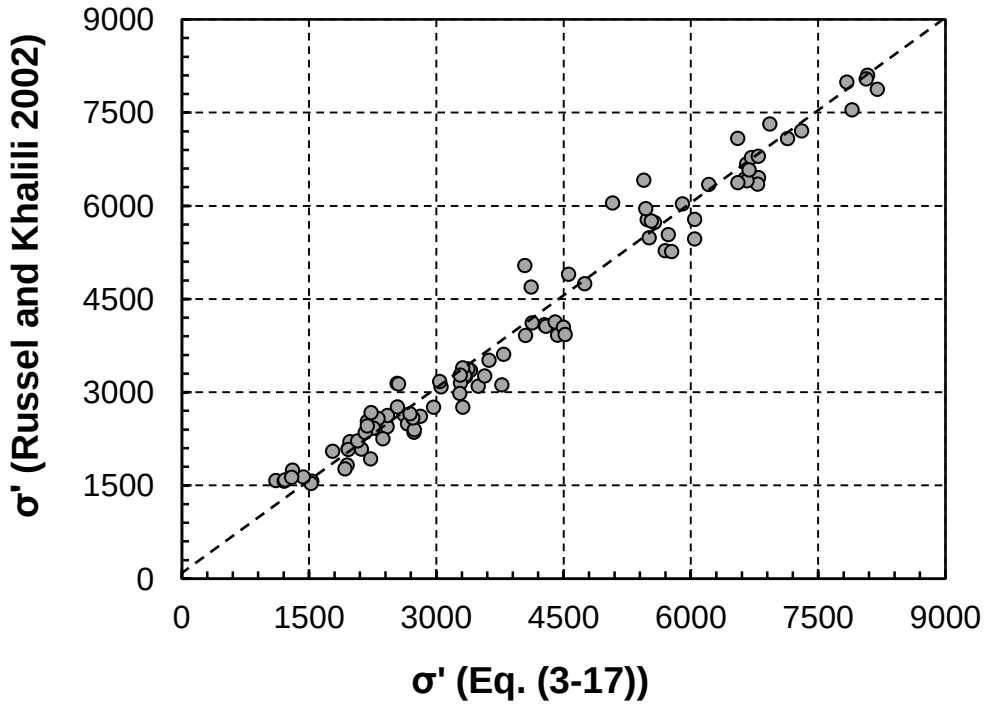

Figure 3-22: Comparison of σ'_c from cavity expansion analysis (Russell and Khalili 2002) and equation (3-17) for CCT on Ticino sand.

3.4.3.3 Comparison with Laboratory Miniature CPT Experiments Results

Figure 3-23 presents normalized CPT resistance (Q_t) from the laboratory CPT experiments performed in the current study and corresponding state parameters produced in the laboratory CPT experiments (based on the CSL of the Barco 71 sand from Omar (2013) and the consolidated void ratio) and estimated from the CPT interpretation methods described above.

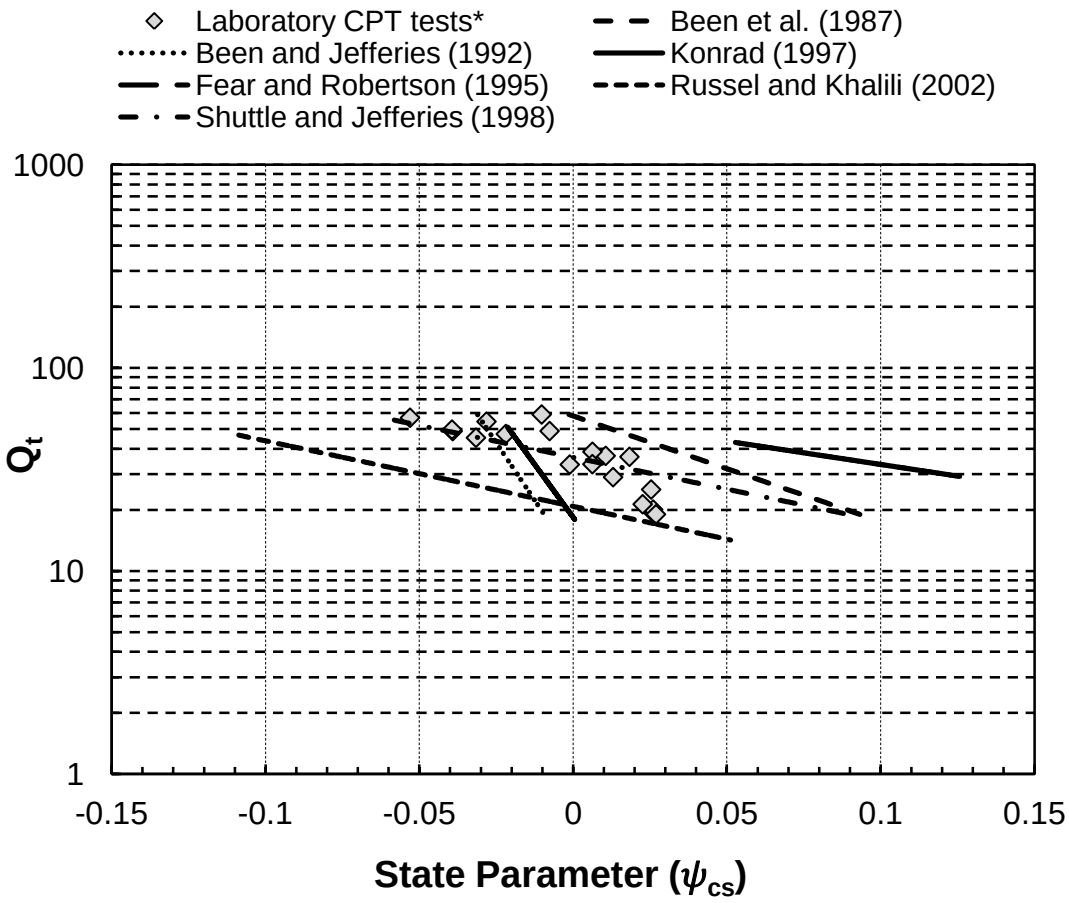

Figure 3-23: Q_c versus ψ_{cs} for Barco 71 from current study (* Note that the state parameters were calculated based on the critical state parameters reported by Omar (2013) for Barco 71)

Figures 3-23 indicates that the method proposed by Been et al. (1987) provides not the best but a reasonable estimate of state parameter for the loose sand tested in the current study using miniature CPT calibration chamber. This method is based on the slope of the CSL, this suggests that there could be some other factors affecting the relationship between state parameter and cone tip resistance which is not included in the empirical equation proposed by Been et al. (1987). Furthermore, results show that including the critical state friction angle by Been and Jefferies (1992) improved the accuracy of the estimations for the loose sands tested in the current study.

Interestingly, the method proposed by Konrad (1997) provided a good estimation of the state parameter for the loose sand tested in the current study, which could be due to the use of precise values for the CSL values.

Finally, the least overall accuracy in estimating ψ_{cs} is provided by the relationship suggested by Fear and Robertson (1995). Note that this method is based on the fundamental relationship between shear wave velocity and void ratio from resonant column laboratory tests and an additional empirical correlation was used for converting shear wave velocity to cone tip resistance (Fear and Robertson, 1995). This additional correlation was calibrated for a very few number of sands, and thus its application for other sands could be subject to greater uncertainty and the observed deviation.

As discussed above, the correlation suggested by Been et al. (1987) provides an estimate of ψ_{cs} with an average deviation of 0.045. This is a very good accuracy considering the difficulties in estimating in-situ void ratio and expenses associated with undisturbed sampling. This empirical correlation could be used in practice as a screening-level procedure to identify liquefiable soils (i.e. $\psi_{cs} > 0$) and liquefaction susceptibility analysis of low risk projects. However, for high risk projects (e.g. large embankments or tailings dams) where a failure could result in loss of lives or substantial financial loss, the application of this correlation for liquefaction analysis need to be supplemented with undisturbed sampling, laboratory shear tests and advanced numerical analysis.

3.5 Conclusions

Available CPT-based procedures to perform a static liquefaction analysis including liquefaction susceptibility, triggering and post liquefaction strength were reviewed and applied to the data from the miniature cone penetration tests performed in the current study and were compared.

Available methods to predict the yield shear strength of the soil based on CPT data were evaluated using the shear strength values reported by Omar (2013). Methods proposed by Olson (2001) and Sadrekarimi (2014), which were based on back analysis of the past case histories, were evaluated. Measured values were lower than the predicted values by Olson (2001) and much closer to the values predicted by Sadrekarimi (2014). The reason was concluded to be the effect of isotropic consolidation in the laboratory tests performed by Omar (2013).

Available methods to predict the liquefied shear strength of the soil based on CPT data were also evaluated using the critical state shear strength values reported by Omar (2013). Methods proposed by Olson (2001) and Sadrekarimi (2014) both predicted the liquefied shear strength of the soil in a good agreement with the measured values. This is justified by the argument that isotropic consolidation has no effect on the shear strength of the soil at large displacements.

Some of the widely used correlations to estimate the soil unit weight and relative density of loose sands were also evaluated. In general, all the methods predicted higher values than the measured values.

References

Baldi, G., Bellotti, R., Ghionna, V., Jamiolkowski, M. and Pasqualini, E. (1986). Interpretation of CPTs and CPTU's, 2nd Part. *Proc 4th International Geotechnical Seminar*, Nanyang Technological Institute, Singapore, 143–156.

Been, K. & Jefferies, M. G. (1985). A state parameter for sands. *Géotechnique,* 35(2): 99-112.

Been, K., Jefferies, M.B., Crooks, J.H.A., and Rothenburg, L. (1987). "The cone penetration test in sands, part 2." General inference of state. *Géotechnique*, 37(3): 285–299.

Been, K., and Jefferies, M.G. (1992). "Towards systematic CPT interpretation." In Proceedings of the *Wroth Symposium*, Oxford, U.K. pp. 44–55.

Casagrande, A. (1940). "Characteristics of cohesionless soils affecting the stability of slopes and earth fills." Contributions to soil mechanics, Boston Society of Civil Engineers, 257–276.

Casagrande, A. (1965). "Second Terzaghi Lecture: the role of "calculated risk" in earthwork and foundation engineering." *Journal of the Soil Mechanics and Foundations Division, ASCE*, 91(SM4), 1-40.

Castro, G. (1969). "Liquefaction of sands." Harvard soil mechanics series, Vol. 81, Harvard University, Cambridge, Mass.

Castro, G., Keller, T.O., and Boynton, S.S. (1989). "Re-evaluation of the Lower San Fernando Dam: Report 1, an investigation of the February 9, 1971 slide." U.S. Army Corps of Engineers Contract Report GL-89-2, Vols. 1 and 2, U.S. Army Corps of Engineers Waterways Experiment Station, Vicksburg, Mississippi.

Doanh, T., Ibraim, E., and Matiotti, R. (1997). "Undrained instability of very loose Hostun sand in triaxial compression and extension." Part 1: Experimental observations. Mechanics of Cohesive–Frictional Materials, 2(1): 47–70.

Fear, C. E., and Robertson P.K. (1995). "Estimating the undrained strength of sand: a theoretical framework." *Can. Geotech. J.* 32: 859-870.

Finge, Z., Doanh, T., and Dubujet, P., (2006). "Undrained anisotropy of Hostun RF loose sand: new experimental investigations". *Can. Geotech. J*. 43: 1195–1212.

Fourie, A.B. and Tshabalala, L. (2005). "Initiation of static liquefaction and the role of K_0 consolidation". *Can. Geotech. J*. 42: 892–906.

Hazen, A. (1918). "A study of the slip in the Calaveras Dam." Engineering News-Record, 81(26), 1158-1164.

Jefferies, M.G., and Been, K. (2006). "Soil liquefaction, a critical state approach." Published by Taylor & Francis.

Kayen, R.E., Mitchell, J.K., Seed, R.B., Lodge, A., Nishio, S., and Coutinho, R. (1992). "Evaluation of SPT-, CPT-, and shear wave- based methods for liquefaction potential assessments using Loma Prieta data. In Proceedings of the 4th Japan-U.S> Workshop on Earthquake Resistant Design of Lifeline Facilities and Counter-measures for Soil Liquefaction, Honlulu, Hawaii. Vol. 1, pp. 177-192.

Konrad, J. M. (1997). "In situ sand state from CPT: evaluation of a unifed approach at two CANLEX sites." *Canadian Geotechnical Journal*, 1: 120-130.

Kulhawy, F. H., and Mayne, P. H. (1990). "Manual on estimating soil properties for foundation design.", Electric Power Research Institute (EPRI), Palo Alto, California.

Lade, P.V. . Yamamuro, J. A, (2011). "Evaluation of static liquefaction potential of silty sand slopes" Canadian Geotechnical Journal, 48(2): 247-264, 10.1139/T10-063

Mayne, P.W., (2007), "Cone Penetration Testing State-of-Practice" NCHRP Project 20-05, Topic 37-14.

Mayne, P.W., Peuchen, J., and Bouwmeester, D, (2010). “Soil unit weight estimation from CPTs.” Proceedings 2nd intl. Symposium on Cone Penetration Testing (CPT’ 10), Vol. 2, Huntington Beach, California; Omnipress; 169-176.

McRoberts, E. C. and Sladen J. A., (1992), “Observations on static and cyclic sand-liquefaction methodologies” Canadian Geotechnical Journal, 29(4): 650-665, 10.1139/t92-072

Muhammad, K. (2012). "Case history-based analysis of liquefaction in sloping ground." PhD, University of Illinois, Urbana.

Olson, S. M. (2001). “Liquefaction analysis of level and sloping ground using field case histories and penetration resistance.” Ph.D. thesis, Univ. of Illinois at Urbana–Champaign, Urbana, Ill.

Olson, S. M., and Stark, T. D. (2002). “Liquefied strength ratio from liquefaction flow failure case histories.” *Can. Geotech. J.*, 39, 629– 647.

Olson, S. M., and Stark, T. D. (2003). “Yield strength ratio and liquefaction analysis of slopes and embankments.” *J. Geotech. Geoenviron. Eng.*, 129_8_, 727–737.

Omar, T. (2013). "Specimen size effect on shear behavior of loose sand in triaxial testing." MESc, Western University, London, Ontario.

Plewes, H. D., Davies, M. P., and Jefferies, M. G. (1992). “CPT based screening procedure for evaluating liquefaction susceptibility.” *Proc., 45th Canadian Geotechnical Conf.*, Vol. 4, BiTech Publishers, Vancouver, BC, Canada, 1–9.

Poulos, S. J., Castro, G., and France, W. (1985). “Liquefaction evaluation procedure.” *J. Geotech. Eng*. Div., 111_6_, 772–792.

Robertson, P. K. (2010). “Interpretation of cone penetration tests—A unified approach.” *J. Geotech. Geoenviron*. Eng. 136:842-853. DOI**:** 10.1061/_ASCE_GT.1943-5606.0000286

Robertson, P. K., et al. (2000). “The Canadian liquefaction experiment: An overview.” *Can. Geotech. J.*, 37, 499–504.

Robertson, P.K., Sasitharan, S., Cunning, J.C., and Sego, D.C. (1995). “Shear wave velocity to evaluate in-situ state of Ottawa sand.” *Journal of Geotechnical Engineering, ASCE*, 121(3): 262-273.

Russell, A. R., and Khalili, N. (2002) “Drained cavity expansion in sands exhibiting particle crushing” *International Journal for Numerical and Analytical Methods in Geomechanics*, 26: 323–340 (DOI: 10.1002/nag.203)

Sadrekerimi, A. (2014), “Static Liquefaction Analysis Considering Principal Stress Directions and Anisotropy.” *Canadian Geotechnical Journal (submitted).*

Sadrekarimi, A. & Olson, S. M. (2011). “Critical state friction angle of sands.” *Ge´otechnique* 61, No. 9, 771–783, http://dx.doi.org/ 10.1680/geot.9.P.090.

Schmertmann, J.H. (1976) “ An Updated Correlation between Relative Density DR and Fugro-Type Electric Cone Bearing, qc.” Contract Report DACW 39-76 M 6646 WES, Vicksburg, Miss., 1976.

Schofield, A., and Wroth, C. P. (1968). “Critical state soil mechanics.” McGraw-Hill, London.

Seed, H. B., and Harder, L. F. (1990). “SPT-based analysis of cyclic pore pressure generation and undrained residual strength.” *Proc., Seed Memorial Symp.,* BiTech Publishers, Vancouver, BC, Canada, 351–376

Seed, H.B., Lee, K.L., and Idriss, I.M. (1969). “Analysis of Sheffield Dam failure.” *Journal of the Soil Mechanics and Foundations Division, ASCE*, 95(SM6), 1453-1490.

Seed, H.B., Seed, R.B., Harder, L.F., and Jong, H. L. (1989). “Re-evaluation of the Lower San Fernando Dam: Report 2, examination of the post-earthquake slide of February 9, 1971.” U.S. Army Corps of Engineers Contract Report GL-89-2, U.S. Army Corps of Engineers Waterways Experiment Station, Vicksburg, Mississippi.

Shuttle, D. A., and Cunning, J. (2007). "Liquefaction potential of silts from CPTu." *Can. Geotech. J.*, 44, 1–19.

Shuttle, D. and Jefferies, M., (1998). "Dimensionless and unbiased CPT interpretation in sand." *International Journal for Numerical and Analytical Methods in Geomechanics*, 22: 351-391.

Stark, T. D., and Olson, S. M. (1995). "Liquefaction resistance using CPT and field case-563 histories." Journal of Geotechnical Engineering, ASCE, 121(12), 856-869.

Taylor, D. W. (1948). "Fundamentals of Soil Mechanics." Published by John Wiley and sons, Inc. New York. United States.

Terzaghi, K., Peck, R. B. & Mesri, G. (1996). "Soil mechanics in engineering practice", 3rd edition. New York, NY, USA: Wiley.

Verdugo, R. & Ishihara, K. (1996). "The steady state of sandy soils." *Soils Foundation*. 36, No. 2, 81–91.

Wanatowski, D. and Chu, J. (2007), "Static liquefaction of sand in plane strain" Canadian Geotechnical Journal , 44(3): 299-313, 10.1139/t06-078

Yamamuro, J.A. and Lade P.V. (1997). "Static liquefaction of very loose sands" Canadian Geotechnical Journal, , 34(6): 905-917, 10.1139/t97-057

Chapter 4

4 Conclusions

4.1 Summary and Conclusions

A miniature cone calibration chamber has been designed and developed in this study with a cone diameter to sample diameter ratio of equal to 25 which has been demonstrated to exhibit negligible boundary condition effects in loose sands. Flexible latex membrane was used around the sample and the cell fluid surrounding the sample was pressurized to apply isotropic pressures to the sample. Therefore, constant stress boundary condition, BC1, was simulated. A pressure transducer was connected to the cone through the hollow shaft and a small tube welded to the cone probe which was used to measure the pore water pressure generated at the tip of the cone during penetration.

Nineteen tests were performed on Ottawa sand and the results were compared to the available data in the literature. The accuracy of the results was validated by comparing the results with the suggested rate for the cone resistance in sands in literature. More specifically, results were compared with the results of the large calibration chamber tests performed on the same soil at University of Florida. Results were in a very good agreement with the literature and data available from large calibration chambers. Different soil identification systems were used to further validate and compare the results.

Repeatability of the data obtained from the developed device was evaluated by repeating one of the tests. Results of the two tests were in a close agreement despite some minor differences due to the possible sample density nonuniformity. The effects of boundary conditions on the data were comprehensively discussed and it was concluded that boundary conditions were not affecting the results for the developed assembly when testing loose sands. The effect of cone penetration rate on the cone tip and sleeve friction was studied by performing two tests on the sample with same properties at the same

stress level but with different penetration rates. Results indicated that penetration rate has no effect on the results of the tests performed on sand which was backed up with the available literature as well. The possibility of particle crushing for the tested material was studied by taking samples from the soil adjacent to the cone probe and performing sieve analysis. No particle crushing was observed for the tested material.

Based on the results of the miniature CPT experiments, available methods for overburden stress normalization were evaluated and compared to find the method with the best performance. The effect of increase in relative density and stress level on penetration resistances was also studied. Both tip resistance and sleeve friction increased with increasing density or stress level.

Available CPT-based procedures to perform a static liquefaction analysis including liquefaction susceptibility, triggering and post liquefaction strength were reviewed and applied to the data from the miniature cone penetration tests performed in the current study and were compared.

Available methods to predict the yield shear strength of the soil based on CPT data were evaluated using the shear strength values reported by Omar (2013). Methods proposed by Olson (2001) and Sadrekarimi (2014), which were based on back analysis of the past case histories, were evaluated. Measured values were lower than the predicted values by Olson (2001) and much closer to the values predicted by Sadrekarimi (2014). The reason was concluded to be the effect of isotropic consolidation in the laboratory tests performed by Omar (2013).

Available methods to predict the liquefied shear strength of the soil based on CPT data were also evaluated using the critical state shear strength values reported by Omar (2013). Methods proposed by Olson (2001) and Sadrekarimi (2014) both predicted the liquefied shear strength of the soil in a good agreement with the measured values. This is justified by the argument that isotropic consolidation has no effect on the shear strength of the soil at large displacements.

Some of the widely used correlations to estimate the soil unit weight and relative density of loose sands were also evaluated. In general, all the methods predicted higher values than the measured values.

Several empirical and numerical techniques have been developed that provide an indirect measurement of the in-situ state parameter from field cone penetration tests. In this study, the accuracies of these methods in estimating the in-situ state parameter were evaluated by comparing their estimates with those from the miniature calibration chamber tests on loose sands performed in the current study.

4.2 Suggestions for Future Research

Based on the capability of the developed device and according to the findings of this research, many modifications could be applied to the current device, for example,

1. Implementation of shear wave velocity measurements;

2. Implementation of electrical resistivity measurements; and

3. Implementation of a mechanism to apply anisotropic consolidation;

Appendix A

(Sensors Calibration Factors)

PRESSURE SENSOR CALIBRATION

Date: August 9, 2013

Sensor Information:

Type:	Pressure Sensor
Mfgr:	Geotac
Model:	SQ226
Serial No:	PS2-288
Range:	200 psi

Standard Information:

Type:	Digital Readout
Mfgr:	Geotac
Serial No:	PS-3012
ID:	
Last Calibration:	

Sensor Exctiation (volts): 9.918106079

Calibration Results:

Corr. Coefficient:	0.999992483
Slope (volts/in)):	0.000497823
Intercept (volts):	-0.000189822
Calibration Factor (in/Vs/Ve):	19922.94437
Offset (volts):	-0.000189822

Standard (psi)	Sensor Output (volts)	Zero Adjusted Sensor Output (volts)	Best Fit Line Sensor Output (volts)	0.00 Best Fit Line error (volts)	0.46 Best Fit Line error (psi)	0.23 Accuracy %FS
0.00	-0.0005176	0	-0.000189	0.000189	0.379857	0.194657
19.48	0.00906742	0.00958497	0.009506	0.000078	0.157632	0.080778
38.97	0.01868886	0.01920641	0.019213	-0.000006	-0.012387	0.006348
58.47	0.02833067	0.02884823	0.028918	-0.000070	-0.140978	0.072244
77.97	0.03800613	0.03852368	0.038627	-0.000103	-0.206692	0.105919
97.50	0.04769388	0.04821144	0.048346	-0.000135	-0.270695	0.138717
116.98	0.05740293	0.05792048	0.058046	-0.000125	-0.251989	0.129131
136.49	0.0671512	0.06766875	0.067757	-0.000068	-0.177150	0.090780
155.95	0.07689771	0.07741527	0.077445	-0.000030	-0.060495	0.031001
175.48	0.08671143	0.08722899	0.087167	0.000062	0.125033	0.064073
195.07	0.09662867	0.09714623	0.096918	0.000228	0.457865	0.234632

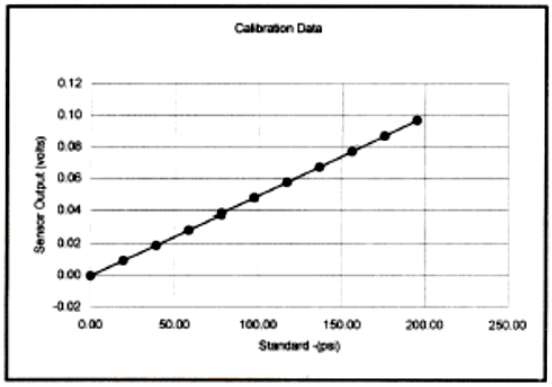

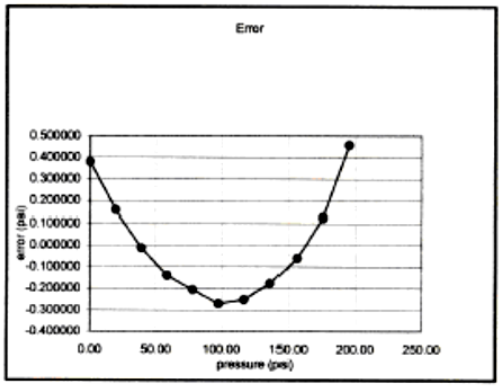

Load Cell Calibration Certificate

Date of Shipment	12/8/2011
Capacity	2000 lb
Input Resistance	464 Ohms
Excitation	10.00 VDC
Test Temp	73.2 degrees F
Linearity (% of R.O.)	0.027
ID Number	474042
Recommended Range	0 to 2000 lb
Output Resistance	353 Ohms
Relative Humidity	36.0%

Applied Load	Load Cell Reading (mV / V)	
Pounds	Tension	% Full Scale*
0	0.0000	0.000%
400	0.3991	0.016%
800	0.7981	0.027%
1100	1.0971	0.023%
1500	1.4959	0.024%
2000	1.9939	0.000%
0	0.0000	

Note: Error Calculated On Best Fit Straight Line Method

Calibration Factor: -1002974.811 lbs/V/V
Correlation Coefficient: 0.99999995

Note: Load cell calibration factor is valid for 1 year after shipment date

Calibration Equipment Used

Dead Weight: 3 klb
Traceability Number: 8511-09

Digital Multimeter:
HP Model Number: 34401A S/N US36133125

Calibrated By: Victor Garcilazo

Calibrated using equipment traceable to NIST in accordance with ISO/IEC 17025:2005 and ANSI/NCSL Z540-1-1994.

LINEAR POSITION SENSOR CALIBRATION

Date: November 8, 2011

Sensor Information:

Type:	LPT
Mfgr:	Geotac
Model:	LPT3
Serial No:	LPT-854
Range:	3 inch

Standard Information:

Type:	Gage block
Mfgr:	HDT
Serial No:	21298
ID:	
Last Calibration:	

Sensor Exctiation (volts): 10.0309

Calibration Results:

Corr. Coefficient:	0.999999865
Slope (volts/in)):	3.319043136
Intercept (volts):	-0.00129759
Calibration Factor (in/Vs/Ve):	3.022226463
Offset (volts):	-0.00129759

Standard (in)	Sensor Output (volts)	Zero Adjusted Sensor Output (volts)	Best Fit Line Sensor Output (volts)	0.00 Best Fit Line error (volts)	0.00 Best Fit Line error (in)	0.03 Accuracy %FS
2	8.886399	6.638601	6.636789	0.001812	0.000546	0.027300
1.8	8.220097	5.972299	5.972980	-0.000681	-0.000205	0.010259
1.6	7.556619	5.308821	5.309171	-0.000350	-0.000106	0.005279
1.4	6.891096	4.643298	4.645363	-0.002065	-0.000622	0.031103
1.2	6.230734	3.982936	3.981554	0.001382	0.000416	0.020815
1	5.564969	3.317171	3.317746	-0.000575	-0.000173	0.008655
0.8	4.902074	2.654276	2.653937	0.000339	0.000102	0.005108
0.6	4.237816	1.990018	1.990128	-0.000110	-0.000033	0.001661
0.4	3.573987	1.326189	1.326320	-0.000131	-0.000039	0.001968
0.2	2.90939	0.661592	0.662511	-0.000919	-0.000277	0.013844
0	2.247798	0	-0.001298	0.001298	0.000391	0.019546

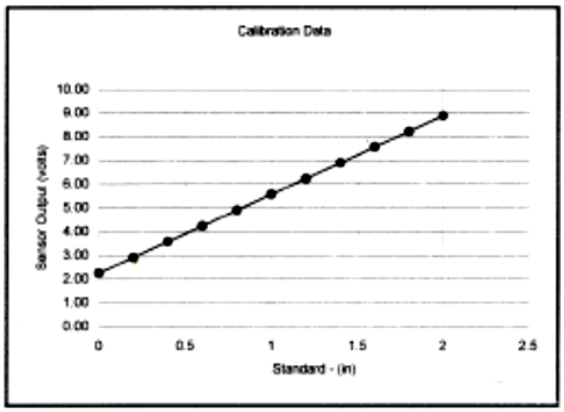

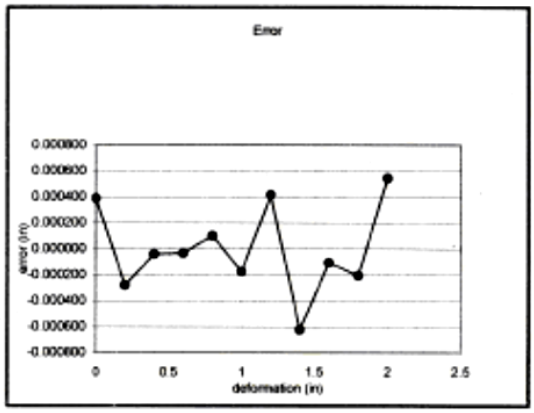

Appendix B

(Photographs of the Developed Device and Experiments)

(a) (b)

Figure B-1: Prepared sample (a) before and (b) after assembling the cell

Figure B-2: Miniature cone calibration chamber assembly

Appendix C

(Repeatability Tests Results)

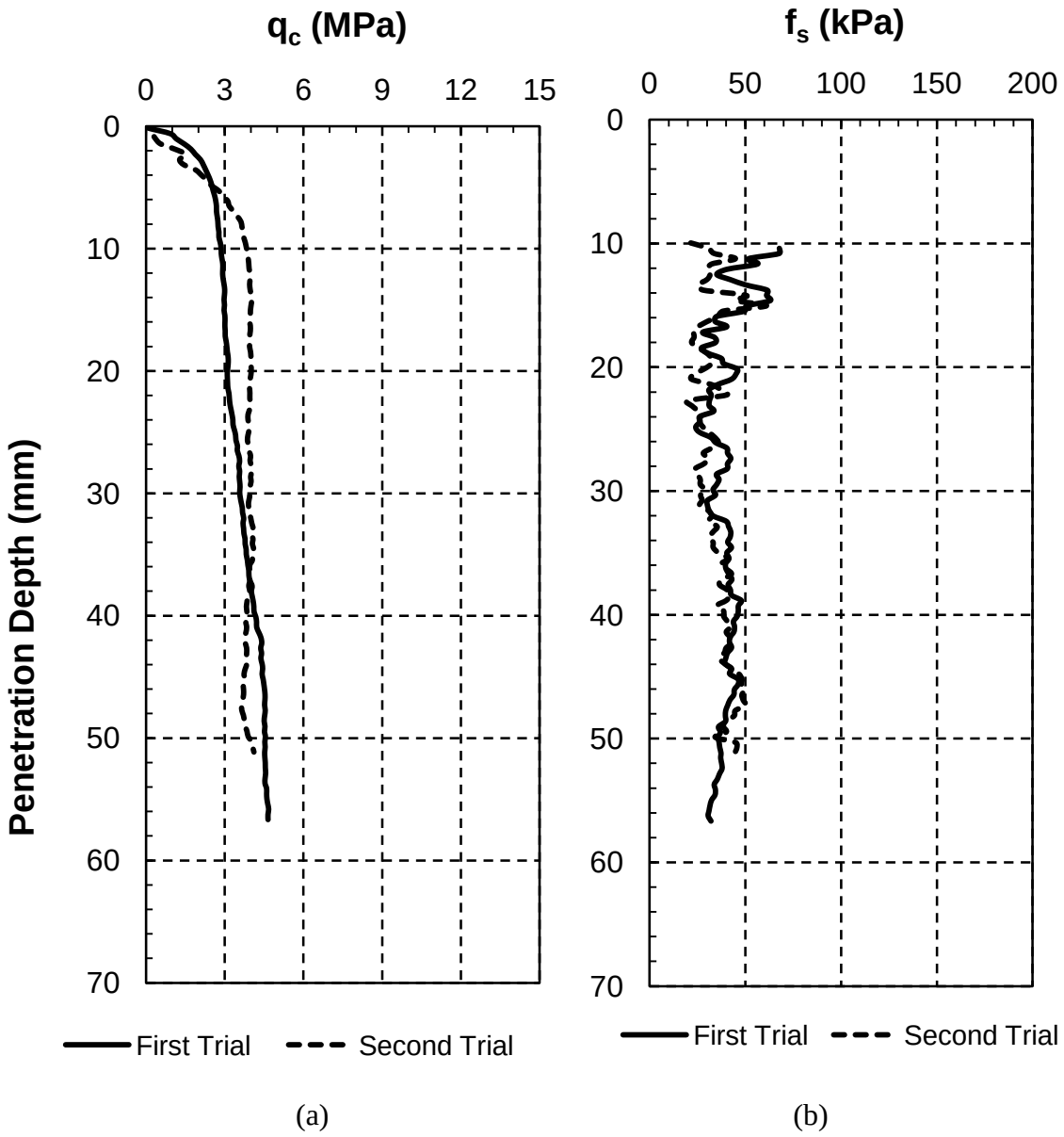

(a) (b)

Figure C-1: Repeatability of penetration resistances for Test No. 4: (a) q_c, (b) f_s

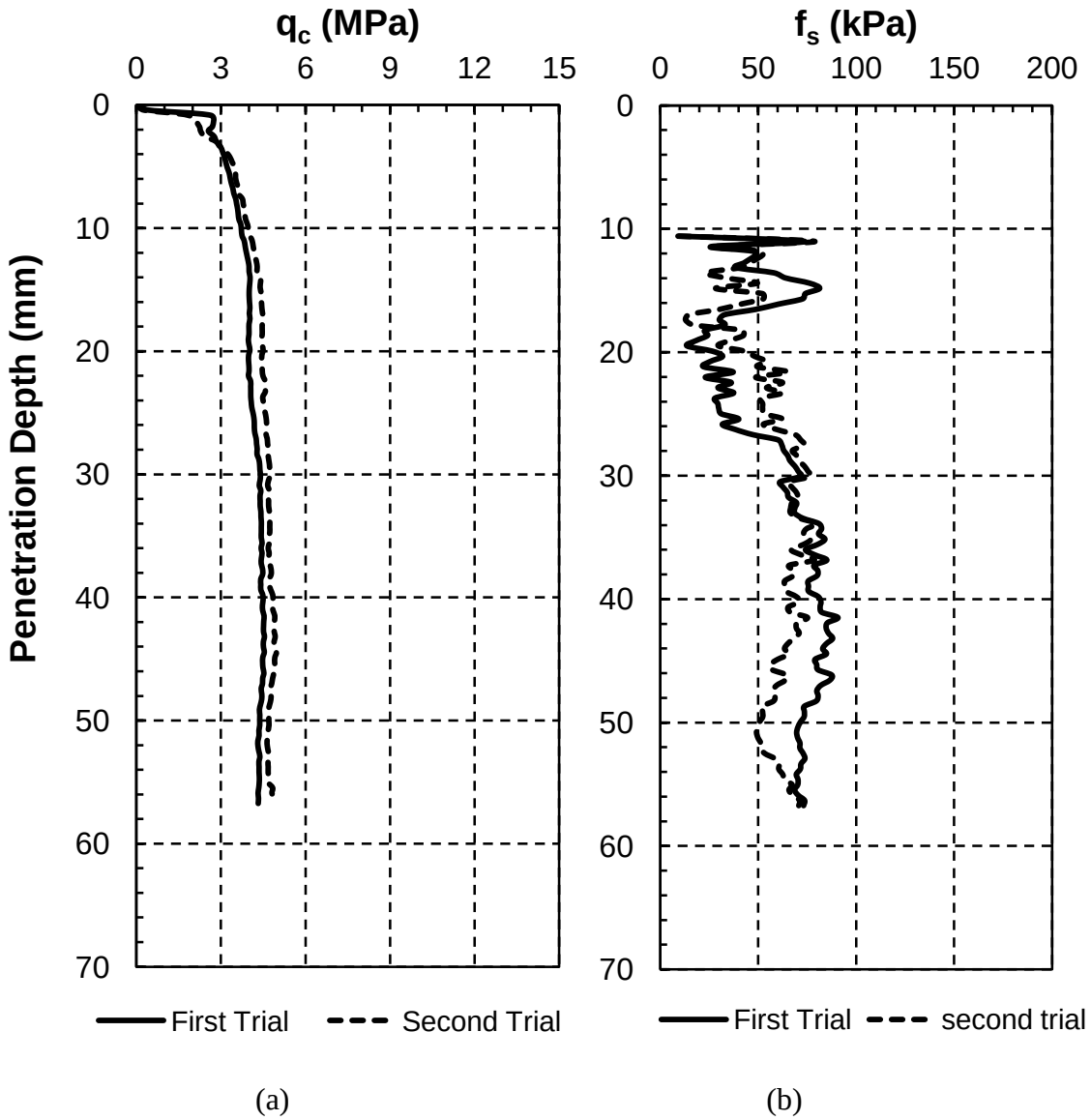

Figure C-2: Repeatability of penetration resistances for Test No. 7: (a) q_c, (b) f_s

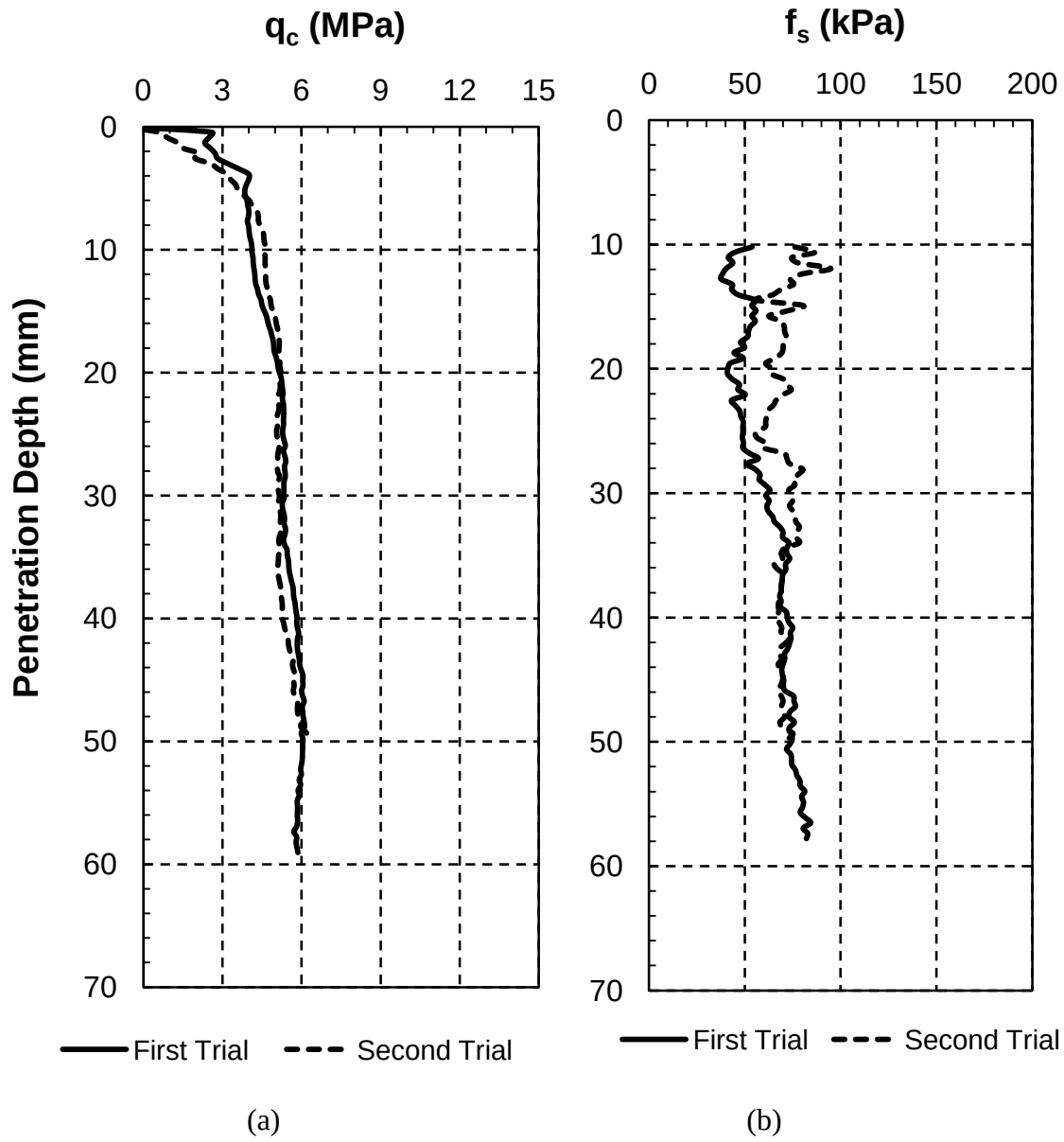

(a) (b)

Figure C-3: Repeatability of penetration resistances for Test No. 10: (a) q_c, (b) f_s

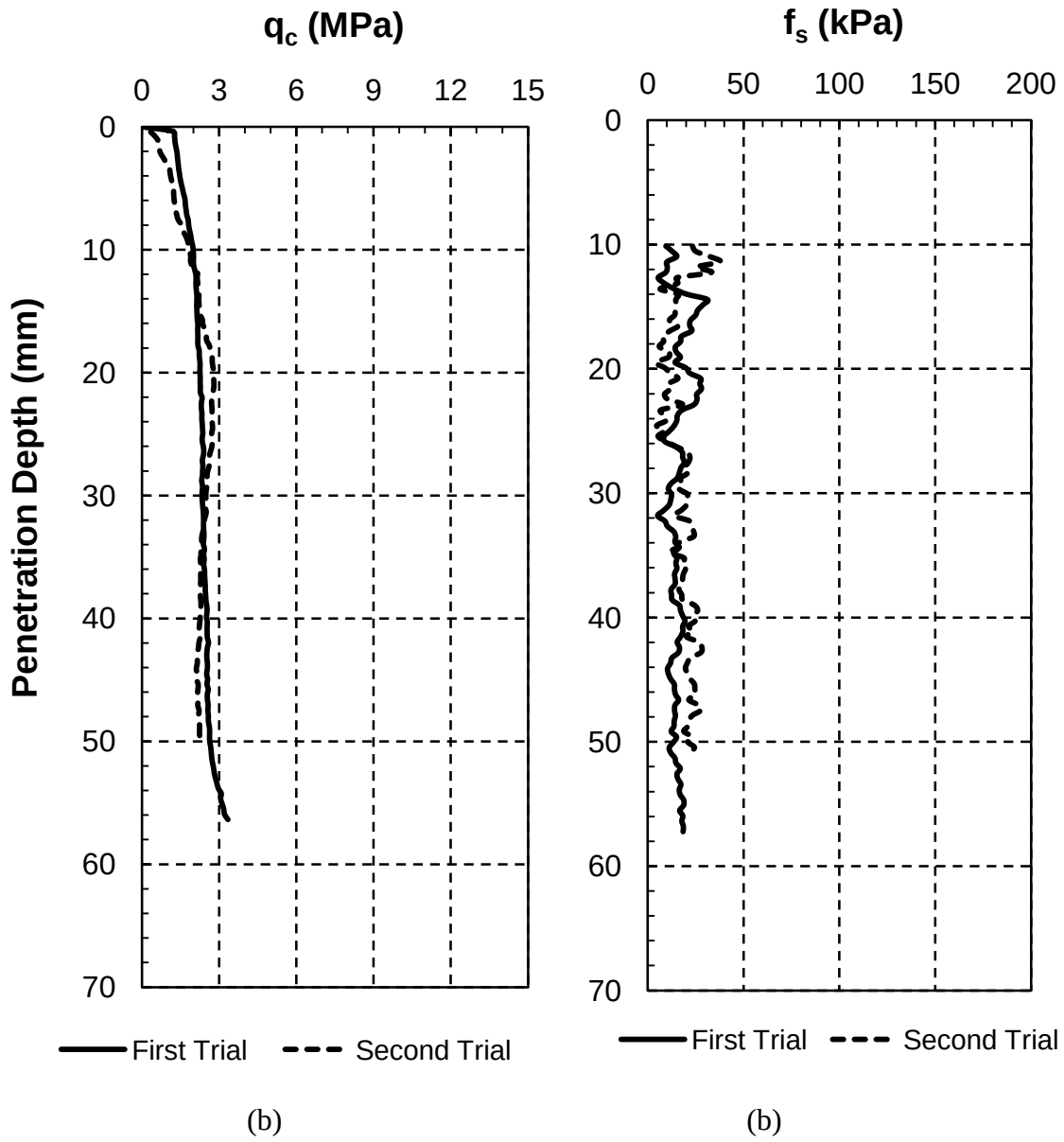

(b) (b)

Figure C-4: Repeatability of penetration resistances for Test No. 12: (a) q_c, (b) f_s

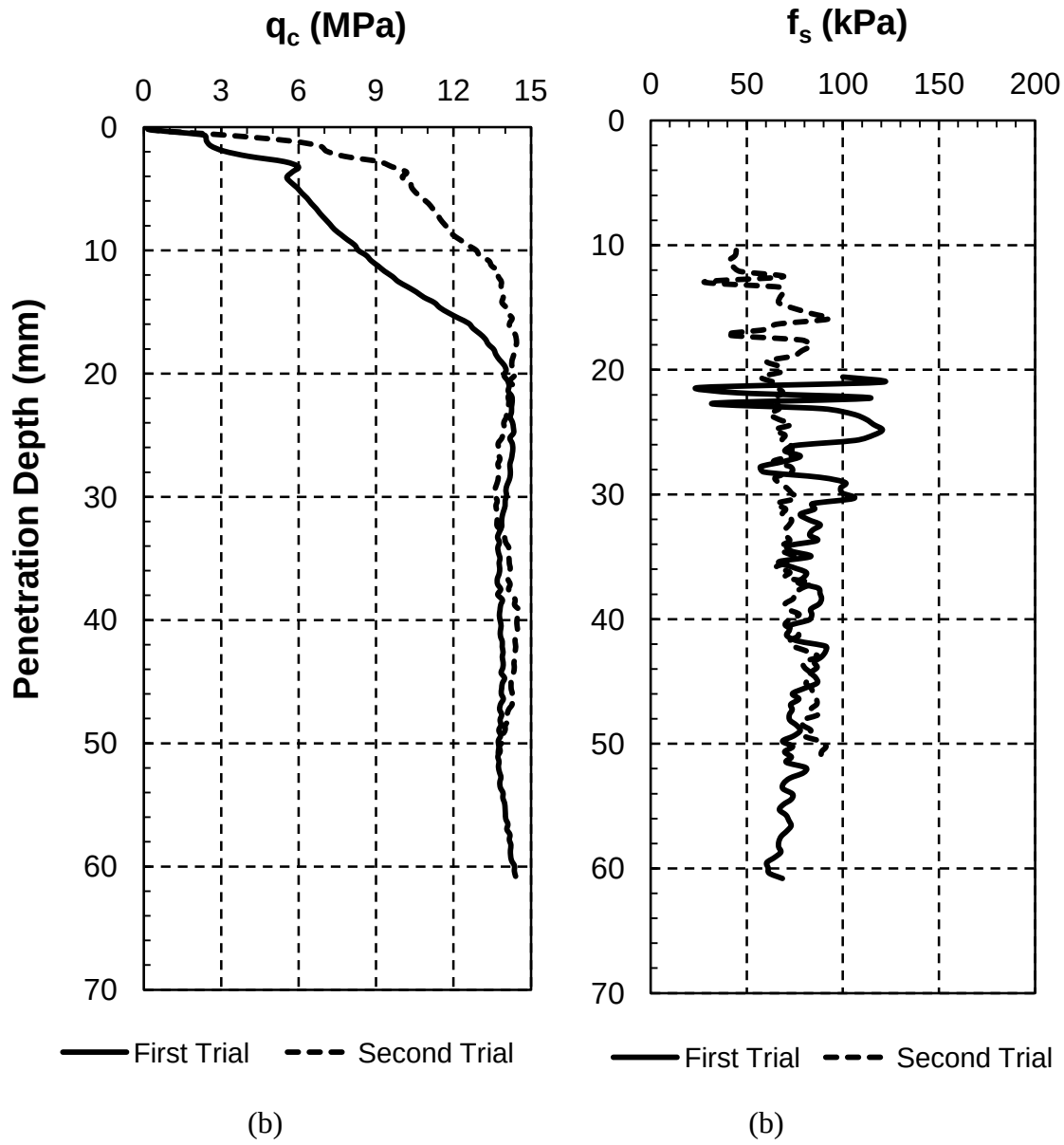

(b) (b)

Figure C-5: Repeatability of penetration resistances for Test No. 19: (a) q_c, (b) f_s

Appendix D

(Triaxial Compression Test Results)

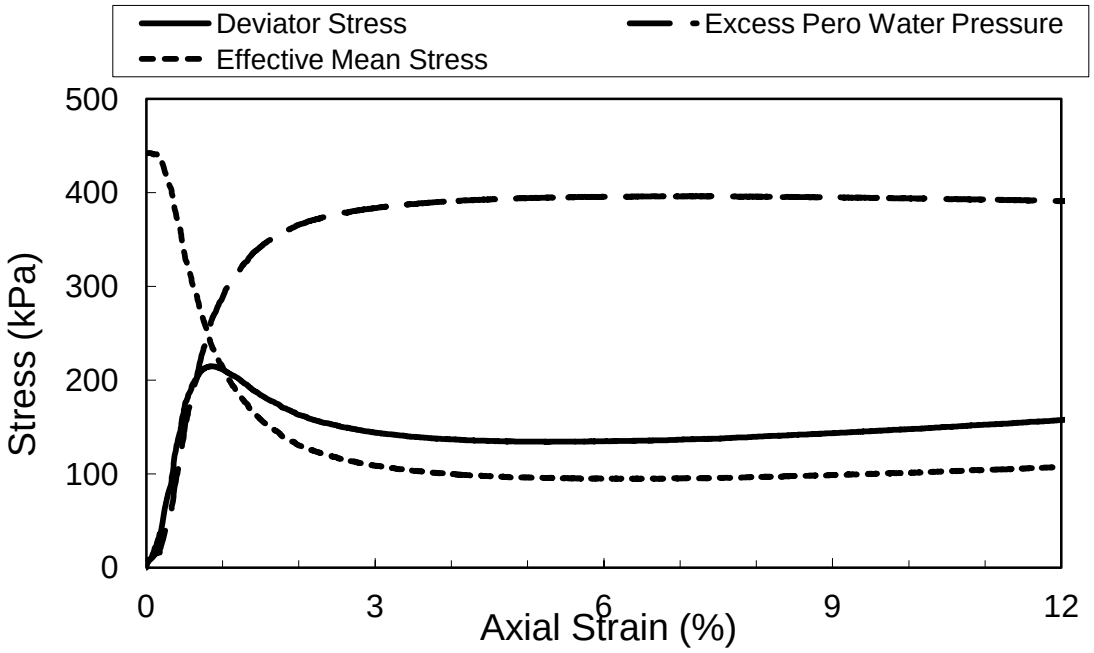

Figure C-1: Stress-Strain response of undrained triaxial compression test on a sample with D_{rc} = 20% at p'_c = 450 kPa (CPT Test No. 17.)

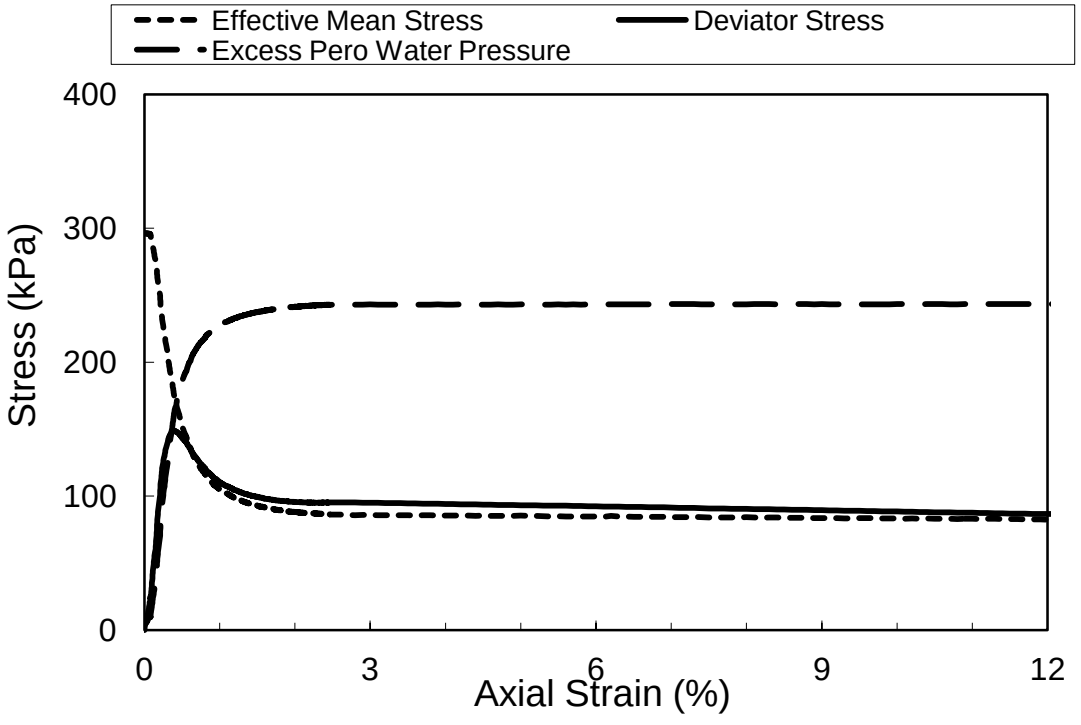

Figure C-2: Stress-Strain response of undrained triaxial compression test on a sample with D_{rc} = 20% at p'_c = 300 kPa (CPT Test No. 16.)

Curriculum Vitae

Name: Sepideh Damavandinejad Monfared

Post-secondary Education and Degrees:
University of Semnan
Semnan, Iran
2005-2009 B.A.

University of Tabriz
Tabriz, Iran
2009-2011 M.ESc.

The University of Western Ontario
London, Ontario, Canada
2012-2014 M.ESc.

Related Work Experience
Teaching Assistant
The University of Western Ontario
2012-2014

Publications:

Damavandinejad Monfared, S., and Sadrekerimi, A. (2013) "An Overview of Existing Methods for Estimating State Parameter from Cone Penetration Test Results." Proceedings of 66th Canadian Geotechnical Conference, Montreal, Canada.

Damavandinejad Monfared, S.(2012) " NUMERICAL STUDY ON THE BEHAVIOR OF INCLINED MICROPILE'' Proceedings of 37th Annual Conference on Deep Foundations Houston, TX October 16-19, 2012.

Sadrekerimi, A and Damavandinejad Monfared, S. (2013) "Numerical Investigation of The Mobilization of Active Earth Pressure on Retaining Walls" Proceedings of the 18th International Conference on Soil Mechanics and Geotechnical Engineering, Paris 2013.